Transparent, Lightweight, High Performance Polymer Films and Their Composites

Yunyin Lin

SUBMITTED IN PARTIAL FULFILLMENT OF THE REQUIREMENTS

OF THE DEGREE OF DOCTOR OF PHILOSOPHY

School of Engineering and Materials Science,

Queen Mary University of London,

London, UK

June 2020

Declaration

I, Yunyin Lin, confirm that the research included within this thesis is my own work or that where it has been carried out in collaboration with, or supported by others, that this is duly acknowledged below and my contribution indicated. Previously published material is also acknowledged below.

I attest that I have exercised reasonable care to ensure that the work is original, and does not to the best of my knowledge break any UK law, infringe any third party's copyright or other Intellectual Property Right, or contain any confidential material.

I accept that the College has the right to use plagiarism detection software to check the electronic version of the thesis.

I confirm that this thesis has not been previously submitted for the award of a degree by this or any other university.

The copyright of this thesis rests with the author and no quotation from it or information derived from it may be published without the prior written consent of the author.

Signature:

Date: 03/06/2020

Acknowledgements

First, I would like to give my greatest and sincere gratitude to my supervisors Prof. Ton Peijs, Dr. Emiliano Bilotti and Prof. Cees Bastiaansen for their generosity in guiding, supporting as well as sharing their knowledge and experience to me. Ton, always coming up with great ideas with his profound knowledge and comprehensive outlook, gave me plenty of constructive comments and supported me in all aspects over these four years. Emiliano's helpful suggestions and encouraging support guided me through the whole process. The intensive discussions with Cees taught me how to think critically and to be rigorous when doing research. Without their patient guidance and precious input, I would not have been able to carry out my research.

I would like to thank the China Scholarship Council (CSC) for their financial support and giving me an opportunity to study abroad. I gratefully acknowledge the facilities and support offered by School of Engineering and Materials Science and Nanoforce Technology Ltd. I also appreciate Dr. Russell Bailey, Dr. Alice Williams, Dr. Rory Wilson, Dr. Thomas Baumard, Dr. Giovanni Santagiuliana, Dr. Theo Saunders, Mr. Maurizio Leo, Ms. Sanam Ghaffari and Mr. Dennis Ife for their technical support.

I greatly appreciate Dr. Wei Tu and Dr. Han Zhang for their useful suggestions and invaluable assistance. A huge thanks to my lovely colleagues and friends Dr. Yi Liu, Dr. Yaqiong Wang, Dr. Nan Meng, Dr. Min Yu, Dr. Hangfeng Zhang, Dr. Kan Chen, Dr. Jiyue Wu, Xintong Ren, Kening Wan, Hanchi Ruan, Xiangyan Yu, Rehan Bhatti, Arnaud Kernin, Leonardo Ventura, Claudia Bertei, Man Zhang and Yichen Wang for all the help in any shape or form. Also I would like to thank undergraduate student Ruhi Patel.

I would also like to greatly acknowledge the support from the Stimuli-responsive Functional Materials & Devices (SFD) Group at Eindhoven University of Technology (Netherlands) and the SFD group members including Prof. Dick Broer, Prof. Albert Schenning, Dr. Lihua Shen, Tom Bus, Rob Verpaalen, Xinlong Pan, Simon Houben, Sarah Lafleur and Yuanyuan Zhan for their help. I spent a fabulous and unforgettable month in Eindhoven.

My special thanks go to my parents and my boyfriend, Jun Cao, for their understanding, support and encouragement which helped me throughout my whole PhD period.

Abstract

This thesis aims to develop novel polymeric material with an excellent balance in high optical transparency and mechanical properties. More particularly, the current thesis reports the processing and characterization of highly oriented transparent polyethylene films and their use in laminated composites.

First, highly transparent high-density polyethylene (HDPE) films with high modulus and tensile strength were developed by regulating solid-state drawing conditions without the need of additives. The effects of drawing parameters like drawing temperature and draw ratio on optical and mechanical properties as well as morphology of these solid-state drawn HDPE films were methodically investigated. It was found that a fairly broad processing window can be utilized to tailor the required balance in optical and mechanical performance.

Subsequently, the production of these ultra-drawn transparent HDPE films was carried out using a scalable and continuous cast-film extrusion and drawing process. High optical transparency of around 91 % was achieved even in the far field. A maximum modulus of ~ 33 GPa and tensile strength of ~ 900 MPa of these solid-state drawn HDPE films was attained without compromising optical transparency, which is an order of magnitude higher than mechanical properties of conventional transparent plastics such as polycarbonate (PC) and poly(methyl methacrylate) (PMMA). The influence of extrusion draw down and two-step drawing on optical and mechanical behaviours was also explored.

Finally, these highly oriented transparent HDPE films were used as the reinforcing phase in high performance transparent composite laminates. The far field light transmittance of

4-layer HDPE-reinforced laminates with either a unidirectional (UD) or bidirectional (BD) lay-up sandwiched between glass or PC skins, was maintained at around 85 %. The fabricated transparent composite laminates were shown to have not only a high tensile strength but also a high energy absorption capability, outperforming existing transparent glazing materials such as laminated glass or PC.

Table of Contents

List of Notations and Abbreviations

ABS	Acrylonitrile butadiene styrene
AFM	Atomic force microscopy
AgBeh	Silver behenate
APET	Amorphous polyethylene terephthalate
aPP	Atactic PP
BD	Bidirectional
BOPA	Biaxially oriented polyamide
BOPEN	Biaxially oriented polyethylene naphthalate
BOPET	Biaxially oriented polyethylene terephthalate
BOPE	Biaxially oriented polyethylene
BOPLA	Biaxially oriented poly(L-lactic acid)
BOPP	Biaxially oriented polypropylene
BZT	2-(2H-benzotriazol-2-yl)-4,6-ditertpentylphenol
CFRPs	Carbon fibre reinforced plastics
CNTs	Carbon nanotubes
CP	Cross-ply
CPET	Semi-crystalline PET
d	Nanovoids' dimension
DBS	1,3:2,4-dibenzylidene sorbitol
DMDBS	1,3:2,4-bis(3,4-dimethyldibenzylidene) sorbitol
DSC	Differential scanning calorimetry
E	Young's modulus
EDS	Energy-dispersive X-ray spectroscopy

EP-RACO	Ethylene-propylene random copolymers
EVA	Ethylene vinyl acetate
EVOH	Ethylene vinyl alcohol
f_c	Hermans' orientation factor
GFRPs	Glass fibre reinforced plastics
HDPE	High-density polyethylene
HDT	Heat deflection temperature
I	Scattering intensity
iPP	Isotactic polypropylene
k	Reinforcing efficiency
L_c	Lamellar thickness
LDPE	Low-density polyethylene
LLDPE	Linear low-density polyethylene
L_p	Long period
LPE	Linear polyethylene
MABS	Methacrylate acrylonitrile butadiene styrene
MD	Machine direction
MDO	Machine direction orientation
MFI	Melt flow index
MMA	Methyl methacrylate
$\overline{M_w}$	Weight-average molecular weight
MWD	Molecular weight distribution
MXD6	Polymethaxylylene adipamide
n	Refractive index
PBT	Polybutylene terephthalate
PC	Polycarbonate

PE	Polyethylene
PEEA	Polyether(ester amide)
PEN	Polyethylene naphthalate
PEO	Poly(ethylene oxide)
PET	Polyethylene terephthalate
PLA	Poly(L-lactic acid)
PMMA	Poly(methyl methacrylate)
POM	Poly(oxymethylene)
PP	Polypropylene
PPO	Poly(propylene oxide)
PS	Polystyrene
PSMMA	Poly(styrene-methyl methacrylate)
PTFE	Poly(tetrafluoroethylene)
PVA	Poly(vinyl alcohol)
PVB	Polyvinyl butyral
PVC	Polyvinyl chloride
PVDF	Polyvinylidene fluoride
q	Scattering vector
RoM	Rule of mixtures
RT	Room temperature
Sa	Surface roughness
SALS	Small-angle light scattering
SAN	Styrene-acrylonitrile
SAXS	Small-angle X-ray scattering
SBS	Poly(styrene-butadiene-styrene)
SEM	Scanning electron microscopy

SIC	Strain or stress induced crystallization
sPP	Syndiotactic PP
SRPP	Self-reinforced polypropylene
t	Thickness
T_d	Solid-state drawing temperature
TD	Transverse direction
T_g	Glass transition temperature
TGA	Thermal gravimetric analysis
T_m	Melting temperature
TPU	Thermoplastic polyurethanes
UD	Unidirectional
UHMWPE	Ultra-high molecular weight polyethylene
UK	United Kingdom
USA	United State of America
UV	Ultraviolet
UV-vis	Ultraviolet-visible spectroscopy
VLDPE	Very low-density polyethylene
WAXS	Wide-angle X-ray scattering
X_c	Crystallinity
$ZnSt_2$	Zinc stearate
ε	Elongation
λ	Solid-state draw ratio
λ_{max}	Maximum solid-state draw ratio
λ_{pre}	Pre-orientation ratio or draw down
λ_{trans}	Maximum transparent solid-state draw ratio
ρ	Density

σ_t	Tensile strength
ΔH_f	Enthalpy of fusion

List of Figures

List of Tables

Chapter 1

Introduction

1.1 Background

Common transparent materials, such as inorganic glass and amorphous polymers like polycarbonate (PC) and poly(methyl methacrylate) (PMMA), possess high optical transparency owing to their non-crystalline or low-crystalline structures with small amount of crystalline phase and have been widely utilized in glazing or window applications. However, the mechanical performance of almost all of these transparent materials is rather limited. For instance, inorganic glass is brittle with low strength (< 50 MPa) and low impact resistance, not to mention the risk from shattering into multiple pieces potentially causing injuries[1]. Typical transparent amorphous polymers including PC and PMMA generally possess relatively low mechanical behaviours such as elastic moduli of 2−3 GPa and tensile strengths of 50−70 MPa[2]. Although some efforts have been made to improve the mechanical properties of these materials by laminating glass, PC and/or PMMA with transparent polymeric interlayers, limited improvements have been obtained so far[3-5]. Therefore, these transparent materials are mostly applied in areas requiring high clarity but not necessarily high mechanical performance.

With regard to semi-crystalline polymers as polypropylene (PP) and polyethylene terephthalate (PET), transparent products can be manufactured by controlling polymer morphology, requiring the dimensions of spherulites to be much smaller than the wavelength of visible light. One way to achieve this is by adding nucleating or clarifying

agents, as in the case of sorbitol-clarified isotactic PP[6]. Furthermore, transparent PET products can be acquired by rapid cooling of the melt to below the glass transition temperature (T_g).

High-density polyethylene (HDPE), a kind of polyethylene (PE) possessing a density above 0.941 g/cm^3, is another type of semi-crystalline polymer and one of the most commonly used plastics. Approaches for making transparent PP and PET are typically not suitable for making PE products transparent because of a too rapid crystallization rate and a low T_g. Typically, HDPE is processed via injection moulding or extrusion-based melt processes, leading to isotropic or near isotropic materials and a relatively low elastic modulus (< 1.1 GPa) and tensile strength (< 35 MPa)[7]. Cast film or blown film extrusion of HDPE can lead to transparent products[8]. Nevertheless, such materials are often stretched in the melt, where chain entropy and chain relaxation prevents effective chain orientation and chain extension. Thus, mechanical properties of such transparent HDPE films are typically low, with moduli of 0.6−3 GPa and strengths of around 30−230 MPa[9-10], which limits their applications mainly to packaging.

Solid-state drawing processes can significantly enhance the modulus and strength of HDPE because chain relaxation phenomena are limited below the melting temperature and hence a high degree of chain orientation and chain extension is generated during solid-state drawing[11]. However, solid-state drawn HDPE fibres or films are normally opaque. For one thing, the size of the crystals, being typically larger than the wavelength of visible light, and the high degree of crystallinity partially accounts for this opacity[12]. Moreover, the introduction of internal voiding and defect structures after ultra-drawing will induce light scattering, resulting in a poor transparency in the visible light regime[13].

High performance composites reinforced by high performance fibres and fabrics such as carbon[14], glass[15], aramids[16] and PE[17] have been increasingly used in automotive, defence, aerospace and civil fields due to their high specific moduli and strengths. Among them, polymeric ultra-high molecular weight polyethylene (UHMWPE) fibres like Dyneema® or Spectra® and aramid fibres like Kevlar® or Twaron® exhibit a relatively high level of toughness and energy absorption capability upon fracture, resulting in various applications where impact resistance is of great importance like bullet-proof vests, armour, helmets and anti-ballistic panels. However, nearly all of today's high performance fibre-reinforced composites are non-transparent due to serious light scattering resulting from the large surface area of fibres and refractive index mismatch between matrix and fibres. Some transparent composites reinforced by S-glass fibres[18-19], nylon fibres[20-21] or drawn PP filaments[22] were previously fabricated by matching refractive indices of matrix and reinforcing phase, but these composites only achieved limited optical transparency especially in the far field as required in windows and visors.

As a result, most of today's polymeric based materials do not possess high optical clarity and high mechanical performance simultaneously. This restricts their application in fields where both high transparency and excellent mechanical properties are required, such as built environment, automotive glazing, safety shields, impact resistant visors and displays for portable electronics.

1.2 Objective of the thesis

The objective of the current work is to develop a methodology to fabricate highly transparent, lightweight and high mechanical performance polymeric films and

composites and to pioneer a new line of research in the area of "high performance transparent polymers and composites".

This research aims to improve the performance, notably optical and mechanical properties, of oriented HDPE films by controlling solid-state drawing parameters, and to produce these transparent HDPE films in a scalable and continuous manner, without adding high cost and/or introducing major changes in the industrial value chain.

The manufactured continuous transparent films are then utilized to fabricate composite laminates with different outer layers. The main attention is devoted to their optical and mechanical performance, notably penetration resistance. Such an approach can potentially yield new, advanced high-end applications with a large profit margin. The potential applications of these optically transparent, lightweight and high performance polyethylene films and laminates lie in flexible plastic packaging, structural glazing for buildings, automotive glazing, safety shields, protective visors or displays for portable electronics where a combination of high transparency, low specific weight and excellent mechanical behaviours is required.

1.3 Scope of the thesis

This research project addresses the processing and properties of highly transparent, high strength HDPE films produced in a lab-scale as well as pilot-scale process and composite laminates based on these highly oriented HDPE films. Chapter 2 gives a comprehensive overview of common transparent materials including inorganic glass and amorphous polymers, the current state-of-the-art to produce transparent products or films consisting of isotropic, biaxially oriented and uniaxially oriented semi-

crystalline polymers, solid-state drawing processing, transparent composite laminates and high performance composites. Chapter 3 presents the fabrication of highly oriented HDPE films with both high transparency and high strength by solid-state drawing and discusses the influence of drawing parameters on drawing, optical and mechanical behaviours in combination with film morphology. Chapter 4 describes a scalable and continuous production process of these ultra-drawn transparent HDPE films using a cast film extrusion and solid-state stretching line. Chapter 5 describes the design, manufacture and properties of high performance transparent composite laminates based on these highly oriented HDPE films with either glass or PC as outer layers. The interfacial, optical, tensile and penetration resistance properties of the resulting HDPE reinforced laminates are discussed. Finally, Chapter 6 summarizes the results of this research and points out potential applications of resulting products as well as some suggestions for future research.

Chapter 2

Literature Review

2.1 Conventional transparent inorganic glass

Generally, optical properties of a material involve transparency, gloss, clarity, haze, absorption of light, fluorescence, etc.[23]. Transparency represents the transmission of visible light. Whether a material is transparent or not highly depends on the amount of the light that is transmitted through the material. It is widely used in the field of glass substitutions, optical appliances and packaging. Gloss is mainly determined by light reflection and a smooth surface usually means high gloss. The gloss of polymers is generally determined by their surface texture, which can originate from extrinsic factors or intrinsic factors. Extrinsic factors like a dusty environment, catalyst residues or surface textures in moulds or calenders can be minimised during processing. Intrinsic factors like the refractive index of the material that create gloss are often more difficult to circumvent. Clarity is a measure of the direct transmission in relation to scattering at low angles (< 2.5 °). A high level of clarity indicates a good resolution of the details of an object when seen through the material. Haze is defined as the part of the transmitted light which is scattered at large angles (> 2.5 °). It denotes the milkiness of a sample. If haze is greater than 30 %, materials will appear translucent, which is still useful in the packaging field. In this thesis, the emphasis is mainly on transparency.

Glass is defined as an inorganic product of fusion that has cooled to a rigid condition without crystallizing. Due to its non-crystalline characteristics, glass generally appears transparent.

The overall light transmission of glass is mainly affected by the reflection on each side of the glass surface, the absorption inside the glass and the thickness of the glass. According to Fresnel equations, reflection mostly depends on incident angle, light wavelength, refractive index of the glass, surrounding medium and the quality of interfaces[24]. In addition, the species of glass, additives, melting and cooling conditions will also influence the transmission of light. For soda-lime glass with a refractive index of 1.50−1.52 in the visible light wavelength range[1], around 4 % reflectance loss occurs at each of the two surfaces when it is normal incidence and absorption is negligible. Thus, approximately 92 % incident visible light will be transmitted through the glass. With lower refractive indices of the glass, more light can be transmitted through the glass. Surface treatments like coating low refractive index layers on glass surfaces will significantly reduce reflection loss and increase transmittance and transparency.

AMIRAN® glass produced by Schott AG is extra-clear glass with anti-reflective coatings. This anti-reflective behaviour is accomplished by dipping glass in several metal oxide solutions. These oxide layers with good mechanical and chemical durability are formed on the glass surface at high temperatures and will effectively reduce reflection. As a result, less than 1 % visible reflectance happens at two surfaces of AMIRAN® glass compared to 8 % for common float glass (see ***Figure 2.1***), contributing to an extremely high light transmission of above 98 % and a crystal-clear appearance. This highly transparent glass offers a good see-through view by the human eye and even camera, and can be applied in showcases and window facades.

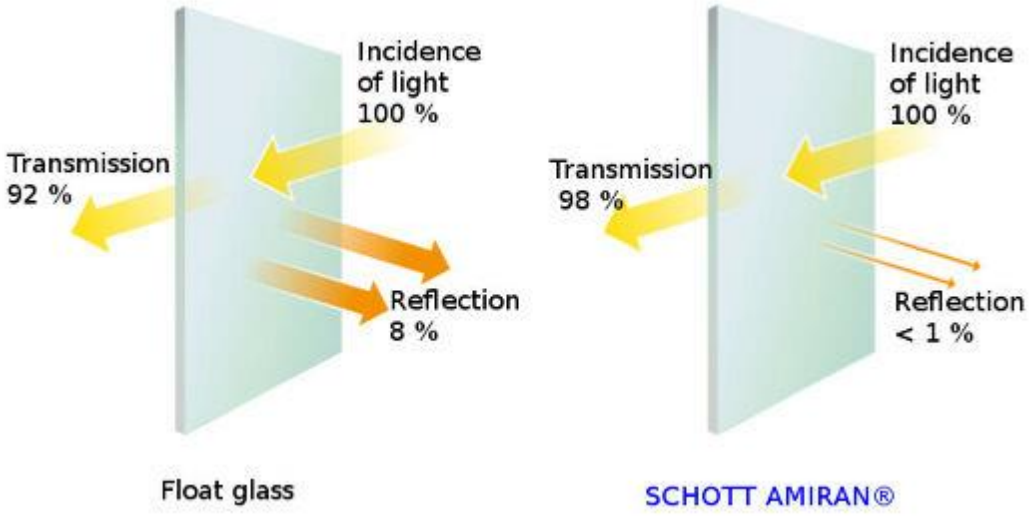

Figure 2.1 *Schematic diagram of reflection and transmission of AMIRAN® glass from Schott AG (right) versus common float glass (left)*[25].

With respect to mechanical performance, most inorganic glasses are rigid but brittle with a low strain at break and no plastic deformation, and hence local stress concentrations cannot be reduced by redistributing stress[1]. Besides, the atoms of inorganic glasses are held together tightly by strong chemical bonds and hard to slip past one another.

Glasses typically possess a Young's modulus of 50−90 GPa. Higher elastic moduli can be achieved when atoms are packed closer to each other so that stronger bonds can prevent deformation[26]. Adding some network formers like aluminium oxide to silicate glass can also increase modulus.

With regards to the tensile strength of glass, the theoretical value is about 17 GPa as calculated by the energy necessary to break Si-O covalent bonds. However, experimental values are typically much lower and only around 50 MPa for normal sheet glass. Differences between theoretical and practical values are primarily due to defects and flaws inside or on the surface of the glass, including scratches, bubbles, inclusions or

inhomogeneous density, leading to stress concentrations at these flaws. When a high enough tensile stress is applied, fracture will be triggered by these stress concentrations, leading to brittle fracture with glass shattering into multiple fragments after breaking, potentially causing injuries. Thus, glass has a poor impact resistance and post-failure behaviour. Most of the flaws on the surface of glass can be eliminated by annealing or acid etching. Additionally, introducing a compressive stress by a secondary treatment, such as ion-exchange, coating, thermal tempering or crystallization gradients, can make glass having higher tensile strengths.

Gorilla® Glass is a brand of specialized toughened glass manufactured by Corning Incorporated. It possesses a layered structure consisting of a tension layer and compression layers. These compression layers are created by an ion-exchange process from small sodium ions to larger potassium ions to provide a compressive stress on the glass surface. This process chemically strengthens glass, and more importantly, protects the core glass from being flawed or scratched, resulting in excellent scratch resistance. It is reported that the latest Gorilla® Glass 6 can survive fifteen consecutive drops from a height of one meter onto coarse surfaces, while normal glass cannot even survive the first drop. Meanwhile, it maintains outstanding optical transparency (> 90.5 %) within a wide wavelength range of 380−2000 nm. Regarding mechanical performance, its Young's modulus and fracture toughness can reach 77 GPa and 0.7 $MPa \cdot m^{1/2}$, respectively[27]. These features make Gorilla® Glass ideal for high-resolution electronic display applications, like smartphone and computer screens. As a consequence, Gorilla® Glass has already been used in more than 6 billion devices by over forty manufacturers.

Based on applications, glass can generally be divided into three categories: flat glass, container glass and glass fibre. Transparent flat glass produced by a float process is used

for windowpanes, while container glass manufactured by blowing or pressing method is mainly used for glass containers, such as jars and bottles for food and beverages. Glass fibres, mostly made by drawing silica-based or other formulated glass into fibres, are usually not transparent because of the large surface area. Glass fibres have widespread applications especially in telecommunication like transatlantic cables[28-29]. They can also be used as a reinforcing agent in composites for building glass fibre reinforced plastics (GFRPs) due to their high specific mechanical properties (properties per unit weight).

2.2 Transparent amorphous polymeric materials

Generally speaking, isotropic transparent polymeric materials can reach similar optical properties as transparent inorganic materials like glass but with significant advantages in other properties such as low density, good impact resistance, flexibility and rapid processing of complex parts, etc. Based on the degree of crystallinity (X_c), polymers can be classified into two main categories: amorphous polymers (non-crystalline or low-crystalline) and semi-crystalline polymers.

Amorphous polymers probably represent the largest group of transparent plastics with major representatives such as polycarbonate (PC), poly(methyl methacrylate) (PMMA), polystyrene (PS), thermoplastic polyurethanes (TPU), polyvinyl butyral (PVB) and copolymer ethylene vinyl acetate (EVA). In general, these amorphous polymers tend to be atactic as in the case of atactic PS, while some polymers like Bisphenol A PC remain in their amorphous state upon cooling because of their extremely slow crystallization kinetics. Also polyvinyl chloride (PVC) can crystallize but typically has a crystallinity of only 10 % and is therefore often classified as an amorphous polymer. Transparency can

also be achieved in plasticized PVC as long as additives are selected carefully. Besides, some intrinsically crystallisable polymers like polyethylene terephthalate (PET) can also be amorphous by suppressing crystallization like quenching the molten PET to below glass transition temperature (T_g), which will be further discussed in Section 2.3.1.1. In amorphous polymers, the absence (or limited size) of the crystalline regions contributes to their high optical transparency, whilst it also leads to no evident presence of a melting temperature. Typically, PC, PMMA or PS have elastic moduli of 2−3 GPa and tensile strengths of around 60 MPa[2].

2.2.1 Polycarbonate (PC)

PC is a thermoplastic polymer with carbonate groups. Most of PC materials are optically transparent with transmittance values of 88−91 % in the visible light wavelength range. It possesses high dimensional stability and can hold up for a long time even under elevated temperatures. Different from most amorphous thermoplastics, PC can withstand high plastic deformation without significant cracking or breaking and shows a high resistance to impact.

However, PC products will appear yellowish after long-term usage because of the long-time exposure to ultraviolet (UV) rays or degradation to smaller molecules. UV stabilizers are thus normally added to PC to prevent them from becoming yellow. In addition, PC has poor scratch resistance and surface coatings are needed for many PC products.

Transparent PC materials have been widely applied in greenhouse construction, building roofs, safety helmets, laboratory appliances like goggles, household appliances, automotive and transportation.

2.2.2 Poly(methyl methacrylate) (PMMA)

PMMA is well known as acrylic glass due to its excellent optical transparency to visible light, whose total transmission values can reach up to 92 % and only 1 % haze[2]. PMMA has good UV tolerance and will not become yellow after a long time. In general, PMMA is cheaper than PC, and PMMA is utilized in fields requiring high optical clarity but relatively low resistance to impact such as shatterproof window, skylights, lenses, optical devices and aircraft canopies.

PMMA is rigid and brittle and it will easily break under stress because the minimum crazing stress, which is the stress level required for crazing to start, is lower than the tensile yield stress[30]. PMMA has a bit higher but still limited scratch-resistance compared to PC. Proper modifications like copolymerization with other monomers or blending with elastomers can toughen PMMA products and make them even more resistant to scratching and impact[2]. However, these modifications often bring light scattering and thus transparency loss.

2.2.3 Polystyrene (PS)

PS is a kind of synthetic thermoplastic commodity plastic polymerized from styrene monomer. Normally, PS in solid form is naturally transparent, with a total transmission of 88−92 %. However, PS is brittle with only 1−3 % elongation, possessing poor resistance to solvent, impact, creep and heat. PS can be copolymerized with methyl methacrylate to produce poly(styrene-methyl methacrylate) copolymer (PSMMA) with higher transparency, better UV and chemical stability. Similar to PMMA, impact resistance, toughness, tensile strength and chemical resistance can be improved by

blending styrene with elastomers like butadiene and/or acrylonitrile to fabricate transparent copolymers or terpolymers such as poly(styrene-butadiene-styrene) (SBS)[31], styrene-acrylonitrile (SAN), acrylonitrile butadiene styrene (ABS)[32] and methacrylate acrylonitrile butadiene styrene (MABS)[33]. Transparent PS and its copolymers are widely used in food packaging, containers, blow-moulded bottles, plastic cutlery and disposable tableware.

2.2.4 Polyvinyl chloride (PVC)

PVC should technically be regarded as a semi-crystalline polymer since it has a crystallinity of around 10 %, but most if not all people will classify PVC as an amorphous polymer. PVC polymerized by vinyl chloride monomer is a durable thermoplastic with excellent cost-performance advantages.

PVC can be categorized into two types: rigid PVC and flexible PVC. By incorporating suitable plasticizers acting as lubricants to reduce crystallinity and chain interactions, more flexible and transparent PVC can be produced. Flexible (or plasticized) PVC with a density of 1.1−1.35 g/cm^3 has better flexibility, better UV resistance, higher impact strength and easier processibility, but worse dimensional stability and lower chemical resistance compared to rigid (or unplasticized) PVC with a density of 1.3−1.45 g/cm^3. However, flexible PVC tends to degrade at high temperatures and its properties will change with time because of the migration of plasticizers. The rigid to flexible range gives PVC a wide spectrum of properties and potential applications. Packing films or sheets, pipes, cables, door and window profiles can be manufactured from PVC.

2.2.5 Thermoplastic polyurethanes (TPU)

TPU is a series of polyurethane elastomers, mostly linear block copolymers incorporating alternating soft and hard segments. As a result, TPU combines the properties of both soft thermoplastics and hard elastomers, and shows good mechanical performance including high flexibility and toughness.

Usually, the hard segments of TPU possess a higher refractive index while the soft segments have a lower refractive index. Light scattering occurs between two segments and results in the opaque appearance of TPU. Transparent TPU products can be produced by matching refractive indices between hard and soft segments, regulating the volume fraction of the two segments or by reducing the size of domains to below the wavelength of visible light in order to avoid light scattering. Transparent TPU products have been applied in automotive interior and exterior accessories, optical lenses and some commodities like snow or ski goggles, mobile phone shell and rain gear. Transparent TPU sheets can also be used as interlayer materials in architectural laminated glass, PC, PMMA or bonding other transparent materials together.

2.2.6 Other transparent amorphous polymers

Apart from the above stated polymers, polyvinyl butyral (PVB) and ethylene vinyl acetate (EVA) are also transparent amorphous polymers which are widely used in composite laminates especially laminated glass.

PVB accounts for the largest market share in laminated glass since PVB can almost completely block UV radiation and possesses high deformation before breakage, excellent adhesion to glass and good optical transparency after lamination. However,

PVB may degrade by weathering conditions. For instance, ambient humidity will decrease its adhesion with glass.

EVA, a copolymer of ethylene and vinyl acetate, has good durability against heat and humidity in combination with long-term reliability. It also has good sound insulating properties even in a high frequency range. However, EVA has worse impact performance compared to PVB at the same thickness.

2.3 Transparent semi-crystalline polymeric materials

Semi-crystalline polymers are composed of both crystalline and amorphous phases. Their high-temperature mechanical performance is often superior to amorphous polymers due to the presence of crystalline regions. However, because the refractive index of these crystallites is usually higher than that of the amorphous phase, visible light can scatter on the boundaries between these crystalline and amorphous regions. This light scattering leads to less light being transmitted through the polymer, resulting in opacity for most of semi-crystalline polymer products.

Besides, the dimensions of the crystals will greatly affect the transparency of a semi-crystalline material. In most semi-crystalline polymers, especially those with a fast crystallization rate such as PE and polyamides like PA-6, the sizes of the crystals are generally larger than the wavelength of visible light, leading to a large amount of light scattering and an opaque appearance.

The following sections are organized according to the methodologies to produce transparent products or films consisting of isotropic, biaxially oriented or uniaxially oriented semi-crystalline polymers.

2.3.1 Isotropic transparent semi-crystalline polymers

Generally, there are three main principles to make transparent products from semi-crystalline polymers: (1) suppressing crystallization and preventing the formation of large crystals by adjusting chemical structure, tacticity or rapid quenching; (2) decreasing the sizes of the crystals to below the visible-light wavelength (usually < 200 nm) by adding nucleating agents or clarifying agents or by copolymerization; (3) matching of refractive indices between two semi-crystalline polymers to produce transparent polymer blends. In many cases, a combination of (1), (2) and (3) is used to generate a high optical transmittance.

2.3.1.1 Suppressed crystallization

Polymers potentially crystallize upon cooling from the melt (thermally induced crystallization), upon mechanical stretching or deformation (strain or stress induced crystallization, SIC) or upon crystallization from solution. During crystallization, the molecular chains of polymers will fold and form ordered regions called lamellae. Crystallinity and crystallization rate, depending on various parameters including chain stiffness, molecular weight, temperature and so on, will determine the amorphous or crystalline state of polymers. For instance, PE possessing a rapid crystallization rate and a low T_g will easily crystallize and normally achieve a crystallinity above 35 %, whilst PC with a very slow crystallization rate can remain in amorphous state upon regular cooling and exhibits a transparent appearance.

If the cooling rate of a polymer melt is higher than the crystallization rate like in the case of quenching, a crystallisable polymer can mostly remain in its amorphous state, preventing the formation of large crystals and spherulites. Amorphous polyethylene terephthalate (APET) films or sheets are transparent with good toughness and can be obtained by quickly cooling the molten PET to below T_g after cast film extrusion from a slot die. PET exhibits moderate crystallization rates and upon rapid cooling, chains do not have adequate time to reorganize themselves into an ordered crystalline structure and the PET will mostly remain in its amorphous state.

Controlling chemical structures and tacticity can influence the crystallization process and the formation of large crystals. A high degree of polymer chain tacticity can facilitate the crystallization process since it is easier for regular chains to pack closely and form ordered crystalline structures. Usually, isotactic or syndiotactic structures result in a certain degree of crystallization, while most atactic polymers do not crystallize and stay in the amorphous state due to the lack of regularity of their polymer chains. Polypropylene (PP) has different stereochemical configurations based on the relative position of adjacent methyl groups as it is polymerized from asymmetric propene monomer. Isotactic PP (iPP) and syndiotactic PP (sPP) are semi-crystalline polymers and their relatively low crystallization speed under homogeneous nucleation leads to the formation of micron-sized crystals, accounting for their poor transparency, whereas atactic PP (aPP) is regarded as an amorphous polymer because the irregular arrangement of its side groups prevents the formation of crystals. Thus, aPP possesses good transparency but has also a low heat deflection temperature (HDT) due to its low T_g. One exception is poly(vinyl alcohol) (PVA). PVA is an atactic polymer but also a semi-crystalline polymer with optical transparency since the OH-groups are very small and can fit in the crystal lattice.

In terms of chain branching, branch content influences both crystallization kinetics and final morphology of lamellae crystals, with increasing branch content resulting in a decrease in crystallization rate as well as crystallinity. Branch length will also affect the final crystal morphology[34]. Homo- or co-polyamides (PA) polymerized by asymmetric (co-)monomers possessing side chains or ring structures can achieve transparent amorphous PA products by disturbing the regularity of aliphatic PA chains, leading to a reduced formation of hydrogen bonds in combination with a lower crystallinity. For instance, the substituent methyl groups of poly(trimethyl hexamethylene terephthalamide) (PA 6-3-T) inhibit crystallization, and it remains amorphous at all temperatures with around 90 % light transmittance[35].

However, the creation of transparent polymers by suppressing crystallization of intrinsically crystallisable polymers may lead to improved clarity but at a significant expense of their high-temperature mechanical properties.

2.3.1.2 Reducing crystal size

There are a few ways to reduce the dimensions of crystals so as to produce transparent semi-crystalline polymer products.

Adding nucleation agents to isotropic semi-crystalline polymers can effectively decrease the dimensions of crystals by accelerating the rate of crystal nucleation and regulating the time scale of crystallization by initiating the crystallization of the polymer at higher temperatures during the cooling of the melt. Nucleation agents are usually inorganic materials with small, average particle sizes (<< 100 nm) such as benzoic acid, kaolin, clay and talc and have a high melting temperature. The nucleation agents remain solid in the polymer melt and act as heterogeneous nuclei as their surface in polymer melts can

decrease the free energy for forming nuclei larger than the critical size[36]. They provide numerous nucleating sites so that the spherulites can form and the polymer chain can crystallize. This process effectively decreases the average size of spherulites and increases the crystallinity.

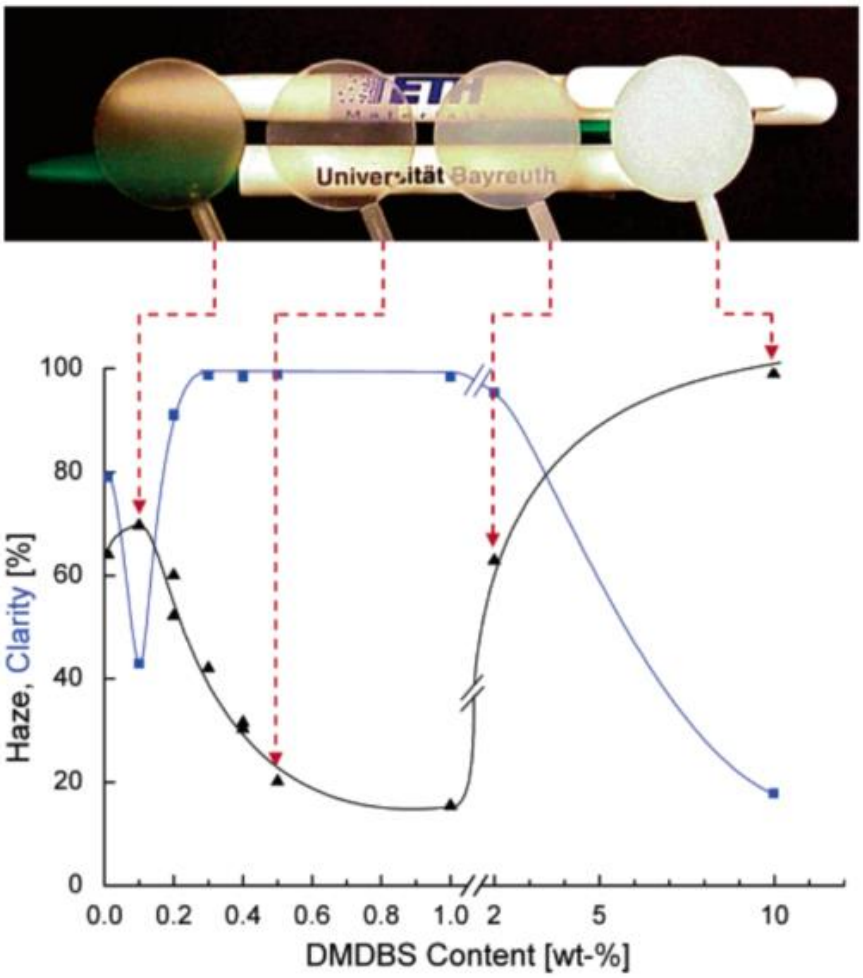

Figure 2.2 *Optical performance of iPP/DMDBS containing different amount of DMDBS*[6].

Clarifying agents, a subcategory of nucleating agents, are generally organic non-polymeric molecules and have a melting temperature within the processing window of the clarified polymer. These transparent clarifiers dissolve in the molten polymer and achieve a homogeneous dispersion. During cooling of the polymer melt, the crystallization of the polymer will start at a higher temperature compared to that without

clarifier, leading to a reduction in the dimensions of the crystals to a size below the wavelength of visible light, which allows light to pass through and hence resulting in a significant improvement in transparency and clarity. Sorbitol and its derivatives such as 1,3:2,4-dibenzylidene sorbitol (DBS)[37-38] and 1,3:2,4-bis(3,4-dimethyldibenzylidene) sorbitol (DMDBS, its clarifying effect is shown in ***Figure 2.2***)[6, 39], salts of rosin acid[40-41], organic phosphates[42] and trisamides[43] are typically used as clarifying agents to fabricate transparent iPP products. Clarifiers like DBS can also enhance the transparency of PET products[44-45].

Adjusting crystallization rate is helpful to reduce the size of crystals in semi-crystalline polymers. Poly(4,4'-aminocyclohexyl methylene dodecanedicarboxylamide), named PA PACM12, is a transparent microcrystalline cycloaliphatic polyamide[46]. The crystallization speed of PA PACM12 is relatively slow and as a result really fine crystalline structures with microcrystalline dimensions smaller than the visible-light wavelength can be formed. As a result, it is transparent with about 92 % light transmittance. Meanwhile, the microcrystalline structures offer excellent processibility, high thermostability as well as good resistance to scratch and abrasion, making it suitable for applications like goggles and sunglasses.

Introducing comonomer for copolymerization helps to destroy the original continuous polymer chain structure and impedes the growth of crystallites, leading to a decrease in crystalline dimensions and overall crystallinity. In the case of PE, nucleating and clarifying agents do not work because the crystallization rate is too high. Reducing their crystal size is usually done by copolymerization with low-density polyethylene (LDPE), linear low-density polyethylene (LLDPE) and/or very low-density polyethylene (VLDPE). PP copolymerized with ethylene or higher α-olefins can reach good optical

clarity. Ethylene-propylene random copolymers (EP-RACO) exhibit better transparency (up to 84.6 %), higher fracture toughness, lower processing temperature, broader softening range and improved low-temperature impact strength in comparison to PP homopolymers, where the ethylene units act as disturbances in the EP-RACO chains and thus impede the crystal growth[47-48]. In addition, random isotactic copolymers of isotactic propylene and 1-butene achieve a transparency of 90 % together with a crystallinity of 30−50 % after quenching followed by aging at ambient temperature. This high transparency is explained by the absence of spherulites and/or the changes of crystal structure and morphology from non-isometric monoclinic lamellae to isometric mesomorphic nodules, with a structure optically less heterogeneous than a spherulitic structure, leading to less light scattering and hence increased light transmission[49].

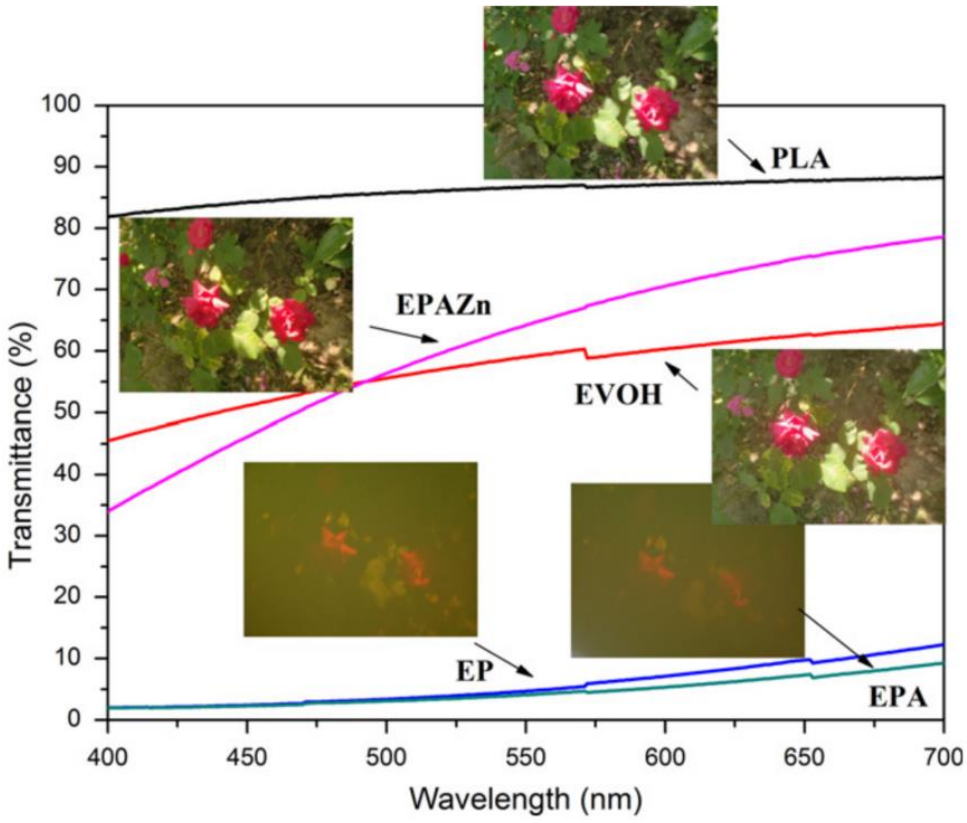

Figure 2.3 *Transmittance and optical appearance of PLA, EVOH, their incompatible blends (EP and EPA) and compatibilized blends (EPAZn)*[50].

Blends of some semi-crystalline polymers can also achieve good clarity by decreasing the domain size of the dispersed phase to below that of the visible-light wavelength. For this purpose, semi-crystalline polymer blends are supposed to have excellent compatibility and the presence of another polymer phase promotes heterogeneous nucleation, leading to a fine morphology. Reactive compatibilization with suitable catalysts is helpful to make originally opaque incompatible polymer blends transparent by stabilizing the dispersed phases to smaller dimensions and lowering interfacial stresses. For instance, the light transmittance of poly(L-lactic acid)/ethylene vinyl alcohol (PLA/EVOH) blends was improved from 9.3 % to 83.5 % after reactive compatibilization with zinc stearate ($ZnSt_2$) as a catalyst (see ***Figure 2.3***). The introduction of EVOH with excellent water vapour barrier properties broadens the application of transparent PLA/EVOH especially in the packaging field[50].

2.3.1.3 Matching refractive indices

Blending of two semi-crystalline polymers of similar refractive index contributes to transparent polymer blends. Some compatibilized blends like PET and polybutylene terephthalate (PBT)[51], PET and polymethaxylylene adipamide (MXD6)[52-53], PET and N-methyl-2,4-dimethyl glutarimide (PMAI)[51] as well as some blends of certain types of polyamides[54] showed good transparency. Among them, PET/PBT blends maintained excellent transparency regardless of the blending ratio because PET and PBT are well miscible. However, decreasing transmittance and increasing haziness were observed in PET/MXD6 blend films when these films were uniaxially or biaxially stretched (***Figure 2.4***) because of induced differences in the anisotropic refractive indices of the two semi-crystalline polymers during stretching.

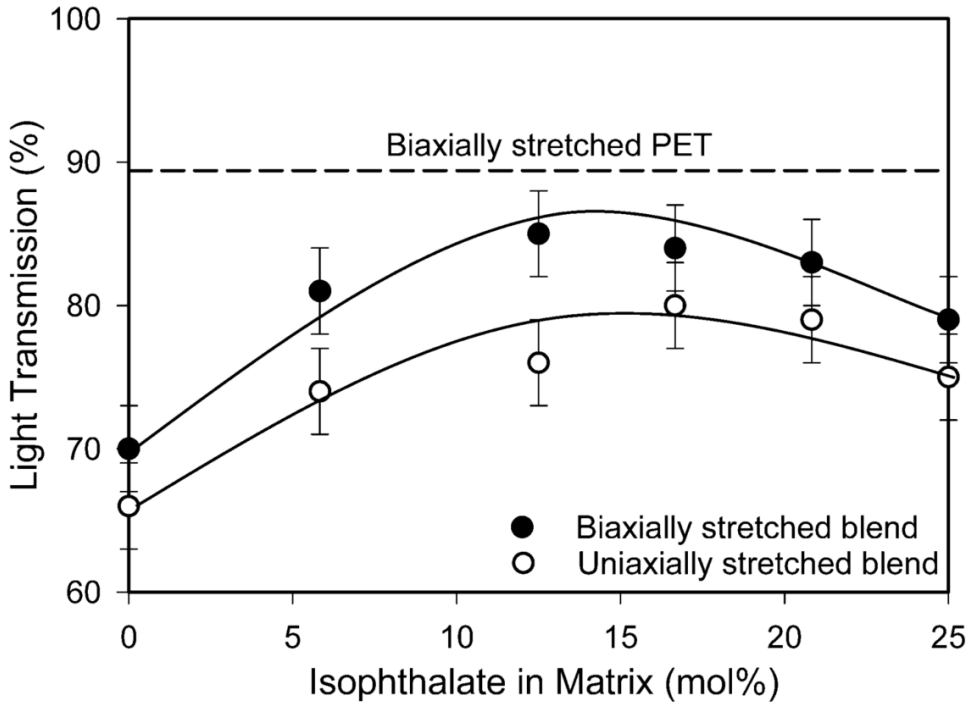

Figure 2.4 *Transmittance of uniaxially and biaxially stretched PET/MXD6 blends with 10 wt.% MXD6 as a function of isophthalate content for modifying PET matrix and PET/MXD6 blend has a transparency of 90 % before stretching*[52].

2.3.2 Biaxially stretched transparent semi-crystalline polymers

Biaxial orientation can improve physical properties in two perpendicular directions (machine direction, MD and transverse direction, TD) and enhance the commercial values of polymer films. Some biaxially oriented semi-crystalline polymer films stretched in the melt state or the solid state are optically transparent due to the reduced crystal sizes induced during the biaxial stretching process. Transparent biaxially oriented polypropylene (BOPP), biaxially oriented polyethylene terephthalate (BOPET), biaxially oriented polyethylene (BOPE) and biaxially oriented polyamide (BOPA) films are representative materials widely used in the packaging industry due to their high clarity, good thermal and chemical stability, good barrier properties as well as low cost.

The approaches to producing transparent biaxially oriented polymer films consist of sequential biaxial stretching in the solid state[55-56], where the films are first uniaxially drawn in MD and then in TD, or through simultaneous biaxial stretching[57-58], where films are drawn simultaneously in both MD and TD, etc. Through biaxial stretching, semi-crystalline polymers can be biaxially oriented to improve thermomechanical stability and mechanical performance by introducing biaxial in-plane molecular orientation as a result of the redistribution of *c*-axis chain orientation[59]. For instance, when biaxial stretching was carried out to reach a draw ratio of 6 in both MD and TD, transparent BOPP films with a high light transmittance (~ 93 %) possessed a modulus of ~ 3.6 GPa and a strength of ~ 230 MPa along both MD and TD[58, 60], compared to the moduli of ~ 0.5 GPa and the strengths of ~ 40 MPa for isotropic PP cast films[61].

Commercial biaxially oriented polymer films are generally manufactured by blown-film, tenter-frame or double-bubble process. In the blown-film process, the semi-crystalline polymer is stretched in the melt state followed by quenching to immobilize chain orientation. As for tenter-frame and double-bubble processes, the semi-crystalline polymer is primarily drawn in the solid state close to but below the melting temperature[62].

With regard to semi-crystalline PET (CPET), thermally induced crystallization, consisting of melt-crystallization (crystallized by cooling from the melt) and cold-crystallization (crystallized during heating above T_g), generally results in large-sized crystals. Thus, thermal crystallized PET products are usually opaque. Strain or stress induced crystallization (SIC) by stretching PET at a temperature above T_g is often used to create transparent PET products like bottles or containers for food and beverages as a result of the formation of small-size crystals even at high degrees of crystallinity[63].

Figure 2.5 *(a) PET preform for stretch-blow moulding process, (b) heat-set PET bottle with standard transparent thread and (c) heat-set PET bottle with post-crystallized opaque thread acquired by annealing*[64].

PET bottles are typically manufactured by a stretch blow moulding process. Here, a tube-like PET preform previously made by injection moulding (see ***Figure 2.5(a)***) is heated and placed into a bottle-shaped mould. Next, a blow pin is inserted into the preform to blow the preform with pressurized air. This blowing process contributes to a biaxial orientation of the molecular chains inside the bottle wall. After stretch blow moulding, the product is quickly cooled to below T_g, which freezes in the molecular orientation, leading to increased strength and toughness. Stretching plus fast cooling facilitates the formation of small-size crystallites, and therefore effectively decreases the light scattering inside the bulk polymer. Thus, the small crystal dimensions resulting from the quenching contribute to the transparent appearance of the sidewalls (***Figure 2.5(b)***). However, often

the post-crystallized and annealed thread (where the cap is applied) still appears opaque (***Figure 2.5(c)***). This is because spherulites here have enough time to grow during annealing and recrystallization, and large spherulites are formed which will significantly scatter light and thus reduce the light transmission.

Apart from the above commercial transparent biaxially oriented polymer products, biaxially oriented poly(L-lactic acid) (BOPLA) films have a good transparency even at a high degree of crystallinity, where oriented crystallization dramatically increases the nucleation density and hence prevents the formation of large crystals[65-66]. Due to their bio-based character, recyclability and under certain conditions compostability, transparent BOPLA films have become attractive for a wide range of packaging applications.

Biaxially oriented polyethylene naphthalate (BOPEN) films have better oxygen barrier properties as well as superior resistance to sunlight and UV exposure compared to BOPET and they are transparent in the visible light range with a transmittance value of around 87 %[67]. However, it was found that when these BOPEN films were biaxially stretched above a certain draw ratio, drawing temperature and/or drawing speed, their appearance becomes milky or opaque. At this specific condition, the drawing temperature is more or less identical to the cold crystallization temperature, which accelerates the crystallization process during stretching and forms large crystals that scatter light[68]. Besides, BOPEN is usually regarded as a specialty film and preferred in high-end applications like displays and electronics due to a higher price as well as larger profit margins in contrast to commodity plastics like PET.

In terms of biaxially oriented polyethylene (BOPE), transparent LDPE, LLDPE, VLDPE and bimodal PE films can be produced by cast film extrusion or film blowing mainly due

to reduced crystal size, processing conditions and film thickness[8, 61]. However, mechanical properties of these films are rarely noteworthy because of the weak inter-molecular forces (van der Waals forces) and the low T_g of PE, leading to a low modulus and tensile strength but good ductility. This limits their applications mainly to packaging. The Young's modulus and tensile strength of cast or blown films based on these polyethylenes are only 100−200 MPa and 20−40 MPa, respectively[61].

High-density polyethylene (HDPE), possessing a density above 0.941 g/cm^3, shows hardly any branching. The chemical structure of these linear polymers, their molecular weight and molecular weight distribution is controlled by selecting proper reaction conditions, catalysts and co-catalysts, reactor design and in some cases additives. Thus, HDPE has a higher crystallinity and tensile strength but worse transparency in comparison to LDPE, LLDPE, VLDPE and bimodal PE. Extrusion film casting or film blowing of HDPE can lead to transparent products, whilst such materials are often stretched in the melt, meaning that chain entropy and chain relaxation prevents effective chain orientation and chain extension[69-70]. As a result, mechanical properties of such transparent cast or blown HDPE films are typically low, with elastic moduli of 0.6−3 GPa and tensile strengths of 30−230 MPa[9-10]. Again, the limiting mechanical properties of such extrusion cast or blown polyethylene products restricts their applications mainly to packaging.

In 2017, Dow Chemical Company introduced novel transparent tenter-frame biaxially oriented polyethylene (TF-BOPE) films[71-72]. These TF-BOPE films with thicknesses of 25−40 μm revealed a transmittance of ~ 90 % and have an excellent optical clarity even after stacking 30 layers. These TF-BOPE films also exhibit better mechanical performance, such as a twice as high stiffness and dart impact resistance in comparison

to conventional blown PE films. They have been used as the interlayer in liquid detergent bags instead of traditional packaging materials including BOPP, BOPET and BOPA. In addition, these printable TF-BOPE films with good colour registration can be incorporated with other kinds of PE films to establish fully recyclable and sustainable all-PE laminates for further packaging applications.

2.3.3 Monoaxially stretched transparent semi-crystalline polymers

Uniaxial solid-state drawing or cold-drawing of semi-crystalline polymers is a simple and low-cost approach to induce high levels of molecular orientation so as to achieve high modulus and tensile strength of polymeric materials along the drawing direction, notably polyolefins[11]. Solid-state drawing is a post-processing method at a drawing temperature below the melting temperature (which will be further discussed in Section 2.4). Drawing in the solid-state is far more effective than melt stretching in improving mechanical properties of polymers because chain relaxation phenomena are limited and hence a high degree of chain orientation and chain extension can be generated[17, 73].

However, often microvoids are formed during the solid-state stretching process, especially at high draw ratios. Two types of microvoids can be observed: microvoids parallel and perpendicular to the drawing direction. Both types of microvoids scatter light and result in non-transparent products. Moreover, uniaxially and solid-state drawn polymers often have a surface texture which influences the overall transmission and the gloss of the samples since light scattering due to the surface roughness is a main cause of transparency loss, especially in the far field[74]. The effect of surface roughness on overall transmittance can be reduced or eliminated by applying suitable surface coatings[75].

On the whole, transparent uniaxially stretched semi-crystalline polymer products can be fabricated by preventing the formation of such voids and defects during the uniaxially stretching process or alternatively by eliminating the refractive index mismatch between the polymer and the voids.

2.3.3.1 Matching the refractive indices between polymer and voids

Light scattering originating from voiding induced by uniaxial drawing can be reduced by matching the refractive indices between the polymer and the voids such as incorporating specific additives or soaking in certain solvents or liquids to fill the voids.

Solid-state drawn HDPE fibres or films are normally not transparent. In these materials, the dimensions of the crystals being typically larger than the wavelength of visible light together with the high degree of crystallinity partially account for the poor transparency[12]. In addition, the introduction of internal microvoids together with the highly fibrillary structures on the surface and in the bulk of the films after ultra-drawing will induce light scattering, resulting in a poor transparency in the visible light regime[13, 17].

Recently, Shen *et al.* studied the relationship between visible-light transparency and weight-average molecular weight ($\overline{M_w}$) as well as molecular weight distribution (MWD = $\frac{\overline{M_w}}{\overline{M_n}}$) in drawn HDPE films. It was found that solid-state drawn HDPE films with $\overline{M_w}$ < 140 kg/mol or MWD < 10 were opaque due to the presence of microvoids parallel to the drawing direction at a draw ratio of 10 to 25. At higher draw ratios (≥ 25), other defects such as perpendicular microvoids and longitudinal separation of fibrils were also observed and resulted in a further decrease in transmittance. The light transmittance of these films could be enhanced by introducing a small (≤ 2 %) quantity of specific

additives like 2-(2H-benzotriazol-2-yl)-4,6-ditertpentylphenol (BZT)[75-76]. The solid-state drawn HDPE films with a draw ratio of 20 showed a 90 % light transmittance with a surface coating to lower surface scattering and a tensile strength of 650 MPa, as shown in ***Figure 2.6(a)***. As this additive has a similar refractive index as HDPE, it could eliminate light scattering by filling voids or defect structures induced in the films, hence lowering the refractive index mismatch between polymer and voids, and thus leading to improved transparency of these oriented films.

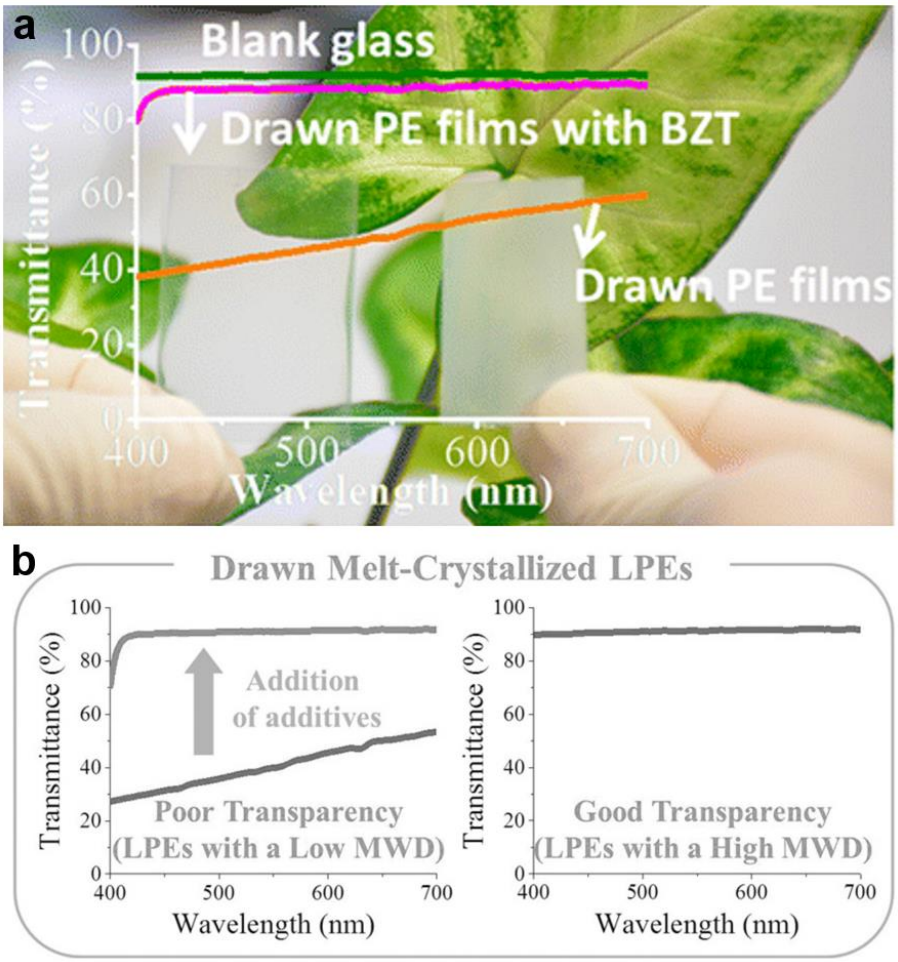

Figure 2.6 *(a) Transmittance and appearance of glass, pure HDPE films and HDPE films with BZT additives[75] and (b) transmittance of drawn melt-crystallized linear polyethylene (LPE) films with different MWDs with and without additives[77].*

At a broad MWD (> 20), the drawn HDPE films revealed a high transparency (~ 90 %) even without incorporating any additives at low draw ratios (~ 10) as shown in ***Figure 2.6(b)***[77]. This is because here the low molecular-weight fraction could function as an additive with a relatively high refractive index that fills the voids.

Figure 2.7 *Appearance of UHMWPE/graphene (left) and UHMWPE/graphene/BZT (right) nanocomposite films*[78].

In terms of ultra-high molecular weight polyethylene (UHMWPE, $\overline{M_w}$ > 1000 kg/mol), Shen *et al.* also found that incorporating a low molecular weight linear polyethylene called POLYWAX™ 1000 ($\overline{M_w}$ ~ 1 kg/mol) was able to dramatically enhance the transparency of UHMWPE films after ultra-drawing[79-80]. Herein, POLYWAX™ 1000 behaved as a solvent, which facilitates chain mobility, processibility, maximum achievable draw ratio and therefore mechanical properties of UHMWPE/POLYWAX™ 1000 blends. A maximum Young's modulus (~ 40 GPa) and a maximum tensile strength (~ 1.5 GPa) could be obtained by incorporating 60 wt.% of POLYWAX™ 1000 in the blends followed by solid-state drawing. Moreover, Pan *et al.* produced clear, ultra-drawn UHMWPE/graphene/BZT nanocomposite films with draw ratios of 30 and 70 by solution casting and solid-state drawing[78]. The above-mentioned BZT was also added in the films

as a second additive in order to fill drawing induced microvoids as well as facilitate the dispersion of graphene, resulting in a high transparency of ~ 90 % (see ***Figure 2.7***). More importantly, these UHMWPE/graphene/BZT nanocomposite films achieved a high thermal conductivity of ~ 75 $W \cdot m^{-1} \cdot K^{-1} \cdot \rho^{-1}$, which is higher than most polymer nanocomposites and some metals.

The clarity after stress-whitening of HDPE due to internal voiding can be improved by saturating pre-stretched samples with diesel after stretching as shown in ***Figure 2.8(a)-(d)***[81]. Here, diesel fuel possessing a close refractive index (n = 1.46−1.52) to HDPE (n = 1.54) worked as an immersion liquid to permeate existing voids. But this method needed much longer immersion time (~ 5 months) to allow diesel entirely fill the existing voids, while the mechanical performance of these diesel-saturated samples was poor.

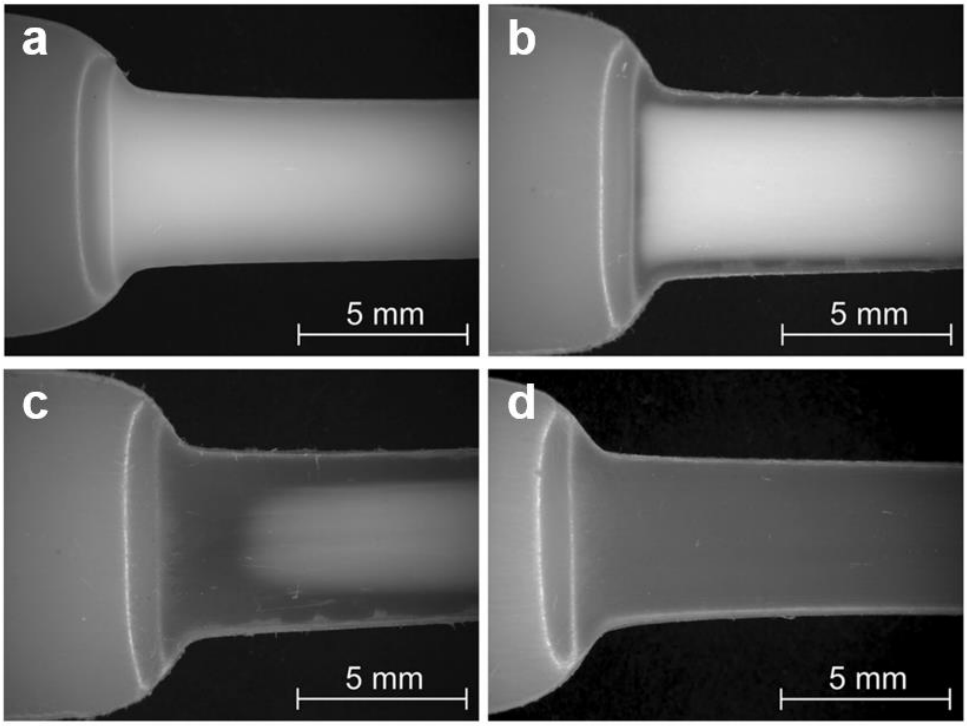

Figure 2.8 *Appearance of stretched HDPE samples (a) without immersion and immersed in diesel after drawing at 60 °C after (b) 1 week, (c) 1 month and (d) 5 months*[81].

It was also reported that drawn PP tapes and fabrics could become more transparent after absorbing a small volume of oil as shown in ***Figure 2.9***[82]. When the tapes absorbed oil, the micro-cavities within the highly drawn PP tapes would be filled with oil. This process resulted in the matching of refractive indices between PP and the oil filled microvoids, leading to a reduction in the amount of light scattering induced by these voids and hence a change in appearance from opaque to semi-transparent.

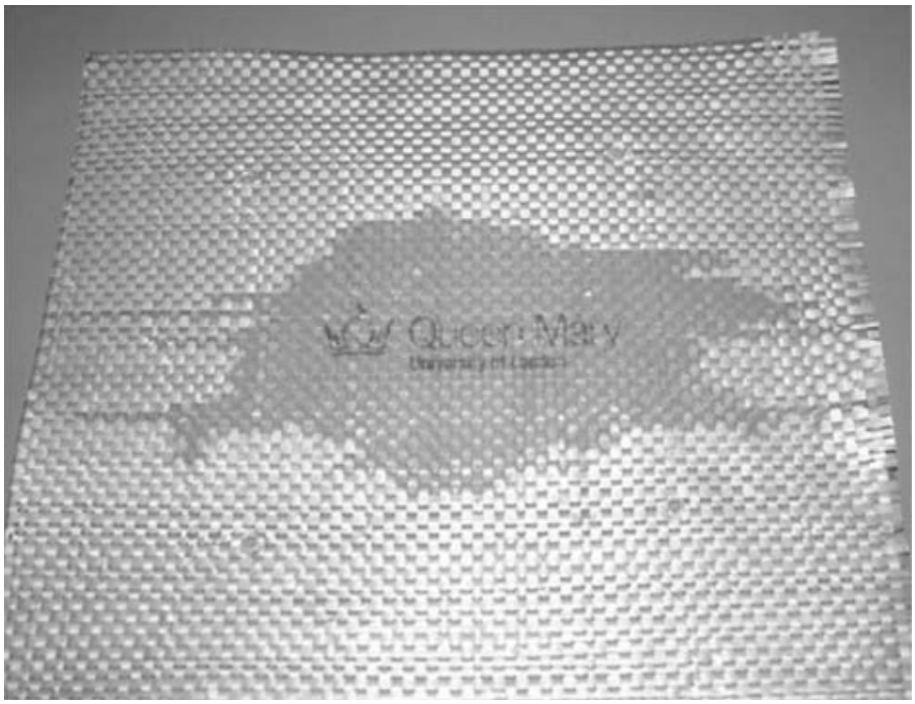

Figure 2.9 *Oil absorption by woven all-PP tapes[82]. The originally opaque tapes become semi-transparent when in contact with a small amount of oil in the centre of the fabric.*

This approach of filling micro- and nanovoids with refractive index matching liquids or resins to create optically transparent composites has also been reported for various cellulose and nanocellulose based composites. Nishino *et al.* created transparent all-cellulose composites by partial dissolution of ligno-cellulose fibres, with the dissolved fibre material filling the spaces between the fibres, creating strong and transparent composites[83-84]. Research by Yano *et al.*[85], Gea *et al.*[86] and others[87-88] reported transparent

nanocomposite films based on bacterial cellulose and other forms of nanocellulose. Here, nanocellulose fibrous networks are typically impregnated with resins to introduce transparency. More recently, Berglund and co-workers created optically transparent wood with transmittance values as high as 85 %, using delignified nanoporous wood. By removing the light-absorbing lignin component, a nanoporous template remained, which after impregnating with refractive-index-matching methyl methacrylate (MMA) resulted in transparent wood/PMMA composites with interesting mechanical properties[89].

2.3.3.2 Preventing the formation of voids

Semi-crystalline polymers can be deformed uniaxially without forming voids by stretching at high temperatures close to their melting temperature. Under these circumstances, plastic deformation is more likely to happen due to the improved mobility of the polymer chain, so no or less cavitation is observed[90].

Porter and his colleagues used a capillary-flowing process using an Instron rheometer with capillaries or a slit die near PE's melting point (130−136 °C) and under a high pressure (~ 200 MPa) to produce transparent and oriented HDPE filaments or films[91-93]. Moreover, they proposed a solid-state co-extrusion technique which could continuously produce transparent ultra-drawn HDPE films with a maximum extrusion draw ratio of 36 and a maximum tensile modulus of 30 GPa under a lower temperature (110−120 °C) and pressure[94]. However, the extrusion speeds of these two methods were fairly low (5 and 16 cm/min, respectively).

For HDPE with a medium $\overline{M_w}$ (~ 408 kg/mol), it was reported that the high density of tie molecules and/or entanglements inside the oriented HDPE films (λ ~ 15) prevents the

formation of interfibrillar voids during deformation and led to a light transmittance of around 90 %[95].

The transparency of drawn HDPE could also be achieved when soaking HDPE in diesel, biodiesel or chloroform before drawing at room temperature (RT)[81, 96-98]. The introduction of diesel or biodiesel could reduce the formation of cavities and voids by increasing the mobility of polymer chains in the amorphous phase, where diesel or biodiesel is regarded as a plasticizer to make HDPE transparent as shown in ***Figure 2.10(a)***. The fuel-induced plasticization also softened polymers and increased its ductility. With increasing concentration of absorbed diesel or biodiesel fuel, Charpy impact strength improved but Young's moduli decreased (< 1 GPa). However, the utilization of diesel or biodiesel may cause severe environmental pollution. Rozanski *et al.* also reported that saturating PP in chloroform or hexane prior to stretching could make PP transparent with similar mechanism[99].

It was also reported that transparent oriented PP copolymer rods with high stiffness (~ 20 GPa) could be achieved by die-drawing at a temperature below the melting temperature[100-101]. At low draw ratios (≤ 17), the samples were transparent with a smooth surface in the post-die deformation area as shown in ***Figure 2.10(b)***. This increase in transparency at low draw ratios was associated with compression stresses perpendicular to the die wall when the polymer is in contact with the wall at the early stages of deformation, suppressing voiding. However, at a high draw ratio of 20, the sample was white and opaque as a result of internal voiding and surface fibrillation upon bending.

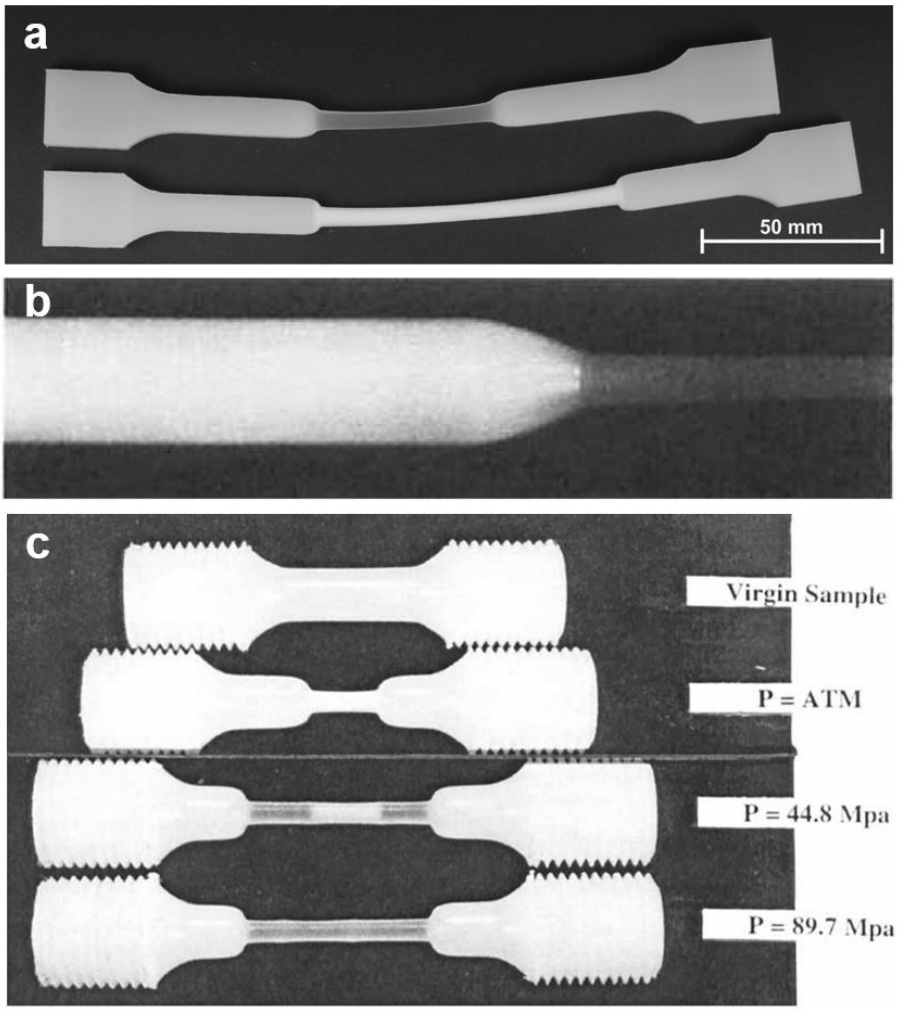

Figure 2.10 *Appearance of (a) drawn HDPE samples with (top) and without (bottom) saturation in diesel prior to drawing*[81]*, (b) drawn PP sample with a draw ratio of 7 by die-drawing*[101] *and (c) HDPE samples without drawing, with drawing and healing at atmospheric pressure and a pressure of around 45 MPa and 90 MPa before redrawing, respectively*[102].

Healing the stress-whitening effects of HDPE or PP at a certain hydrostatic pressure at RT in between drawing processes could also reduce the size of existing voids and improve transparency (see ***Figure 2.10(c)***). Here, HDPE or PP samples were first drawn at atmospheric pressure with stress-whitening, healed at a pressure of around 90 MPa and then redrawn at atmospheric pressure to reduce the size of the voids[102].

Polyvinylidene fluoride (PVDF) is generally opaque as a result of large crystals and a high crystallinity (35−70 %). It was discovered that the transparency of PVDF was significantly improved when quenched in ice-water followed by cold-drawing at 25 °C because the formation of voids is prevented under this condition (see ***Figure 2.11***)[90].

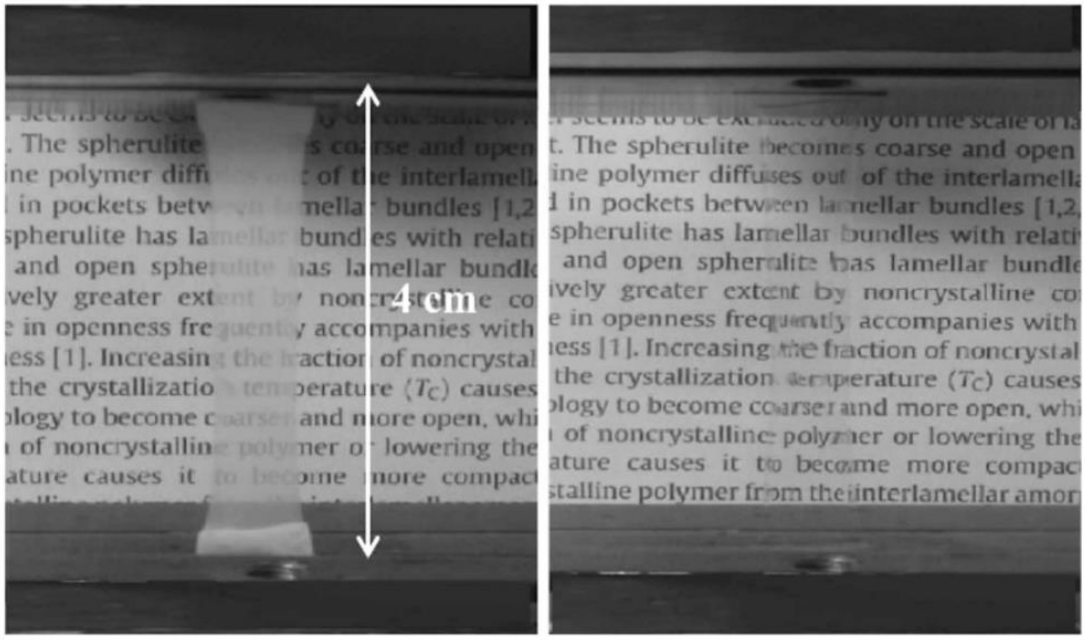

Figure 2.11 *Optical appearance of PVDF films crystallized at 30 °C (left) and in ice water (right) followed by cold-drawing to* $\lambda = 3$[90].

2.3.3.3 Whitening after overdrawing

Overdrawing is typically defined as a certain draw ratio after which the optical appearance of a fibre or tape is changed from transparent to opaque[103]. Due to the formation of microvoids, whitening occurs after overdrawing. Usually, overdrawing is accompanied with the changes of mechanical properties as well as surface and internal morphology of the specimen.

Transparent uniaxially stretched iPP films with good mechanical performance can be obtained after a solid-state drawing process. Schimanski *et al.* found that transparent iPP films or tapes could be produced by melt-extrusion in combination with solid-state post-drawing at a temperature of 145 °C in an oven[103-104]. With post-draw ratios below or equal to 10, the corresponding iPP tapes were transparent; however, the appearance of these tapes changed from transparent to opaque at $\lambda \geq 11$ (***Figure 2.12(a)***), which was explained by overdrawing and micro-voiding. As for mechanical properties, Young's modulus and tensile strength of these iPP tapes continuously increased with draw ratio (see ***Figure 2.12(b)-(c)***). However, the draw ratio of 10 represented a demarcation point where appearance changed from transparent to opaque, with the tape having a modulus of ~ 10.5 GPa and a strength of ~ 400 MPa.

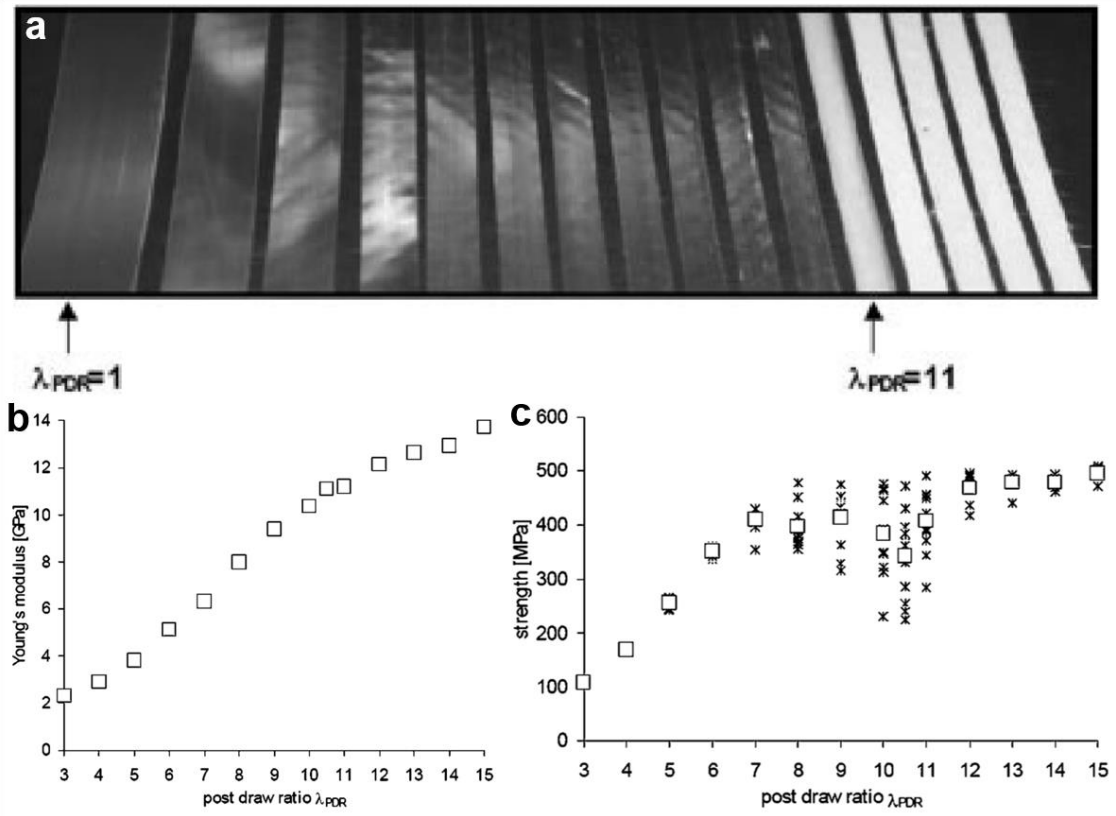

Figure 2.12 *(a) Optical appearance, (b) Young's modulus and (c) tensile strength of the post-drawn iPP tapes with different draw ratios after solid-state post-drawing*[103].

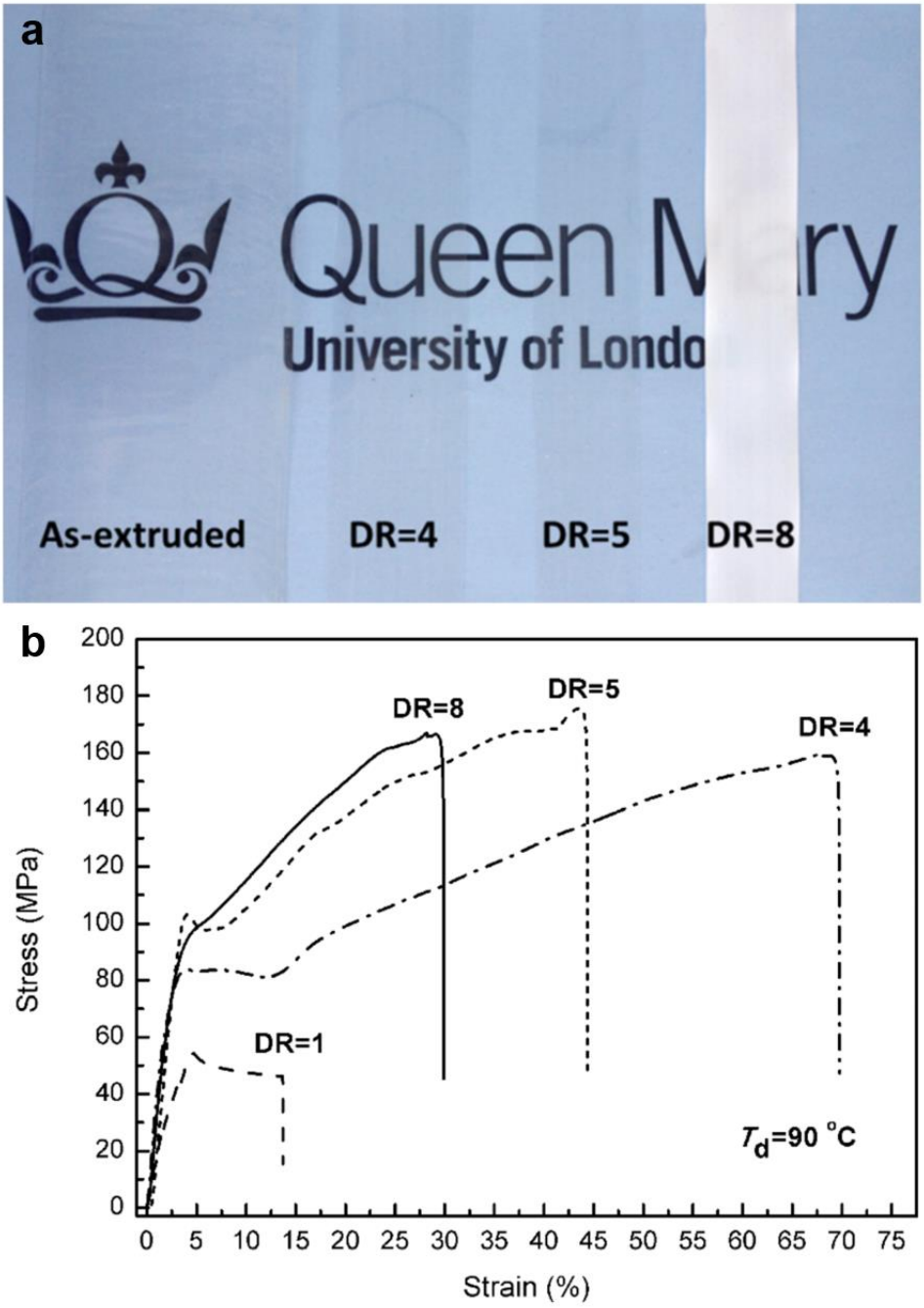

Figure 2.13 *(a) Optical appearance and (b) stress-strain curve of PLA tapes with different draw ratios drawn at 90 °C*[105].

Also, PLA tapes had a transparent appearance after uniaxial solid-state drawing at a drawing temperature of 90 °C to a certain draw ratio[105-106], but also here obvious whitening happened at higher draw ratios (***Figure 2.13(a)***). Here the mechanical

behaviours of PLA tapes with $\lambda = 8$ were similar to those for transparent tapes of $\lambda = 5$, with the Young's moduli of ~ 4.0 GPa and ultimate strengths of ~ 170 MPa in ***Figure 2.13(b)***, which again resulted from the development of micro-voiding during overdrawing.

An important implication of orientating polymer chains as mentioned above is the introduction of birefringence. Birefringence is an optical phenomenon where polymer samples exhibit different refractive indices for light with plane polarization in two vertical directions[62]. Birefringence effects happen in crystalline phases in polymers or unordered phases by applying an orientation field, like biaxial or uniaxial orientation. Under specific illumination conditions like low incoming angle of direct sunlight, birefringence will lead to undesired optical effects such as colours originating from polarization and wavelength dispersion effects[107].

All above mentioned semi-crystalline polymers appeared transparent mostly in the near field at relatively low solid-state draw ratios, whereas whitening happened at higher draw ratios as a result of overdrawing and micro-voiding, leading to a change in appearance from transparent to opaque. Because of the lower maximum transparent draw ratio of PP ($\lambda \sim 10$) and PLA ($\lambda \sim 5$) in combination with the much lower theoretical crystal modulus of PP and PLA compared to PE, these transparent PP or PLA films possessed significantly lower mechanical properties than transparent HDPE or UHMWPE films[78].

Table 2.1 summarizes common approaches for producing transparent films categorized by the type of semi-crystalline polymer.

Table 2.1 *Summary of methodologies for creating transparent semi-crystalline polymer products.*

Materials	Methods
PE	• Casting or blowing LDPE, LLDPE, VLDPE, bimodal PE and HDPE[8, 61, 69-70] • Incorporating certain co-monomers for copolymerization[47-48] • Adding specific additives prior to solid-state drawing of HDPE[75-76] • Use of medium $\overline{M_w}$ or high MWD HDPE at low draw ratios[77, 95] • Adding low molecular weight linear polyethylene to UHMWPE[79] • Soaking HDPE with diesel, biodiesel or chloroform before drawing[81, 96-99] or after drawing for a prolonged time[81]
PP	• Amorphous atactic PP (aPP) • Adding clarifying agents[6, 37-43] • Incorporating certain co-monomers for copolymerization[47-49] • Saturating PP in chloroform or hexane prior to drawing[99] • Absorbing small amounts of oil[82] • Die drawing for oriented PP copolymer rods[100-101] • Solid-state drawing at relatively low draw ratios[103-104]
PET	• Rapid cooling of PET melt to create amorphous PET (APET)[64] • Adding clarifying agents[44-45] • Stretching PET at a temperature above T_g for strain or stress induced crystallization (SIC)[63]
PA	• Amorphous homo- or co-PA polymerized by asymmetric (co-)monomers possessing side chains or ring structures[35] • PA with microcrystalline structures by adjusting crystallization rate[46]
PLA	• Solid-state drawing at relatively low draw ratios[105-106]
Cellulose	• All-cellulose composites[83-84] • Impregnated with resin[85-86, 89]

PVDF	• Quenched in ice-water followed by cold-drawing[90]
Biaxially oriented	• BOPP, BOPET, BOPE, BOPA, BOPLA, BOPEN, etc.
Blends	• Improving compatibility of blends by reactive compatibilization[50] • Matching refractive indices of two semi-crystalline polymers[51-54]

2.4 Solid-state drawing

Mechanical properties of polymeric materials predominantly depend on (i) internal structure, consisting of chemical structure, configuration and conformation of molecular chains, which is primarily dependent on the polymer chain itself; and (ii) morphology and molecular packing, including orientation and chain extension of molecular chains, and crystallization morphology, mainly determined by processing conditions[108].

Solid-state drawing, as previously mentioned in Section 2.3.3, is a post-processing method carried out at a drawing temperature close to but below the melting temperature (T_m) and above the glass transition temperature (T_g) or α-relaxation temperature of a polymer[11]. During the solid-state drawing process, chain relaxation phenomena are limited and hence a high degree of molecular orientation and chain extension can be generated in the drawing direction[17]. More importantly, since molecular mobility is negligible in the solid state, molecular orientations are locked into the final product, leading to large-scale effective morphological reorganisations[109]. Thus, drawing in the solid-state can significantly improve mechanical properties including Young's modulus and tensile strength of polymers, especially polyolefins. For instance, the Young's modulus and tensile strength of ultra-drawn HDPE fibres can reach values as high as 70 GPa and 1.5 GPa, respectively[110-112]. In the case of UHMWPE, solid-state drawing is

widely used in combination with solution-processing or solvent-free techniques[113-115]. Here, Young's moduli and tensile strengths have been reported of 100−180 GPa and 2−5 GPa, respectively.

Based on Peterlin's molecular deformation model[116-117], the morphology of semi-crystalline polymers will transform from isotropic spherulites into newly formed anisotropic micro-fibrils during the solid-state drawing process. This deformation can generally be divided into three stages[118-119] as shown in ***Figure 2.14***: (1) elastic and plastic deformation of the spherulites at low draw ratios; (2) nearly discontinuous transformation from a spherulitic structure to a fibrillar structure (typically at draw ratios above 5 in polyolefins); (3) plastic deformation of fibrillar structure usually above a draw ratio of 15. These three stages of molecular deformation are sometimes intermixed during the necking process and the boundaries between each stage are not always clear.

The initial material has low strength and high ductility. At the initial stage of stretching, chain slipping and tilting happens. Typically, stage (1) corresponds to low draw ratios (< 2) from isotropic to the initial yield point.

During stage (2), the molecular chains in the crystalline phases are oriented along the drawing direction and this stage usually gives rise to necking. The formation of necking leads to the inhomogeneous deformation and a non-uniform distribution of stress and strain in the sample. The necking behaviour is affected by processing conditions such as initial morphology and molecular weight[119-120]. In the necking region, the morphology shows reformed small aligned lamellar blocks connected by stretched non-crystalline tie molecules or crystalline bridges[116]. The increased continuity of the loading lamellar blocks correspond to a high modulus and tensile strength after further solid-state drawing, together with only slightly increased molecular orientation and crystallinity at high draw

ratios. At this stage, the sample usually does not show a sharp load drop at the onset of plastic deformation but typically the load remains relatively constant.

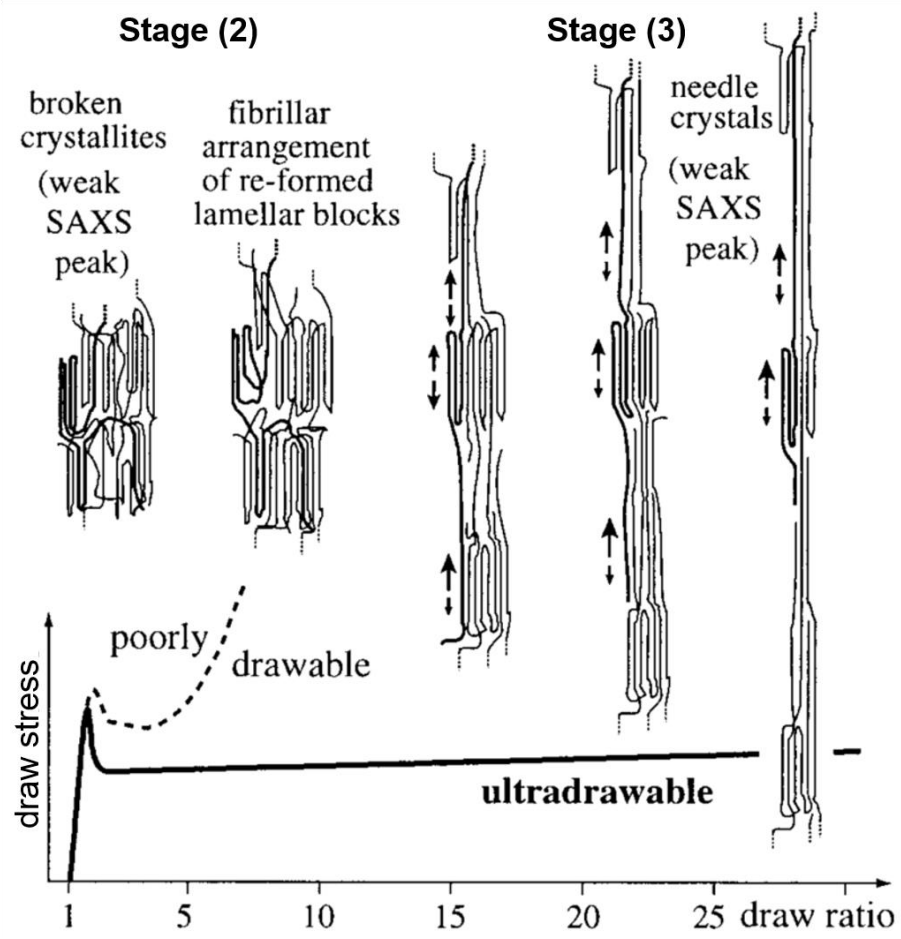

Figure 2.14 *Schematic diagram of the draw stress as a function of draw ratio and the local morphology change in three stages during solid-state drawing*[118].

Further drawing to stage (3) can be regarded as ultra-drawing ($\lambda > 15$). The representative ultra-drawable semi-crystalline polymers include PE, iPP, poly(tetrafluoroethylene) (PTFE), poly(oxymethylene) (POM) and poly(ethylene oxide) (PEO). In stage (3), the extent of chain folding gradually reduces and molecular chains become more extended and oriented with further stretching, forming the long needle-like crystals (protofibrils)[121]. The molecular chain extension and orientation during ultra-drawing contributes to high draw ratios and thus a significant enhancement in modulus and strength. The deformation

in this stage of the drawing is relatively homogeneous in a clearly defined geometrical manner because it consists of drawn material which has passed through the neck[119]. The achievement of stage (3) by solid-state drawing requires polymers possessing an α_c-relaxation and at a fairly low degree of entanglements[118]. α_c-relaxation takes place above a temperature where the motion of polymer chains inside the folded crystals will occur. For PE, the α_c-relaxation usually corresponds to a temperature around 80 °C[122]. When the molecular chains are highly extended at a high draw ratio, further stretching will only result in longitudinal sliding of the chains past each other. This process is limited by interfibrillar tie molecules and will lead to ductile failure. Therefore, polymers possessing a high molecular weight with many interlamellar links typically show a smaller maximum draw ratio than the ones of lower molecular weight[116]. In terms of melt-crystallized linear polyethylene, maximum draw ratio generally reduces with increasing weight-average molecular weight ($\overline{M_w}$) under optimized conditions regarding drawing temperature and thermal treatment[123].

At high drawing temperatures, the polymer is likely to recrystallize and molecular chains may slide over each other with less hindrance, leading to a specimen possessing a particular high draw ratio but with inferior properties compared to the one drawn at a lower temperature. Thus, high drawing temperatures may lead to viscous flow, a higher degree of recrystallization and a lower tensile modulus[119]. Besides, lower drawing temperatures generally reveal a higher degree of strain hardening phenomenon during stretching. More strain hardening results in more effective drawing in terms of improving the chain orientation and properties of the drawn product[120].

Figure 2.15 shows typical solid-state deformation processes. Batch-wise tensile drawing is typically carried out by hand or using a tensile tester[124-125] (***Figure 2.15(a)***) and can

only be used to make samples with limited dimensions. The draw ratio attained in the necking area is effectively controlled by the polymer, which is the so-called "natural draw ratio"[109]. Continuous drawing of melt-spun filaments[126] (***Figure 2.15(b)***) has also restrictions in the initial fibre diameter (< 2 mm). Hydrostatic extrusion of polymers in the solid phase through a conical die[127-129] (***Figure 2.15(c)***) can, however, lead to slightly larger products with diameters of 1 to 25 mm, but this is still a batch-wise process and needs to be carried out under high pressure with high levels of flow stress, resulting in a limited maximum attainable draw ratio (~ 7 under hydrostatic extrusion conditions in contrast to a draw ratio of ~ 20 for uniaxial tensile drawing in the case of PP). Applying a tensile haul-off force to the extrudate (as F_1 in ***Figure 2.15(c)***) can enhance extrusion production rates, while at higher extrusion ratios, this effect will be small as the haul-off stress is lower compared to the extrusion pressure.

Die drawing of originally isotropic polymers through a temperature-controlled converging die at temperatures below T_m[100-101] is previously mentioned in Section 2.3.3.2. As shown in ***Figure 2.15(d)***, isotropic polymer encounters the die at line A-A while deforming parts are no longer in contact with the die at line B-B, and an axial tensile force F is applied to a heated solid-state polymer billet. The die drawing process can operate in a continuous, stable and controllable manner with a high production rate especially at high draw ratios to achieve large diameter rods. The controllability is affected by the die design and affects stress, strain and strain rate as well as temperature control to reach certain draw ratios and thus to attainable properties. The steady state of die drawing can be realised with the polymer possessing strong strain hardening behaviour, which allows for the stabilisation of neck formation over a wide range of drawing temperatures and speeds. A wide range of products consisting of engineered elevator cores, marine cables, construction products, pipes, bioresorbable shape memory products for bone and soft

tissue fixation, stents as well as some hollow products have been produced by die drawing[109, 130].

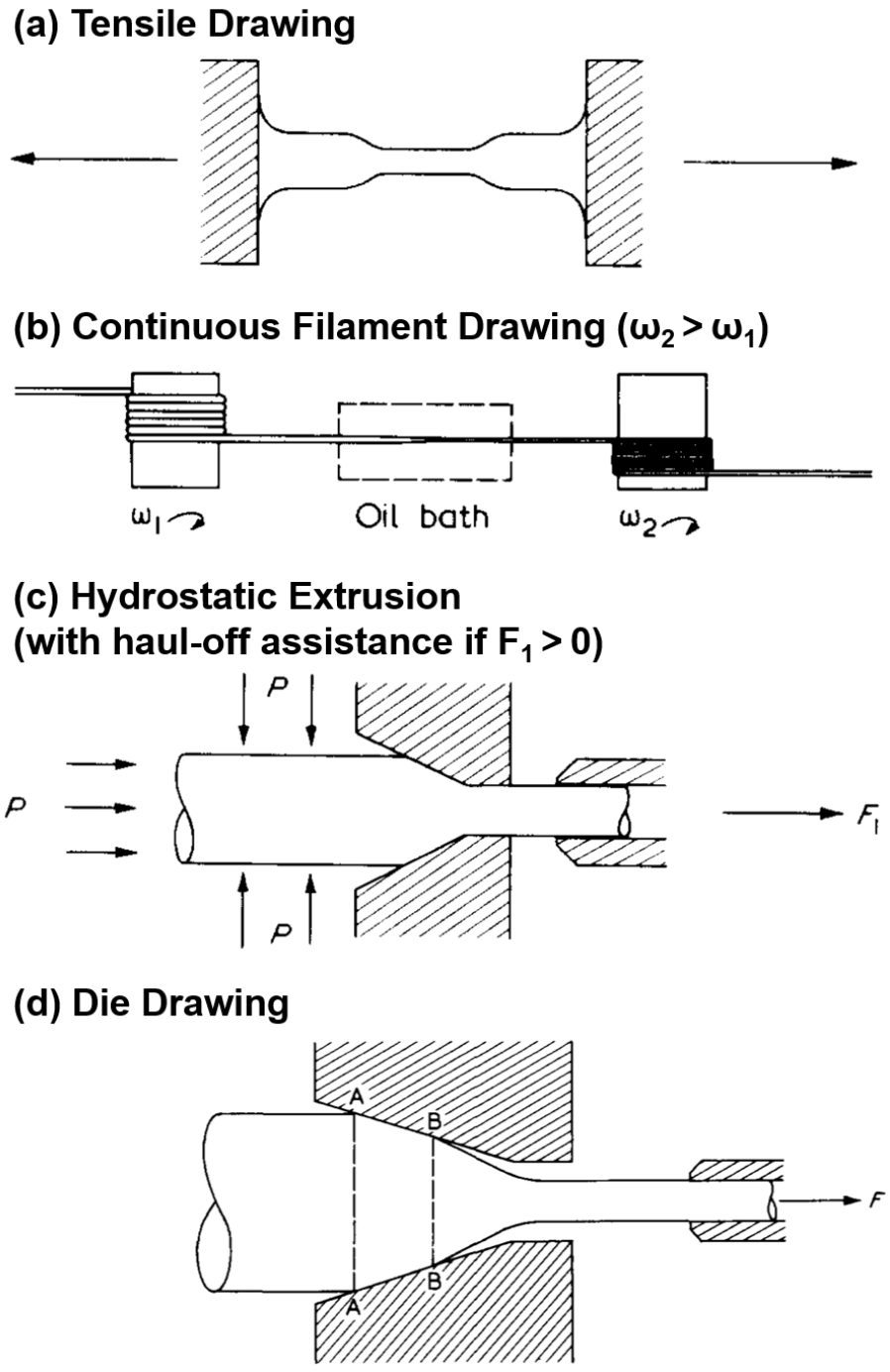

Figure 2.15 *Common solid-state deformation processes[100].*

2.5 Transparent composite laminates

Lamination can improve the strength of a panel or component, lowering the risk of catastrophic failure when a single layer breaks as others will work to prevent further crack propagation as well as enhance the post-failure behaviour of composite laminates[131]. Thus, when it comes to damage tolerance, multilayer composites are often considered to be more favourable over monolithic structures.

Laminated glass contains two or more glass panes bonded together with transparent plastic interlayers. These interlayers can adhesively bond the glass panes together under heat and pressure. Autoclaving is the most common lamination process for manufacturing laminated glass. In the case of PVB interlayers, a temperature of ~ 140 °C and a pressure of ~ 0.8 MPa assures good adhesion between the glass and the polymer interlayer[1]. In comparison to sheet glass, the fracture behaviour, impact resistance and failure mode are significantly improved in laminated glass.

The polymeric interlayers used in laminated glass can commonly be classified to three categories based on the thermo-mechanical properties controlled by molecular structures: (1) thermoplastics with linear or branched polymer chain structures, like polyvinyl butyral (PVB) and copolymer ethylene vinyl acetate (EVA); (2) elastomers with long cross-linked polymer chains, including thermoplastic polyurethane (TPU); (3) thermosets with highly cross-linked polymer chains, such as acrylic adhesive, polyester resin and epoxy[132-133]. In laminated glass, the existence of interlayers can bond glass fragments after fracture in combination with enhancing mechanical behaviours like fracture toughness, residual structural integrity and impact resistance[3, 134].

Laminated glass is considered as a type of safety glass due to its excellent post-failure behaviour, while it also possesses some other desirable properties like enhanced safety, security, fire resistance as well as sound diffusing and attenuation. It has been widely used in glazing, automobile, architectural, structural and defence fields.

Besides laminated glass, there are other composite laminates based on transparent inorganic glass and/or amorphous polymers as mentioned in Section 2.1 and 2.2 that simultaneously demonstrate a high transparency and good mechanical performance.

The two most common polymeric glasses PC and PMMA display fairly different mechanism by which energy is absorbed during impact. PC can absorb large amounts of energy through yielding like many other ductile materials. For more brittle PMMA, the creation of surface area (crazing) during failure is a main source of energy absorption[135], and its brittle failure behaviour allows dissipation of energy during impact into cracking. It was previously discovered that PC outperforms PMMA at low impact speeds, whilst the ballistic impact performance of PMMA is superior to PC[136-137]. Thus, the combination of PC and PMMA can integrate their merits in composite laminates. It is reported that transparent multilayer all-plastic laminates consisting of PC and PMMA sheets can be created by bonding them together using adhesives[138-139], welding with solvents (e.g. methylene chloride)[135] or using multilayer coextrusion techniques[140-141]. These laminates show good ballistic impact properties due to the introduction of PMMA with the feature of high strain-rate sensitivity as an intermediate layer. More importantly, these laminates maintain good visibility even after projectile impact tests, making them suitable for applications like transparent armour[137].

Some studies focused on glass-plastic laminates when sheet glass is also involved in these PC and/or PMMA laminates[142-143]. These glass-plastic laminates are lightweight and

show better post-failure behaviour and higher impact resistance in comparison to ordinary laminated glass. The impact performance of these laminates can be further improved when ion-exchange strengthened glass is used and a ballistic limit speed of 974 m/s can be reached while these laminates still possess over 83 % light transmittance[144-145].

Polyester resin composite laminates with the reinforcement of unidirectional (UD) and cross-ply (CP) E-glass fibre mats can reach a maximum light transmittance of ~ 85 % because of matching refractive indices between polyester resin and E-glass fibres[146-147]. However, the transmittance drops with increasing glass fibre content (***Figure 2.16(a)***). Glass ribbons could also be applied in transparent composite laminates as reinforcing parts instead of cylindrical glass fibres. Transparent soda-lime silicate glass ribbon/epoxy resin UD and cross-ply laminated panels with over 86 % light transmittance and below 4 % haze were successfully fabricated by Velez *et al.* as shown in ***Figure 2.16(b)***[148-149]. The features of lightweight and high resistance to stress and impact made these transparent laminates of interest for aircraft windows and windshields.

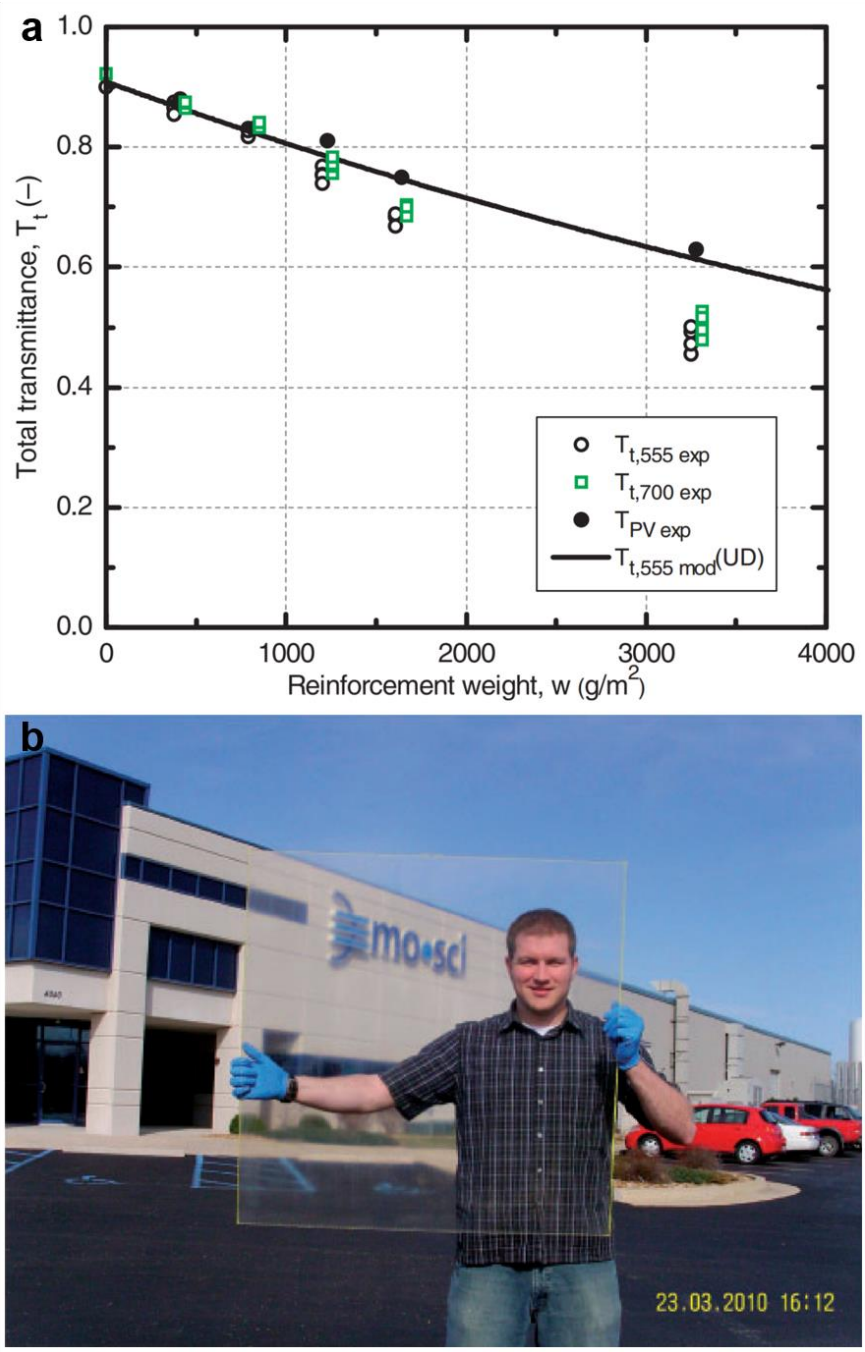

Figure 2.16 *(a) Experimental and analytical transmittance of UD glass fibre/polyester resin composite laminates at a wavelength of 555 nm and 700 nm*[146] *and (b) optical appearance of glass ribbon/epoxy resin cross-ply composite laminate*[148]*, showing excellent near field transparency but reduced far field transparency.*

2.6 High performance composites

High performance or advanced composites, generally refers to composites reinforced by high performance fibres and fabrics based on carbon fibres[14, 150-151], glass fibres[15], UHMWPE fibres[17, 152] and aramids[16]. They are increasingly used in aerospace, automotive, sports and other fields like renewable wind energy owing to their high specific modulus and strength.

Compared to carbon fibres and glass fibres, UHMWPE and aramid fibres exhibit higher strains at break, better flexibility in combination with high specific mechanical properties owing to the low density of these polymers ($\rho \approx 1-1.5$ g/cm^3). They possess not only high specific stiffness and tensile strength but also relatively high levels of toughness with the ability to absorb large amounts of energy upon tensile loading. These features make them outstanding reinforcing materials in energy absorbing composites.

Composites reinforced by highly oriented UHMWPE fibres exhibit high mechanical performance in tension and impact[153-154]. The extended chains with well-oriented tie molecules after ultra-drawing result in the high stiffness and strength and the highly oriented fibrous structure ensures that cracks will not propagate perpendicular to the drawing direction. There are two common reinforcing modes: woven fabrics and cross-plied UD tapes[152]. For woven fabrics, one sample is based on UHMWPE fabrics using LDPE films to stack them together layer by layer, which possesses the advantages of easy production and post-processing. With regard to cross-plied UD reinforcements, UHMWPE composites reinforced by cross-plied UD fibre laminates have been widely used in commercial ballistic products, like Spectra Shield® developed by Allied Signal (now Honeywell) and Dyneema® UD produced by DSM as shown in ***Figure 2.17***. These composites reinforced by UHMWPE fibres or textiles possess excellent mechanical

behaviours especially with respect to ballistic resistance since they can rapidly disperse energy to surrounding areas due to the fully aligned fibre structure, and can absorb a large amount of energy as a result of the high modulus as well as high elongation at break[17, 155] (***Figure 2.18***). The corresponding composite products have been widely applied in armour, vests, helmets and blankets[156-157].

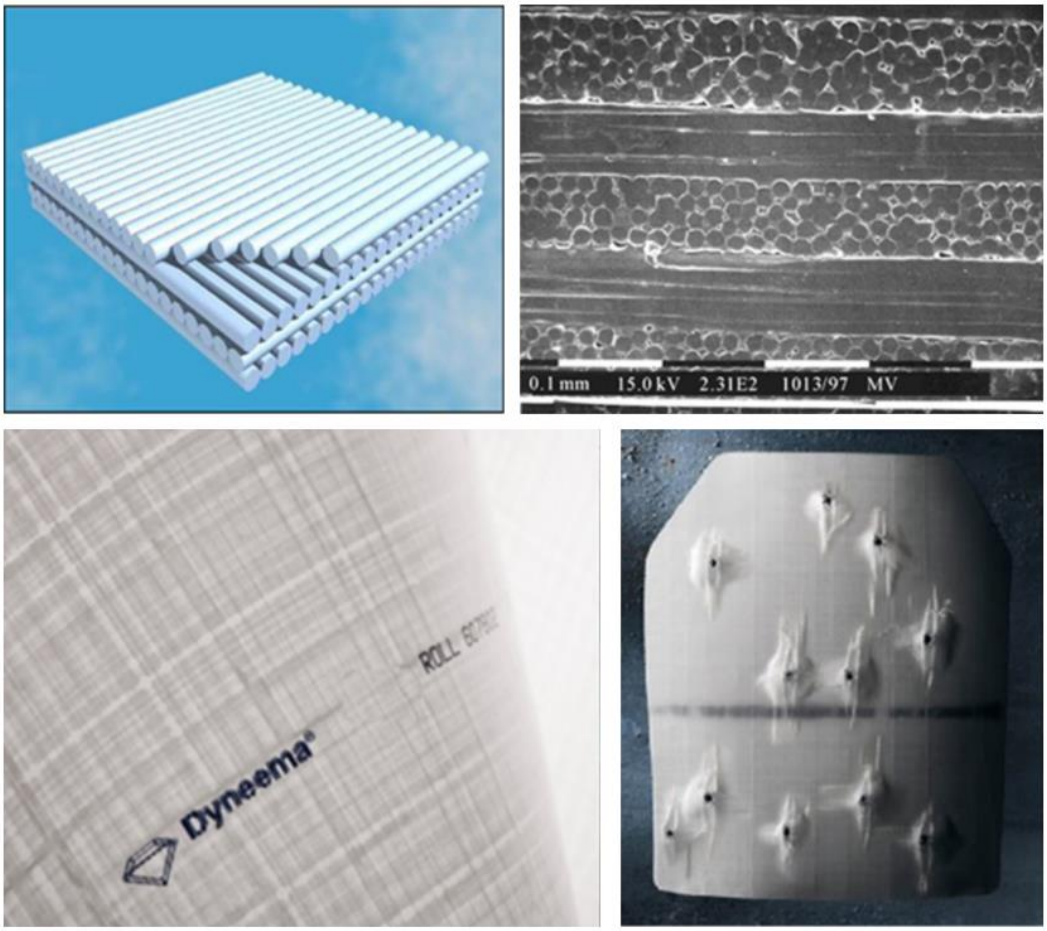

Figure 2.17 *Dyneema® UD is a cross-ply laminate based on a unidirectional UHMWPE composite material[152].*

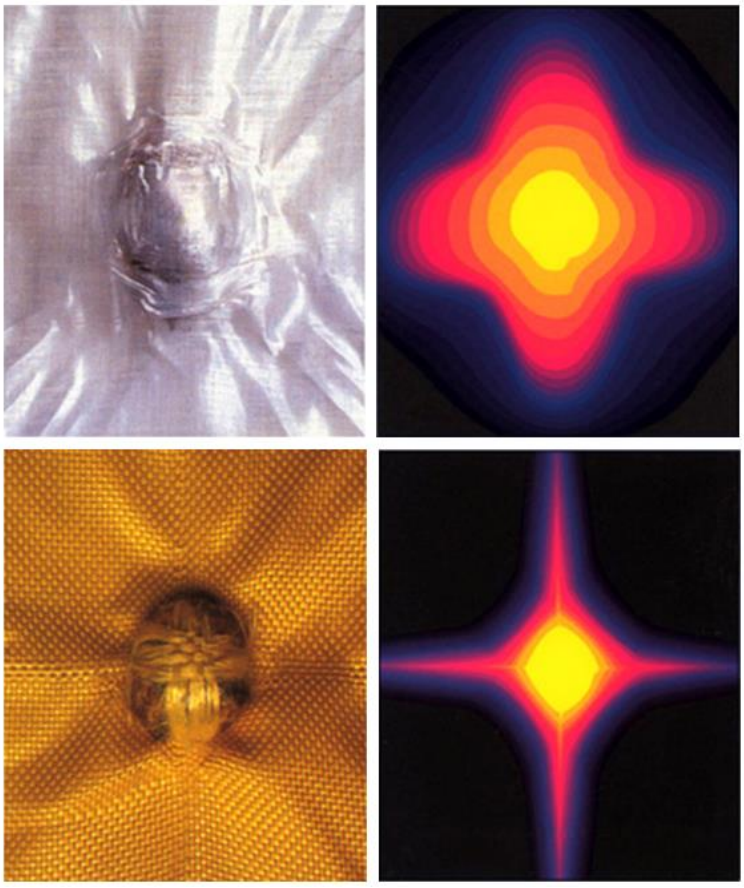

Figure 2.18 *Energy dispersion pattern of Spectra Shield® (above) versus woven aramid fabric (below). Spectra Shield® shows a wider, less localised energy dissipation area, which improves ballistic performance*[152].

Aramids (aromatic polyamides) manufactured under the trade names of Kevlar® by DuPont and Twaron® by Teijin Aramid have also been fabricated to lightweight products with good resistance to impact from fragments or bullets, high temperature and chemicals and have been used in anti-ballistic and aerospace materials[158-159].

However, most of today's high performance fibre-reinforced composites are non-transparent due to light absorption by fibres, light scattering effects caused by the large surface area of reinforcing fibres and/or differences in refractive indices between fibres and matrix. Some efforts were made in fabricating transparent composites by matching

the refractive indices of the polymer matrix and the reinforcing phase, including S-glass fibres[18-19], glass ribbons[148-149], nylon fibres[20-21], cellulose nanofibres[85, 160-161] and drawn PP filaments[22]. However, most of these transparent composites only achieved certain degree of transparency in the near field and limited transparency in the far field as required in windows and visors.

2.7 Summary

In this chapter, we reviewed common transparent materials including inorganic glass and amorphous polymers, the current state-of-the-art to fabricate transparent semi-crystalline polymers as well as some transparent composite laminates mainly based on glass, PC and/or PMMA. The methods to make isotropic semi-crystalline polymers transparent generally consist of suppressing crystallization, decreasing the dimensions of crystals or matching refractive indices in polymer blends. For oriented semi-crystalline polymer products after drawing, biaxially stretched semi-crystalline polymers such as BOPP, BOPET, BOPE, BOPA, BOPLA and BOPEN can exhibit optical transparency. In terms of monoaxially stretched semi-crystalline polymers, transparency can be achieved by matching the refractive indices of the polymer and the drawing induced voids, filling or preventing the formation of voids during stretching. Solid-state drawing can effectively enhance the mechanical performance of polymers, whereas severe light scattering by microvoids formed during solid-state drawing usually results in non-transparent products. High performance composites reinforced by high performance fibres have excellent mechanical properties, but nearly all of them are non-transparent due to light absorption by the reinforcing fibres, the large surface area of the fibres and/or the mismatch in refractive indices between fibre and matrix.

From the above, it can be concluded that most of today's materials do not demonstrate both a high optical transparency and high mechanical behaviour. This restricts these materials to applications where either high clarity or high mechanical properties are needed. The following chapters aim to address this discrepancy between high transparency and high mechanical properties by developing highly transparent high performance polyethylene films and composites.

Chapter 3

Highly transparent high strength polyethylene films by tuning drawing parameters

This chapter is partially reproduced from: (1) Y. Lin, R. Patel, J. Cao, W. Tu, H. Zhang, E. Bilotti, C. W. M. Bastiaansen, T. Peijs, *Polymer* **2019**, *171*, 180-191. and (2) Y. Lin, T. Peijs, C. W. M. Bastiaansen, GB1820429.7, Applicant: Queen Mary University of London, priority date filling: 14 December **2018**.

3.1 Introduction

As reviewed in Chapter 2, most common transparent materials exhibit high transparency levels but relatively unsatisfactory mechanical properties. For example, glass is typically brittle and of low strength (< 50 MPa), not to mention the risk from shattering into multiple pieces potentially causing injuries[1]. Other typical transparent amorphous polymers like PC and PMMA generally possess a low modulus (2−3 GPa) and strength (~ 60 MPa)[2].

For HDPE, one of semi-crystalline polymers, cast or blown film extrusion of HDPE can lead to transparent products[8, 70]. However, such materials are often stretched in the melt, meaning that chain entropy and chain relaxation prevents effective chain orientation and chain extension. As a result, mechanical properties of such transparent HDPE sheets are

typically low, with elastic moduli of 0.6−3 GPa and tensile strengths of 30−230 MPa[9-10], which restricts their application area mainly to packaging.

Solid-state drawing can significantly improve mechanical properties of polyolefins including modulus and strength as stated in Section 2.4. However, solid-state drawn HDPE fibres or films are normally not transparent due to large crystal dimensions, high degree of crystallinity, and/or introduction of internal voiding and defect structures after ultra-drawing.

Thus, most of the today's materials do not combine high transparency and high mechanical behaviour as needed for applications such as built environment, impact resistant windows, automotive and protective glazing.

In this chapter, high transparency and high mechanical performance were simultaneously introduced into HDPE films by regulating drawing conditions without the need to incorporate additives. The influence of drawing conditions, especially drawing temperature, on optical performance of solid-state drawn HDPE films is systematically explored for the first time. Moreover, this chapter further investigates the impact of drawing parameters on drawing behaviour, film morphology, mechanical and thermal properties.

3.2 Experimental

3.2.1 Materials

Borealis VS4580 (Borealis AG, Austria) was used as HDPE. This polymer grade has a melting temperature (T_m) of 134 °C, a pellet density of 0.958 g/cm^3 and a melt flow index

(MFI) of 0.6 g/10 min at 190 °C/2.16 kg and 21 g/10 min at 190 °C/21.6 kg. Clearly, the HDPE grade selected will have a major effect on drawability and ultimate mechanical properties of the films. For example, only homopolymer grades without long chain branching will lead to high draw ratios and mechanical properties. In this chapter, the HDPE grade selected was based on the seminal work on drawing of HDPE fibres by Ward and coworkers[110, 123, 162], and Wu and Black[112]. They performed a comprehensive study on different grades to achieve ultimate mechanical properties in melt-spun solid-state drawn HDPE fibres. TPU ST-6050 sheets with a thickness of 0.36 mm were provided by Schweitzer-Mauduit International, Inc. (USA). Glass slides with a thickness of 1−1.2 mm were purchased from Fisher Scientific (UK).

3.2.2 Preparation of specimens

Isotropic HDPE sheets with a thickness of 0.2−0.5 mm were manufactured by compression moulding using a Dr. Collin P300E (Germany) hot press at 160 °C for 3 min, followed by cooling down to room temperature (RT). For optical properties, optical microscopy and thermal characterizations, rectangular-shaped samples with gauge dimensions of 20 mm × 10 mm were cut from these hot-pressed sheets. For surface morphology imaging as well as mechanical tests, dumbbell-shaped specimens were cut from these isotropic sheets according to ASTM D638 Type V with gauge dimensions of 9.53 mm × 3.18 mm. All these samples were then uniaxially drawn at different drawing temperatures (T_d) from 70 °C to 125 °C in an Instron 5900R84 (UK) universal tensile tester equipped with an environmental chamber. The drawing temperature was defined as the air temperature surrounding the samples during solid-state drawing process, which was measured by thermocouples in the environmental chamber, rather than the real

temperature on the surface and/or inside the samples. Drawing speed was varied between 100 mm/min to 500 mm/min (corresponding to a strain rate of 5−25 min^{-1} for rectangular-shaped specimens and 10.5−52.5 min^{-1} for dumbbell-shaped specimens, respectively), although most of the drawing was performed at 100 mm/min. Draw ratio (λ) was measured by the length ratios before and after drawing using ink marker lines initially spaced every 1−2 mm. The average thickness (t) of the drawn HDPE samples was calculated by weighing the samples, and using the following equation:

$$t = \frac{m}{\rho \times l \times w} \tag{3.1}$$

where m is the mass of the oriented HDPE films, ρ is the density of the oriented HDPE films (0.958 g/cm^3), and l and w are the length and width of the films after solid-state drawing, respectively. At least three specimens were used for each test.

Specimens for optical appearance and properties as well as optical microscopy consisted of drawn HDPE films sandwiched between TPU interlayers and two glass slides (see ***Figure 3.1(a)*** in Section 3.3.1) in order to remove surface scattering from the uniaxially oriented films. Compression moulding of this laminated structure was performed using a Rondol (UK) hot press at 100 °C for 5−10 min and a pressure of 3 bar.

3.2.3 Characterization

Transmittance spectra of the HDPE/TPU/Glass laminates were obtained using a PerkinElmer Lambda 950 (USA) UV-vis spectrometer equipped with an integrating sphere with 100 mm diameter in the wavelength range of 400−700 nm at an interval of 1 nm, measured at least three times for each sample. UV-vis tests were carried out at a sample-to-detector distance of 5 cm and 40 cm (see schematic diagrams in ***Figure 3.4(a)***

and ***Figure 3.4(b)*** in Section 3.3.1). Optical microscopy of laminates was performed using an Olympus BX60 (USA) microscope in transmission-mode. The percentage of area coverage by microvoids in the drawn HDPE films was calculated from optical microscopy images using ImageJ software.

Atomic force microscopy (AFM) images of drawn HDPE films were taken using a NT-MDT NTEGRA (Russia) system with a Mikromasch probe. The probe had a resonant frequency of around 160 kHz and a spring constant of 5 N/m. The AFM images were captured at a frequency of 0.5−1 Hz and a set point ratio of 2.0. The surface roughness of drawn HDPE films was calculated from the AFM images by SPIP software analysis. Scanning electron microscopy (SEM) of drawn HDPE films was carried out using FEI Inspect F (Netherlands) with an acceleration voltage of 5 kV.

Differential scanning calorimetry (DSC) of drawn HDPE films was carried out using a TA Instruments (UK) DSC 25. Samples of 5−10 mg were placed in aluminium pans with a single heating-cooling cycle performed under a flow of nitrogen gas at a constant heating rate of 10 °C/min. At least three tests were carried out for each condition. The melting point (T_m) and enthalpy of fusion (ΔH_f) of the drawn films were obtained from the first heating scan. The crystallinity (X_c) was calculated using the following equation:

$$X_c = \frac{\Delta H_f}{\Delta H_f^0} \times 100\ \% \tag{3.2}$$

where ΔH_f^0 is the enthalpy of fusion of 100 % crystalline polyethylene crystals, which is equal to 293.0 J/g[163].

The maximum draw ratio which still produced transparent films was judged by visual inspection during the solid-state drawing process. Above a specific draw ratio, whitening

occurred in the drawn films. The maximum transparent draw ratio (λ_{trans}) was defined at this critical point, which was different from the maximum draw ratio (λ_{max}) which was defined as the draw ratio at break. Young's modulus and tensile strength of drawn oriented HDPE films were measured using an Instron 5566K1071 (UK) universal tensile tester at a crosshead speed of 100 mm/min at RT. Specimens with gauge lengths of 60−100 mm (60 mm for λ = 10, 80 mm for λ = 15 and 100 mm for λ = 20, respectively) were tested using manual wedge action grips, which corresponds to a strain rate of 1.67 min^{-1} for λ = 10, 1.25 min^{-1} for λ = 15 and 1 min^{-1} for λ = 20, respectively. Young's modulus was calculated from the tangent of the engineering stress-strain curve at a strain below 0.5 %. The mean and standard deviation of the Young's modulus and tensile strength were calculated from at least five samples in most cases as required by the common tensile test standards. However, in the case of the oriented HDPE films drawn at T_d = 110 °C and λ = 20 as well as T_d = 120 °C and λ = 15, only three or four samples were used to calculate the mean and standard deviation of modulus and strength as the inhomogeneous drawing process with localised necking easily happened under these conditions as a result of the weak strain hardening behaviour.

3.3 Results and discussion

3.3.1 Some effects on optical properties of drawn HDPE films

In order to remove the influence of surface scattering when evaluating the optical properties of uniaxially oriented HDPE films, these films were sandwiched between two glass slides with TPU interlayers as schematically shown in ***Figure 3.1(a)***. Typically, the values of refractive index vary with draw ratio, orientation degree as well as the position

in the specimen, and hence the average optical properties were focused on here. The chosen TPU interlayers have an average refractive index (n = 1.50) similar to glass (n = 1.52)[164] and HDPE (n = 1.54)[7], reducing the degree of light reflections at the interfaces. After being sandwiched between glass and TPU, a more clear appearance with higher transmittance values is observed for the oriented HDPE films (***Figure 3.1(b)*** and ***Figure 3.1(c)***), which means that the TPU interlayers successfully eliminate the light scattering at the surface of the HDPE films.

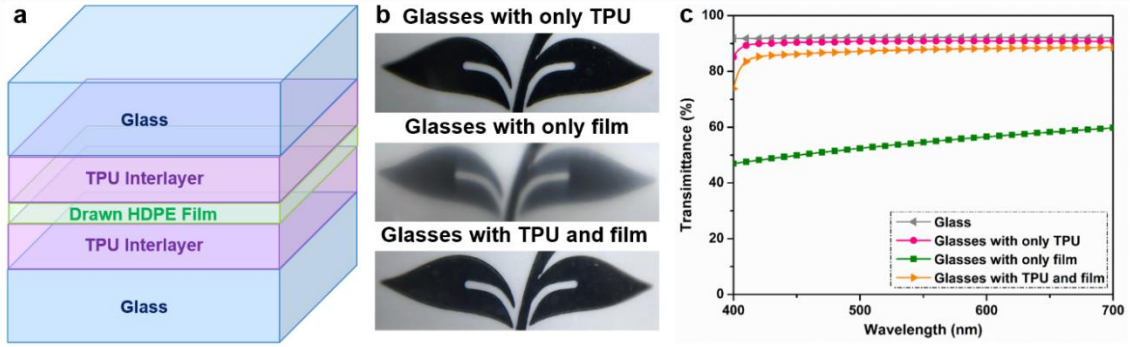

Figure 3.1 *(a) Schematic diagram of the laminated structure consisting of drawn HDPE film sandwiched between glass slides and TPU interlayers, (b) photographs and (c) transmittance of glass, TPU interlayers sandwiched between two glass slides, drawn HDPE films sandwiched between two glass slides with or without TPU interlayers versus visible light wavelength tested at a sample-to-detector distance of 40 cm. In (a), relative thickness of the different layers is drawn to scale.*

The thickness of the films also affects their optical performance. Thinner films usually possess higher transparency (***Figure 3.2***) since they contain fewer defects or dust particles that can scatter light. HDPE films with a thickness of ~ 275 μm after drawing (shown as the blue line in ***Figure 3.2***) were drawn from compression-moulded films with a thickness of around 1 mm. These films still possessed a transmittance of ~ 81 % at 550 nm. However,

above this thickness, with the current set-up it became hard to carry out the solid-state drawing process.

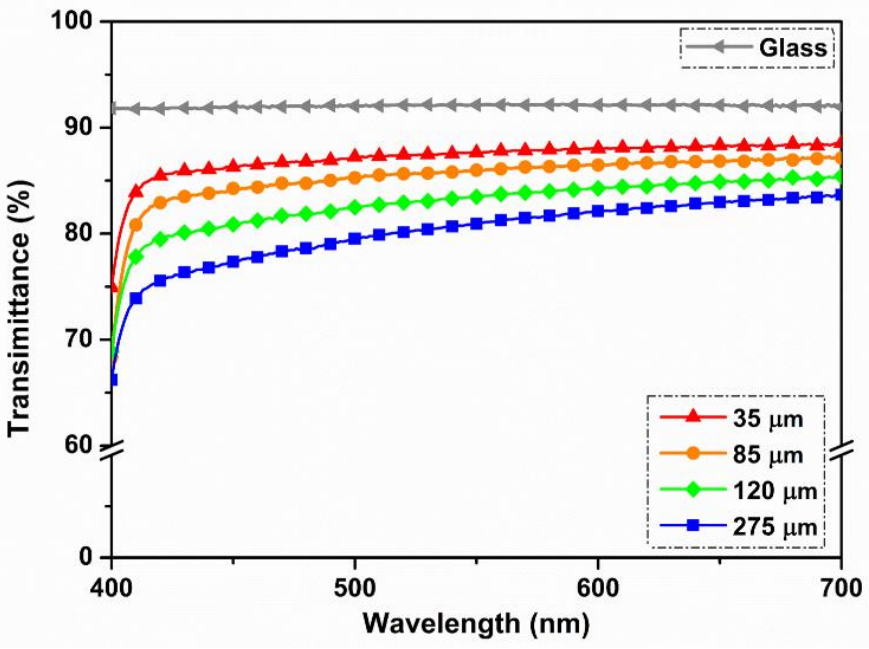

Figure 3.2 *Transmittance of HDPE drawn films with different thicknesses at a drawing temperature of 110 °C and a draw ratio of 10. Drawn films were sandwiched between glass slides and TPU interlayers and tested at a sample-to-detector distance of 40 cm.*

Nearly all studies in the literature that are concerned with optical transparency use photographs of sample appearances by positioning the sample at a very close distance to an object, often involving placing the "transparent" film or sheet directly on top of a background image[6, 165-166]. However, according to ASTM D1746-15, regular transmittance usually refers to the ability of an observer to "see-through" a specimen in order to clearly distinguish a relatively distant object, analogous to the visibility of the distant scenery seen through a window. Here, the optical appearance of the oriented HDPE films (λ = 15) drawn at different temperatures is shown when placed close to an object but also at a relatively far distance from an object (***Figure 3.3***). It is shown that the drawn films are completely opaque at a drawing temperature T_d = 70 °C and 80 °C.

However, when the drawing temperature is increased from 80 °C to 90 °C, the appearance of the drawn HDPE films changes from opaque to transparent. Films drawn above 100 °C have a highly transparent appearance with little differences in optical appearance. Moreover, the visibility as seen through opaque films (T_d = 70 °C and 80 °C) or translucent films (T_d = 85 °C) when placed at a far distance from an object (***Figure 3.3(b)***) is less than when placed close to an object (***Figure 3.3(a)***). It is noteworthy that in the case of translucent films drawn at 85 °C, an object is still slightly visible when the HDPE film is placed close to the object, whereas it is not at all visible when the film is placed at a distance. This once more highlights the importance of evaluating transparency not only at a short sample-to-object distance (near field) but also at a long sample-to-object distance (far field).

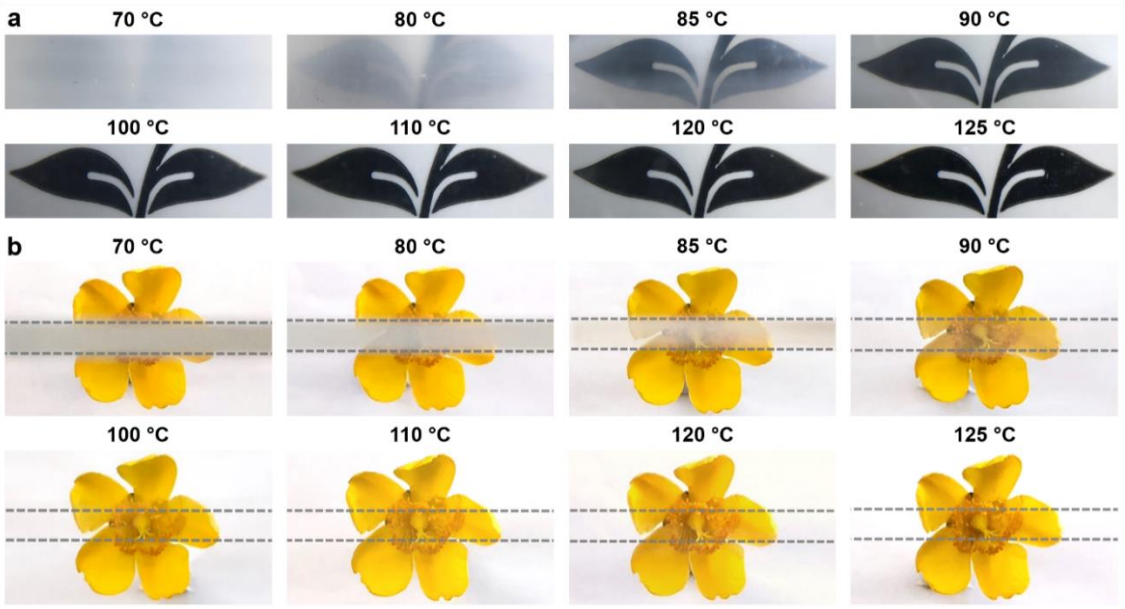

Figure 3.3 *Photographs of oriented HDPE films (λ = 15) drawn at different drawing temperatures (a) when placed directly on top of an object (near field) and (b) when placed at a 40 cm distance from an object (far field). HDPE films were sandwiched between glass slides and TPU interlayers. In (b), the films are marked and located between the dashed lines. The thickness of the drawn HDPE films is around 80 µm.*

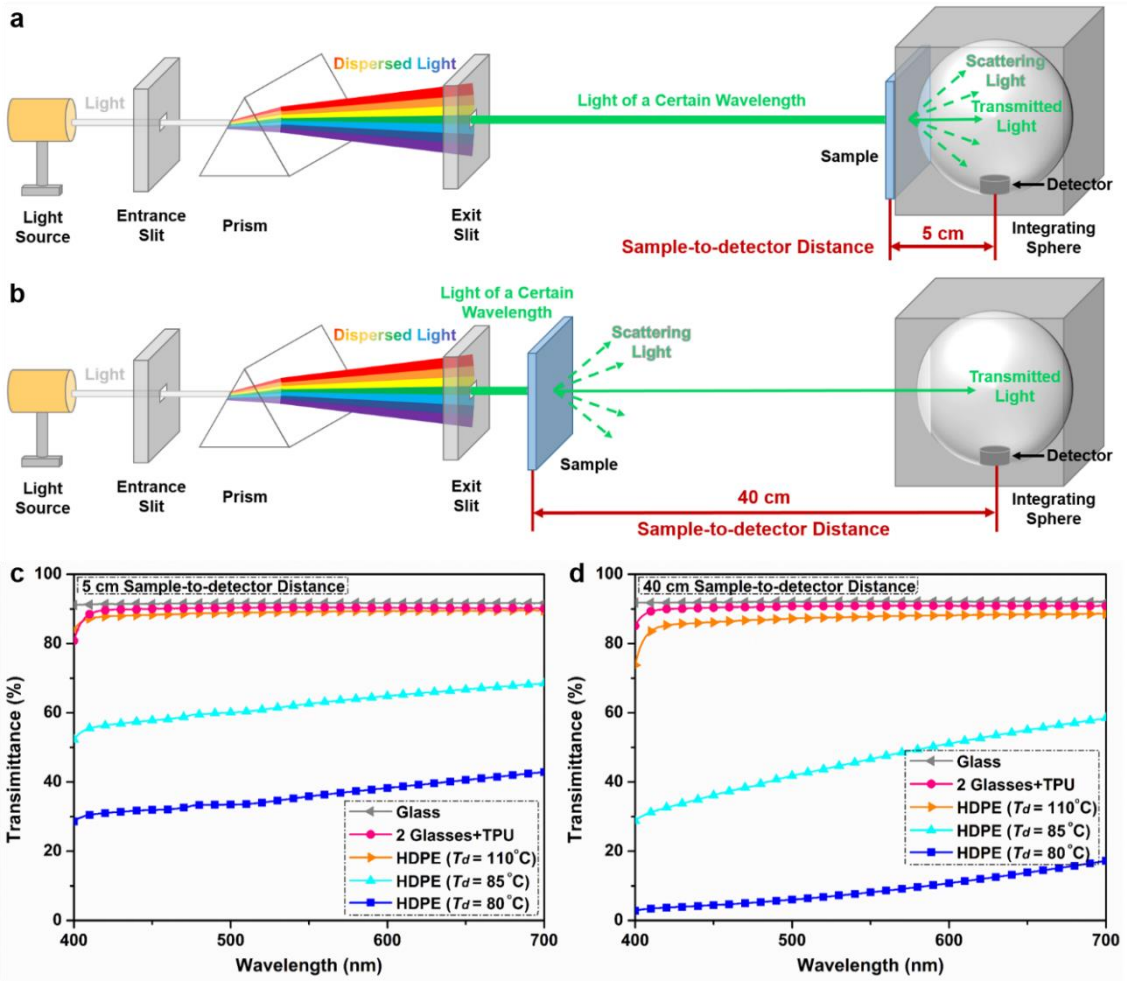

Figure 3.4 *Schematic diagrams of the beam path inside the UV-vis machine, corresponding to two different sample-to-detector distances of (a) 5 cm and (b) 40 cm together with transmittance data versus wavelength tested at a sample-to-detector distance of (c) 5 cm and (d) 40 cm. Drawn HDPE films (λ = 15) were sandwiched between glass slides and TPU interlayers.*

Similarly, also transmittance spectra for solid materials are customarily measured in the near field using a short sample-to-detector distance (typically below 5 cm) in a UV-vis machine[167-168]. Here, optical performance was tested at both a short (near field) and a relatively long sample-to-detector distance (far field). For a sample-to-detector distance of 5 cm, the sample was placed at the entrance port of the integrating sphere (***Figure***

3.4(a)). In this case the transmittance spectra contain the light scattered in the forward direction. At a sample-to-detector distance of 40 cm, the specimen was placed further away from the integrating sphere which gives more relevant transmittance data (***Figure 3.4(b)***).

Transmittance spectra at both sample-to-detector distances are shown in ***Figure 3.4(c)*** and ***Figure 3.4(d)***. Transmittance values measured at both distances are around 92.0 % for glass and 90.5 % for a single TPU interlayer sandwiched between two glass slides. For HDPE film drawn at 110 °C sandwiched between two glass slides and TPU interlayers, the transmittance at 40 cm sample-to-detector distance is 1−2 % lower than the value measured at a distance of 5 cm. However, differences in transmittance as high as 16 % or 28 % are obtained at these two distances for HDPE films drawn at 85 °C or 80 °C, respectively. This discrepancy in transmittance values for different sample-to-detector distances is in accordance with the optical appearance at different sample-to-object distances (see ***Figure 3.3(a)*** and ***Figure 3.3(b)***). Bearing in mind potential practical applications for transparent high strength HDPE films, subsequent optical tests were all performed at a sample-to-detector distance of 40 cm (far field).

3.3.2 The influence of drawing temperature on properties and structures of drawn HDPE films

The engineering stress-strain curves of HDPE films during solid-state drawing at different drawing temperatures are shown in ***Figure 3.5(a)***. With increasing drawing temperature, the yield stress significantly drops from 13.8 MPa to 3.6 MPa for drawing temperatures ranging from 70 °C to 120 °C. Also, strain hardening behaviour becomes less pronounced with increasing drawing temperatures. At $T_d \leq 110$ °C, strain hardening results in stable

neck formation and homogeneous deformation even at high draw ratios (λ). However, the solid-state drawing process becomes inhomogeneous with localised necking at low draw ratios when T_d > 110 °C as a result of the weak strain hardening. In fact, heterogeneous drawing with highly deformed regions and close to non-deformed regions were always observed under these conditions and consequently proper and reproducible samples were difficult to obtain due to the lack of strain hardening. ***Figure 3.5(b)*** shows the maximum draw ratio (λ_{max}) and the maximum transparent draw ratio (λ_{trans}) as a function of drawing temperature, where λ_{max} is related to the maximum extensibility of the molecular network above which further drawing would lead to failure, i.e. no further orientation would develop, whereas λ_{trans} is the maximum draw ratio before "whitening" starts to occur and the film becomes opaque. At T_d = 80 °C, the highest λ_{max} is obtained for this grade of HDPE, indicating an optimum drawing temperature of 80 °C for ultimate mechanical performance. Similar optimum drawing temperatures for ultimate mechanical properties of oriented HDPE were also reported by both Jarecki and Meier[169] and Capaccio *et al.*[162]. However, all uniaxially oriented films are opaque at $T_d \leq$ 80 °C. Conversely, transparent films are obtained at $T_d \geq$ 90 °C. Both λ_{max} and λ_{trans} are reduced with further increasing drawing temperatures due to less strain hardening. Hence, transparent oriented HDPE films and homogeneous drawing even at high draw ratios were obtained in a temperature window between 90 °C and 110 °C.

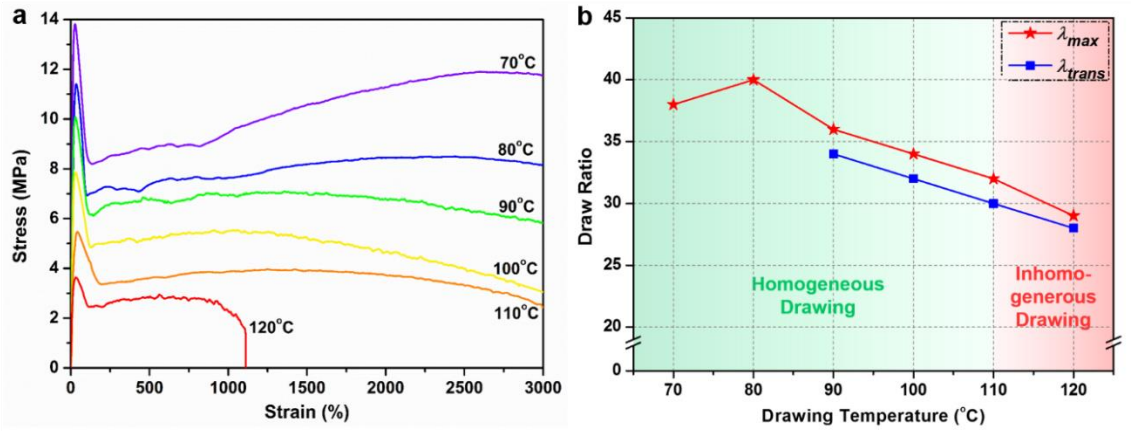

Figure 3.5 *(a) Stress-strain curves at different drawing temperatures and (b)* λ_{max} *and* λ_{trans} *of oriented HDPE films as a function of drawing temperature at a drawing speed of 100 mm/min. The background colour change from green to red signifies the transition from homogeneous to inhomogeneous drawing and indicates the processing window for creating highly oriented polymer films.*

The influence of drawing temperature on transmittance in the visible light range is shown in ***Figure 3.6(a)*** and ***Table 3.1***. At $T_d \leq 80$ °C, transmittance values of drawn HDPE films at $\lambda = 15$ are all below 18 %. Transmittance of the uniaxially oriented films increases to over 75 % when T_d increases to 90 °C. More importantly, with further increasing drawing temperatures ($T_d \geq 100$ °C), optical transmittance can exceed 89 % at high wavelengths within the visible spectrum, which is only 3 % lower than glass (~ 92 %). Higher chain mobility resulting in fewer defects at elevated drawing temperatures may account for this increase in transparency. It is well known that the most sensitive wavelength to the human eye is around 550 nm within the visible spectrum. ***Figure 3.6(b)*** gives the change in transmittance with increasing drawing temperature at this wavelength. Transmittance of drawn HDPE films at $\lambda = 15$ is significantly improved within the T_d range of 80−90 °C. Transmittance becomes even better (≥ 86 %) for $T_d \geq 100$ °C, with films showing a consistent tendency of improved optical clarity with increasing drawing temperature.

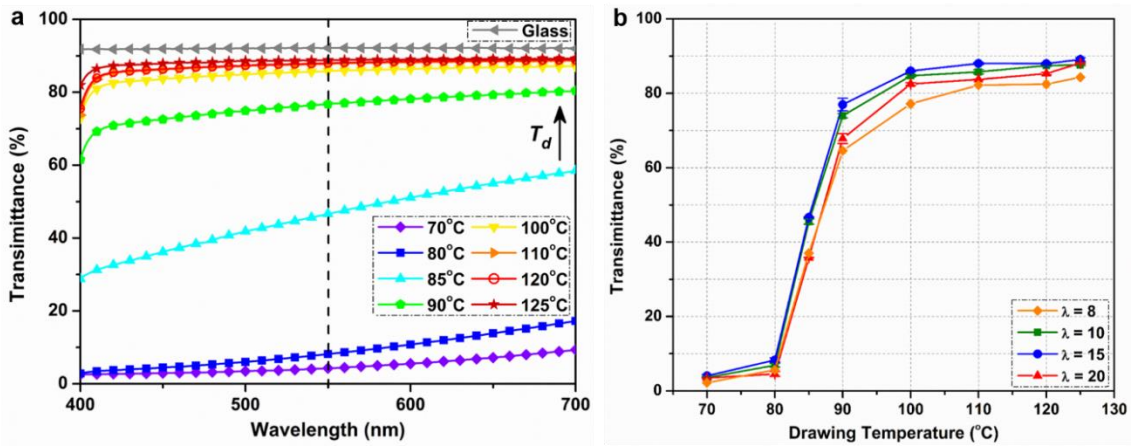

Figure 3.6 *Transmittance of drawn HDPE films (a) at λ = 15 at different drawing temperatures versus visible light wavelength and (b) at different draw ratios as a function of drawing temperature at a wavelength of 550 nm, indicating maximum transmittance at $T_d \geq 100$ °C. Drawn HDPE films were sandwiched between glass slides and TPU interlayers and tested at a sample-to-detector distance of 40 cm. The thickness of the drawn HDPE films is about 80 µm.*

Table 3.1 *Transmittance values of drawn HDPE films (λ = 15) at different drawing temperatures at a wavelength of 700 nm, 550 nm and 400 nm measured at a sample-to-detector distance of 40 cm.*

Wavelength	70 °C	80 °C	85 °C	90 °C	100 °C	110 °C	120 °C	125 °C
700 nm	9.3 %	17.2 %	58.5 %	80.5 %	87.1 %	88.5 %	88.9 %	89.2 %
550 nm	4.3 %	8.2 %	46.6 %	76.7 %	85.8 %	87.8 %	88.0 %	88.9 %
400 nm	2.5 %	2.8 %	28.8 %	61.5 %	73.1 %	73.8 %	75.5 %	82.0 %

The outcomes of these optical experiments indicate that by simply raising the drawing temperature in the solid-state drawing process, transparency of oriented HDPE films can be significantly enhanced. For the purpose of exploring the mechanism behind this improvement in transmittance with increasing drawing temperatures, optical microscopy

images of drawn HDPE films at different T_d were taken (***Figure 3.7***). It can be seen that a number of parallel interfibrillar microvoids along the drawing direction are present in films drawn at 70 °C and 80 °C. As a result, less light can penetrate through these films due to light scattering effects by these microvoids which contributes to the darkened images. When T_d is raised to 90 °C, the amount of parallel interfibrillar microvoids clearly diminishes. The area covered by these parallel microvoids as quantified by ImageJ software drops from 42.7 % at T_d = 80 °C to 4.2 % at T_d = 90 °C. This implies that more light can pass through films produced at T_d = 90 °C because less light is scattered, resulting in a much brighter image. The number of interfibrillar microvoids is even further reduced for $T_d \geq$ 100 °C, with only 0.1 % coverage by parallel microvoids at T_d = 120 °C. This is consistent with the highly transparent appearance and high transmittance values of films drawn at high temperatures (see ***Figure 3.3*** and ***Figure 3.6***).

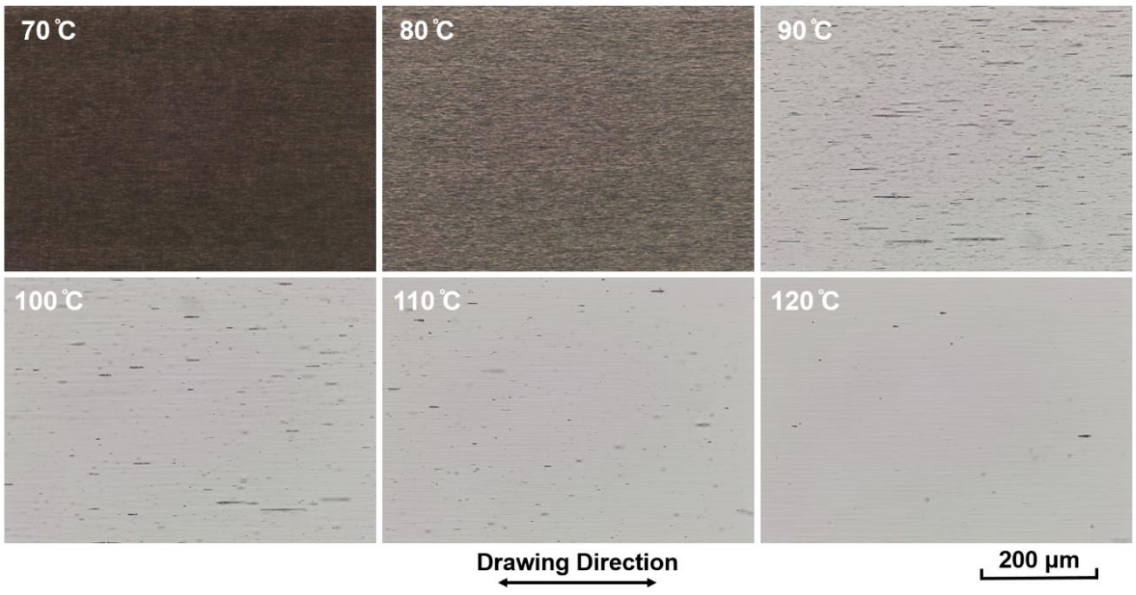

Figure 3.7 *Optical microscopy images of drawn HDPE films (λ = 15) at different drawing temperatures taken at the same light intensity in the optical microscope, showing a reduction in parallel microvoids with increasing drawing temperature. Drawn HDPE films were sandwiched between glass slides and TPU interlayers.*

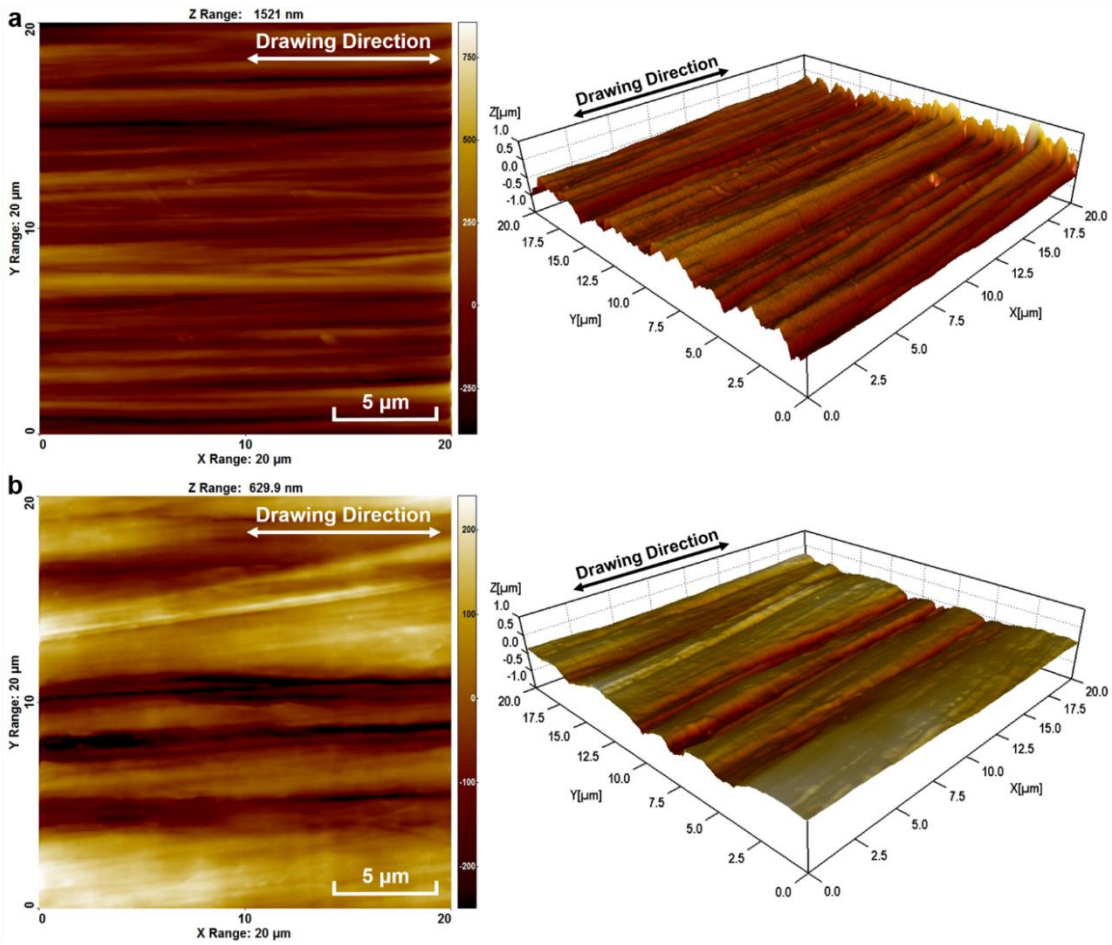

Figure 3.8 *2D and 3D AFM images of drawn HDPE films (λ = 15) drawn at (a) T_d = 80 °C and (b) T_d = 110 °C, showing a smoother surface morphology at higher drawing temperature.*

AFM images in ***Figure 3.8*** reveal the surface structure of drawn HDPE films (λ = 15) at a drawing temperature of 80 °C and 110 °C. The films drawn at T_d = 80 °C display obvious fibrillar and wrinkled surface structures (***Figure 3.8(a)***), with an average surface roughness (*Sa*) of 118 nm. According to Peterlin's molecular model of the drawing of polyolefins[116, 170], the morphology of semi-crystalline polymers will change from a spherulitic structure to a newly generated fibrillar structure during drawing. In comparison, films drawn at T_d = 110 °C reveal a smoother surface structure (***Figure 3.8(b)***) with a lower average surface roughness (*Sa*) of 89 nm. This reduction in surface

roughness at high drawing temperatures is again the result of higher chain mobility and relaxation at these elevated temperatures[171-172].

SEM images (***Figure 3.9***) further reveal the change in surface morphology of HDPE films (λ = 15) drawn at 70−120 °C. With increasing drawing temperatures, the fibrillar microstructure with fibrils along the drawing direction appears less pronounced and the width of the fibrils broadens. Higher drawing temperatures will give rise to relaxation of oriented chains, facilitating the mobility of polymer chains as well as reducing the separation of fibrils in drawn HDPE films[13]. The decreasing number of interfibrillar voids then contributes to reduced interfibrillar scattering, and hence enhanced transparency together with an optically clear appearance at higher drawing temperatures.

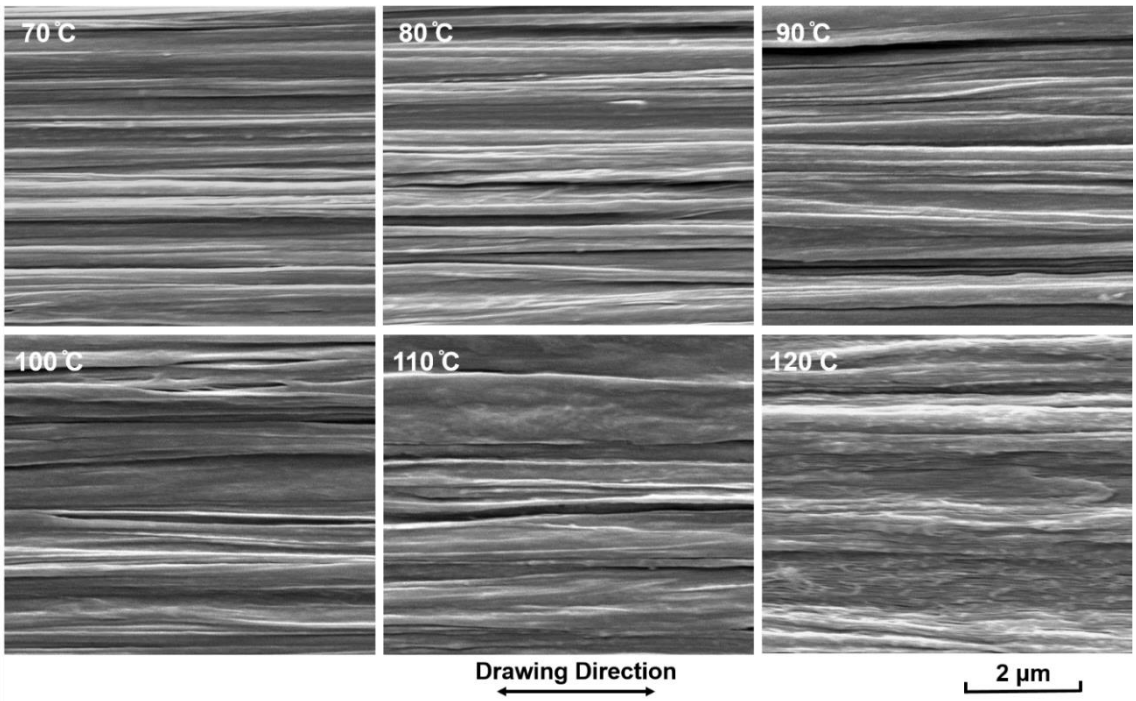

Figure 3.9 *SEM images of drawn HDPE films (λ = 15) at different drawing temperatures, showing less interfibrillar defects with increasing temperature.*

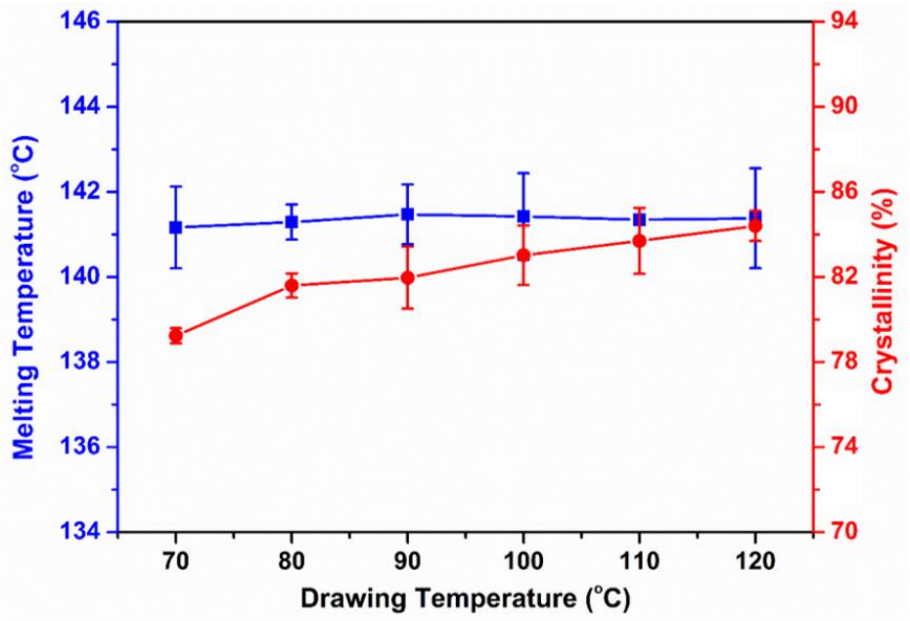

Figure 3.10 *DSC results of T_m and X_c of drawn HDPE films as a function of drawing temperature at λ = 15.*

In terms of thermal properties, the melting temperatures (T_m) of drawn HDPE films fluctuate at around 141 °C for T_d = 70−125 °C and therefore T_m can be regarded as independent of drawing temperature for a draw ratio of 15 (see ***Figure 3.10***). It signifies that drawing temperature has limited impact on the thermal properties of drawn HDPE films at this draw ratio, which is in agreement with previous studies[169]. However, crystallinity (X_c) did slightly increase (~ 5 %) with increasing T_d.

3.3.3 The influence of draw ratio on properties and structures of drawn HDPE films

Figure 3.11 demonstrates the influence of draw ratio on optical transparency of drawn HDPE films. It is shown that for all drawing temperatures, transmittance is maximum at around λ = 15, with transmittance decreasing at higher draw ratios. This initial increase

in transmittance is most likely related to the change in polymer morphology from an isotropic spherulitic structure to an oriented structure[116]. The slight decrease in optical properties at high draw ratios can be attributed to the formation of defects in the highly fibrillar structure, leading to light scattering. The observation of an optimum draw ratio for high transparency is in accordance with previous research in the area of transparent HDPE films using additives to enhance transparency[75]. Another remarkable observation is that transmittance values of drawn HDPE films show only little improvement for $T_d \geq$ 100 °C for each draw ratio, indicating that a plateau in optical transparency is reached around this temperature.

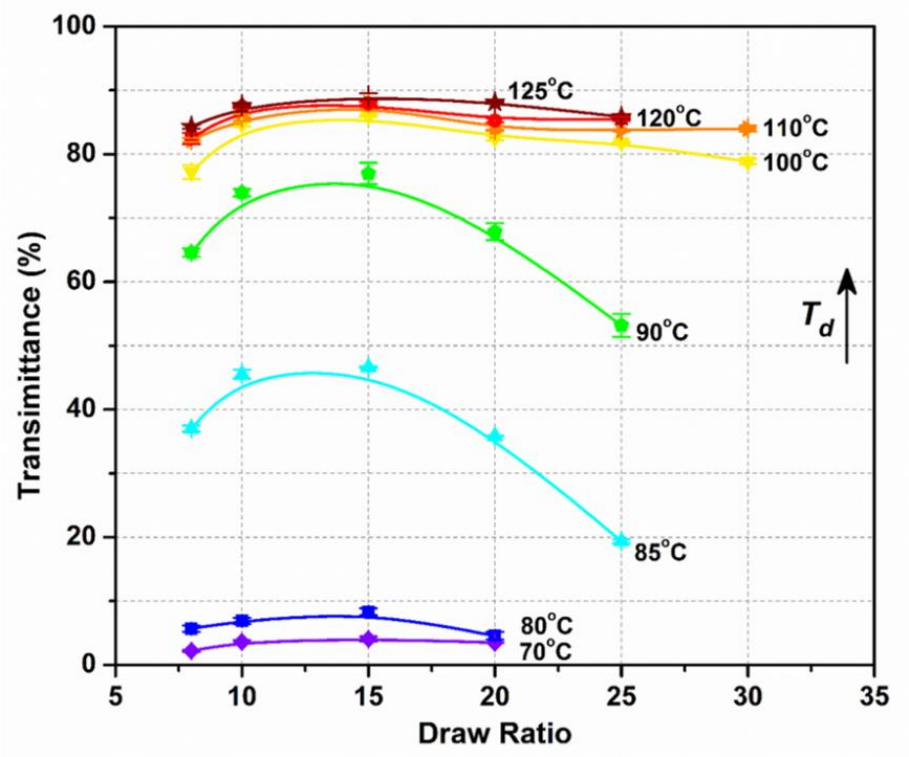

Figure 3.11 *Transmittance of drawn HDPE films at different drawing temperatures as a function of draw ratio at a wavelength of 550 nm, indicating maximum transmittance at λ = 15. Drawn HDPE films were sandwiched between glass slides and TPU interlayers and tested at a sample-to-detector distance of 40 cm. The thickness of the drawn HDPE films is about 80 μm.*

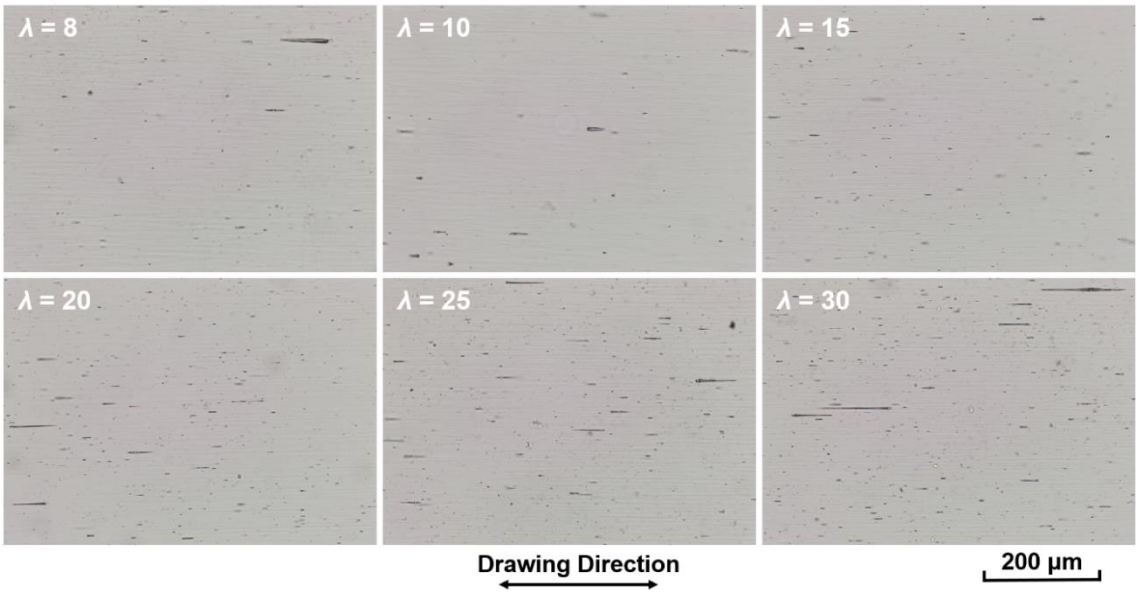

Figure 3.12 *Optical microscopy images of drawn HDPE films with different draw ratios at T_d = 110 °C taken at the same light intensity in an optical microscope, showing an increase in parallel microvoids at high draw ratios. Drawn HDPE films were sandwiched between glass slides and TPU interlayers.*

To further investigate the effect of draw ratio on films' optical performance, optical microscopy and SEM images of drawn HDPE films with different draw ratios at T_d = 110 °C are shown in ***Figure 3.12*** and ***Figure 3.13***, respectively. It is found that the number of microvoids parallel to the drawing direction increases markedly above λ = 20 (see ***Figure 3.12***), with 0.4 % area coverage by parallel microvoids at λ = 15 and 1.5 % coverage at λ = 30. The increase in parallel microvoids explains the reduced transparency for drawn HDPE films of high draw ratios (λ > 15) because of the induced interfibrillar light scattering. Similar changes in transparency at high draw ratios were also observed in solid-state drawn PP tapes[103] and PLA tapes[173].

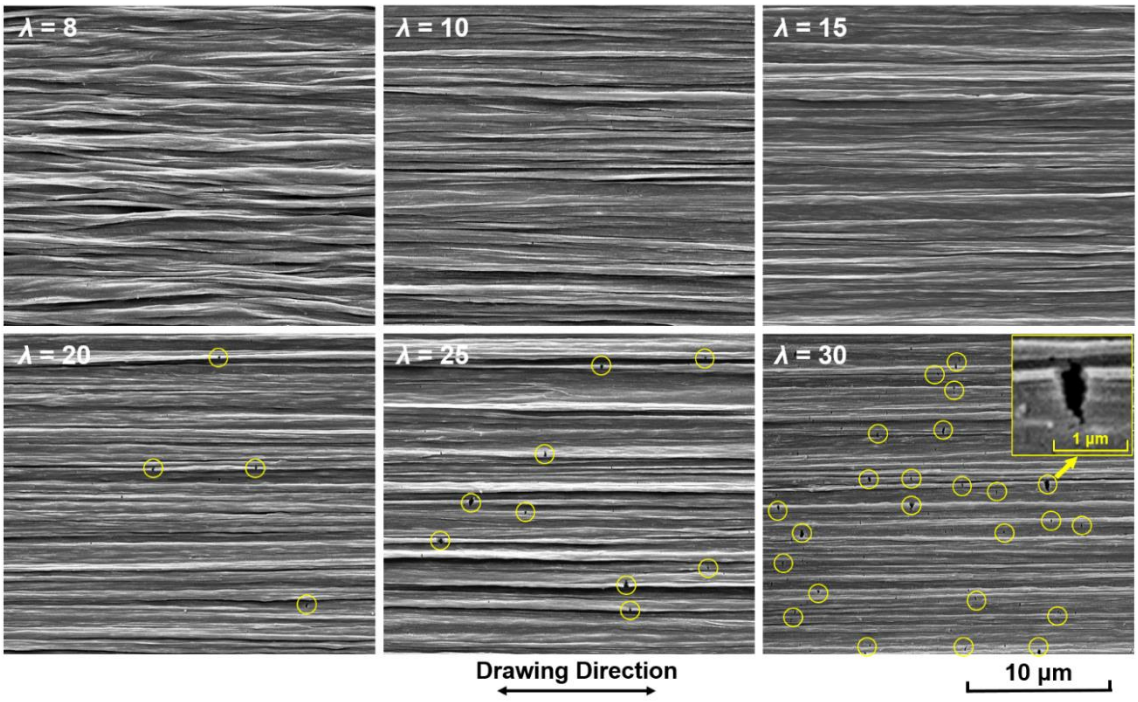

Figure 3.13 *SEM images of HDPE films drawn at T_d = 110 °C at different draw ratios, showing a clear increase in defects at high draw ratios. The circles mark the microcracking defects perpendicular to the drawing direction. The inset in the image for λ = 30 shows a higher magnification image of this type of microcracking defect.*

Furthermore, significant microcracking perpendicular to the drawing direction (indicated by the circles in ***Figure 3.13***) can be seen in SEM images at $\lambda \geq 20$, which may also lead to severe light scattering inside the films and hence a decrease in transparency. Similar transverse cracking and associated changes in appearance from transparent to opaque were also observed by Schimanski *et al.*[103] for PP. These perpendicular microcracks, which are often associated with overdrawing, also restrict further deformation and orientation of molecular chains, resulting in a trend of decreasing λ_{max} and λ_{trans} above T_d = 80 °C (see ***Figure 3.5(b)***). Microvoids along the drawing direction occur at relatively low drawing temperatures or at relatively high draw ratios are predominately feature in the bulk of the oriented films[75]. Hence, they hardly present in SEM images (***Figure 3.9***

and ***Figure 3.13***) but do show in optical microscopy images under transmission-mode (***Figure 3.7*** and ***Figure 3.12***). In conclusion, micro-voiding both along and perpendicular to the drawing direction of the polymer films induced at relatively low drawing temperatures ($T_d \leq 80$ °C) or high draw ratios ($\lambda \geq 20$) will increase the amount of light scattering inside the drawn HDPE films, hence leading to a deterioration in optical transparency.

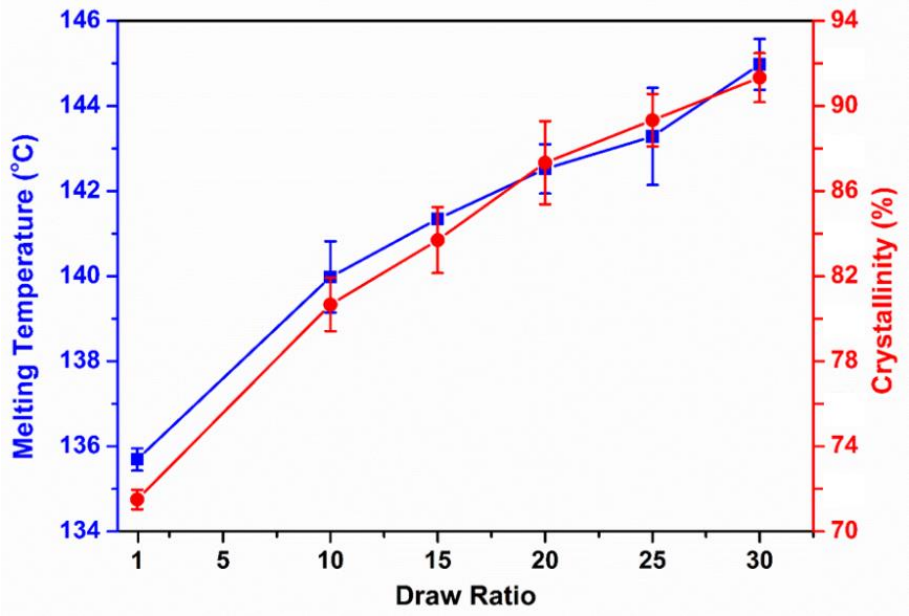

Figure 3.14 *DSC results of T_m and X_c of drawn HDPE films as a function of draw ratio at T_d = 110 °C.*

With respect to thermal properties, both T_m and X_c gradually increase with increasing λ. In ***Figure 3.14***, the increase in T_m and X_c between HDPE films ($\lambda = 30$) drawn at 110 °C and the original isotropic hot-pressed film is shown to be around 10 °C and 20 %, respectively. Based on previous studies[174-175], this can be explained by orientation of the amorphous phase during drawing, leading to an increase in density of the amorphous region. As a result, chain relaxation is hindered by the dense chain packing

and taut tie molecules during heating, and consequently results in the increase of T_m and X_c.

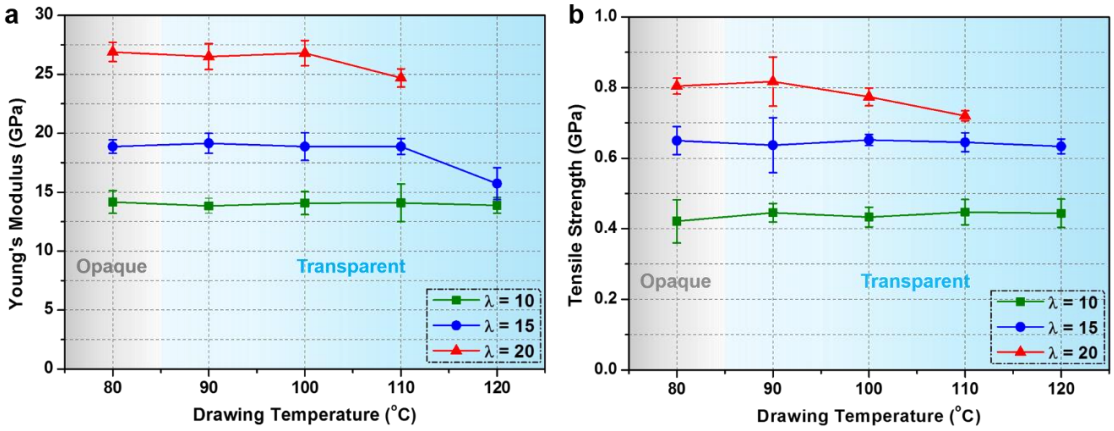

Figure 3.15 *(a) Young's modulus and (b) tensile strength of drawn HDPE films along the drawing direction at different draw ratios as a function of drawing temperature. The background colour change in (a) and (b) from grey to blue indicates the transition from opaque to transparent films.*

The Young's modulus and tensile strength of drawn HDPE films along the drawing direction are shown in ***Figure 3.15*** at different drawing temperatures and draw ratios. First, with increasing draw ratio, elastic modulus and tensile strength along the drawing direction are improved as a result of the unfolding of molecular lamellae and the high degree of chain orientation induced by solid-state drawing. Young's modulus is independent of drawing temperature for $T_d \leq 100$ °C and draw ratios between 10 and 20 (***Figure 3.15(a)***), with modulus values of around 19 GPa for drawn HDPE films at the highest transparent draw ratio ($\lambda = 15$). Moreover, a modulus of around 27 GPa can be achieved for drawn HDPE films at $\lambda = 20$ and $T_d = 80-100$ °C owing to the formation of taut tie molecules induced by the deformation and orientation of polymer chains in the drawn films[116]. These well-oriented tie molecules effectively connect crystalline regions

and therefore contribute to a high modulus. For drawing temperatures below 100 °C, the tensile strength is about 650 MPa and 800 MPa at λ = 15 and λ = 20, respectively (***Figure 3.15(b)***). Nevertheless, both modulus and strength drop with increasing T_d above 100 °C at high draw ratios, with values of around 24 GPa and 700 MPa for λ = 20 at T_d = 110 °C, respectively. This decrease in modulus and strength along the drawing direction is the result of a higher degree of molecular chain relaxation at higher drawing temperatures, and therefore a reduction in the number of taut tie molecules and degree of molecular chain orientation. In addition, the development of parallel microvoids and perpendicular microcracks at high draw ratios can also contribute to this reduction in properties[13, 169] (see ***Figure 3.12*** and ***Figure 3.13***). Uniaxially oriented polyethylene films and fibres are highly anisotropic and mechanical properties of ultra-drawn polyethylene films perpendicular to the drawing direction are typically low. As measured in some of our earlier work[176], the Young's modulus and tensile strength perpendicular to the drawing direction of polyethylene tapes with a draw ratio of 20 is around 2 GPa and 15 MPa, respectively. Our drawn HDPE films (λ = 20) are expected to have similar values of modulus and strength in transverse direction.

Clearly, depending on the required performance, an optimum combination of optical and mechanical performance can be obtained after carefully tuning draw ratio and drawing temperature. For instance, if high mechanical performance is preferred, a draw ratio of 20 should be used, yielding a much higher modulus and strength at similar optical transparency (see ***Figure 3.11***). Thus, depending on specific applications, transparent and high strength HDPE films can be achieved within a wide processing window for solid-state drawing between 90 °C and 110 °C.

3.3.4 The influence of drawing speed on properties of drawn HDPE films

Besides drawing temperature, the drawing speed also influences the solid-state drawing process of HDPE films. Both the yield stress and strain hardening increases with increasing drawing speed (see ***Figure 3.16(a)***). As a result of this increase in strain hardening, drawing behaviour becomes more stable, leading to an increase in λ_{max} and λ_{trans} with drawing speed (see ***Figure 3.16(b)***). In accordance with time-temperature equivalence[177], this trend is opposite to that of drawing temperature (***Figure 3.5(a)*** and ***Figure 3.5(b)***).

However, as illustrated in ***Figure 3.17***, transmittance values gradually decrease with increasing drawing speed at similar draw ratio. Accordingly, combining with ***Figure 3.6***, an optimized combination of drawing temperature and drawing speed should be aimed for when requiring high optical clarity. Actually, during solid-state drawing process, the work of deformation will be partially transformed to the heat of the samples, resulting in a higher actual drawing temperature compared to the drawing temperature as defined in Section 3.2.2, so the actual drawing process is not isothermal. Ideally, the actual sample temperatures should have been checked by high-speed thermal camera during experiment. In addition, a higher drawing speed usually gives rise to a more significant heating effect, which means that the drawing temperature and drawing speed are in fact not totally independent and will affect each other.

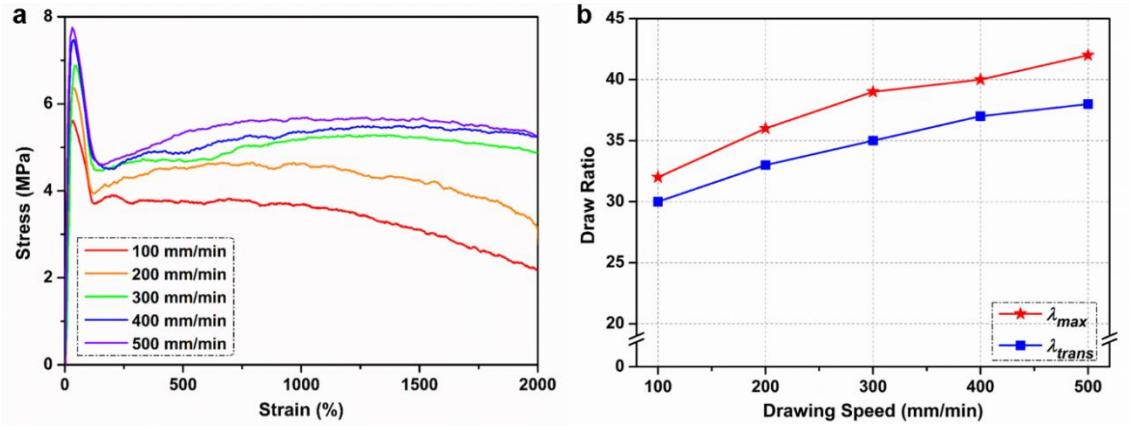

Figure 3.16 *(a) Stress-strain curves of the solid-state drawing process with the influence of drawing speed at 110 °C and (b) λ_{max} and λ_{trans} as a function of drawing speed at 110 °C.*

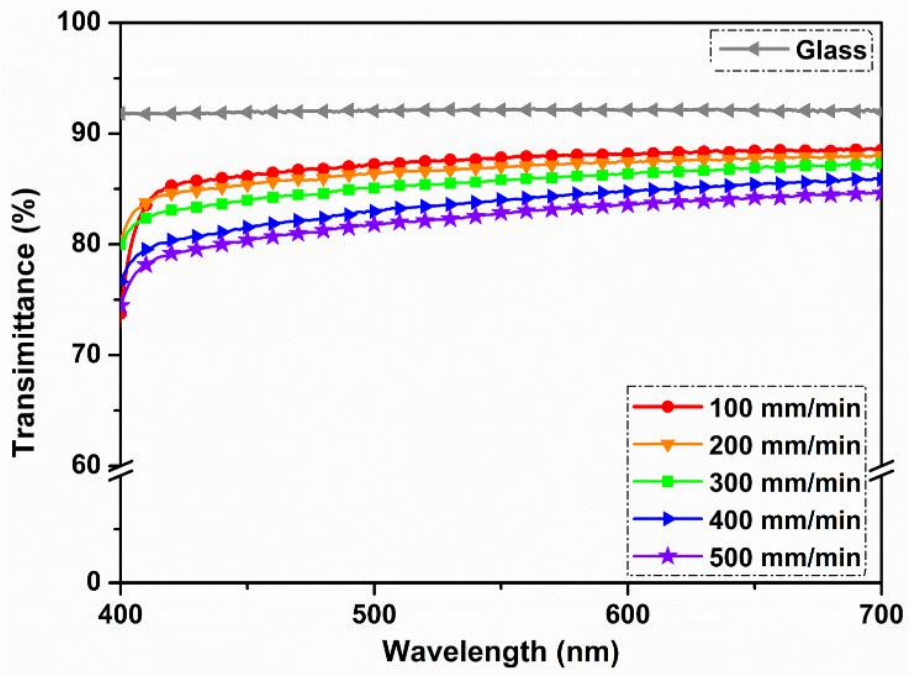

Figure 3.17 *Transmittance of HDPE films (λ = 15) drawn at different drawing speeds at T_d = 110 °C. The films were sandwiched between glass slides and TPU interlayers and tested at a sample-to-detector distance of 40 cm. The thickness of the drawn HDPE films is around 80 μm.*

3.4 Conclusions

In this chapter, transparent, glass-like HDPE films with outstanding mechanical properties were successfully prepared by solid-state drawing at elevated temperatures without the need of additives. The underlying mechanism and the effect of various parameters were systematically explored. HDPE films drawn at $T_d \geq 90$ °C had a transparent appearance, with a maximum transmittance of around 90 % at higher drawing temperatures. Increasing drawing temperatures led to higher transmittance values, however at the expense of mechanical properties, resulting in a practical drawing temperature window for transparent high strength HDPE films of 90−110 °C. Optical transmittance of the solid-state drawn HDPE films was optimum for a draw ratio of 15. Morphological observations revealed a reduction in microvoids parallel to the drawing direction with increasing drawing temperature most likely due to greater chain mobility and the formation of less interfibrillar defects. Microcracking perpendicular to the drawing direction was observed after ultra-drawing ($\lambda \geq 20$), leading to severe light scattering and reduced transparency in these highly fibrillar structures. At a drawing temperature of 90 °C and 100 °C, transparent solid-state drawn HDPE films ($\lambda = 20$) exhibited excellent mechanical properties with a maximum Young's modulus of 27 GPa and a maximum tensile strength of 800 MPa along the drawing direction. Thus, through carefully controlling drawing parameters, especially drawing temperature and draw ratio, highly oriented HDPE films could be obtained with high levels of optical clarity without the need for additives combined with mechanical properties which are more than 10 times greater than those of common transparent polymers like PC, PMMA and PS.

Chapter 4

A scalable continuous extrusion and drawing process for producing transparent high strength HDPE films

This chapter is partially reproduced from: Y. Lin, W. Tu, R. C. P. Verpaalen, H. Zhang, C. W. M. Bastiaansen, T. Peijs, *Macromol. Mater. Eng.* **2019**, *304* (8), 1900138.

4.1 Introduction

In Chapter 3, highly transparent ultra-drawn HDPE films with high mechanical properties were obtained by uniaxially stretching isotropic HDPE films in a specific temperature window in the solid state to a draw ratio of around 20. A transmittance of 90 % in the visible light range was achieved in both the near and far field, and a high modulus and strength of 27 GPa and 800 MPa were obtained when drawing was performed in a temperature window between 90 and 110 °C. Also, as mentioned in Section 2.3.3, Shen *et al.* added up to 5 wt.% of a 2-(2H-benzotriazol-2-yl)-4,6-ditertpentylphenol (BZT) additive to HDPE films which were then drawn to high draw ratios (~ 20), resulting in highly oriented polymer films with transmittance values of 90 % and a tensile strength of 650 MPa[75].

However, these oriented transparent HDPE films either with or without additives were all produced at lab-scale using batch-wise fabrication and drawing procedures. These procedures typically involved micro-compounding in the case of additives, compression moulding of films followed by solid-state drawing using a universal tensile tester equipped with a thermostatically controlled environmental chamber. Although a proof-of-principle was established, the process only yielded narrow (< 0.5 cm) films or tapes of limited length (< 30 cm), which seriously limits the use and evaluation of these films in single or multilayer laminates of larger dimensions.

In this chapter, a cast film extrusion and solid-state stretching line was employed for the scalable and continuous production of oriented HDPE films of high transparency and strength. The benefit of this processing approach lies in the use of conventional polymer processing equipment, which allows for a direct implementation into an industrial environment. The effects of using a specific drawing temperature as well as the addition of BZT on the degree of molecular orientation and microstructure, and optical and mechanical performance of the drawn HDPE films are explored in this chapter. In addition, the influence of pre-orientation as a result of extrusion draw down and two-step drawing is investigated as these variables could not be investigated in the batch-wise process in Chapter 3.

4.2 Experimental

4.2.1 Materials

One of the used HDPE grade was again Borealis VS4580 (Borealis AG, Austria), which has a number-average molecular weight ($\overline{M_n}$) of 37 kg/mol, a weight-average molecular

weight ($\overline{M_w}$) of 134 kg/mol and a molecular weight distribution (MWD) of 3.6. In Section 4.3.1−4.3.3, the used HDPE grade was all referred to Borealis VS4580; in Section 4.3.4, it was referred as HDPE 1. Another HDPE grade was Total M5510EP (Total Ecosolutions, Belgium) using metallocene as the catalyst, which was referred as HDPE 2 in Section 4.3.4. Total M5510EP has a T_m of 134 °C, a pellet density of 0.955 g/cm^3, a MFI of 1.2 g/10 min at 190 °C/2.16 kg, a $\overline{M_n}$ of 28 kg/mol, a $\overline{M_w}$ of 77 kg/mol and a MWD of 2.7. 2-(2H-benzotriazol-2-yl)-4,6-ditertpentylphenol (BZT) with molecular formula of $C_{22}H_{29}N_3O$ and a density of 1.170 g/cm^3 was provided by BASF (Germany, TINUVIN® 328). According to the datasheet of TINUVIN® 328, the weight loss of pure BZT substance is 1.0 % at a temperature of 183 °C measured with thermal gravimetric analysis (TGA) at a heating rate of 20 °C/min in air. TPU ST-6050 sheets were supplied by Schweitzer-Mauduit International, Inc. (USA).

4.2.2 Processing

For producing HDPE pellets with 2 wt.% BZT, a Dr. Collin ZK 25 × 40 (Germany) laboratory twin-screw compounder was used at 80 rpm and a die temperature of around 175 °C. At this mixing temperature, the weight loss of BZT particles is less than 1.0 % of the total amount of BZT which means that BZT has a high stability at this temperature. The BZT concentration used was based on a previous study by Shen *et al.*[75] who showed that drawn HDPE films containing 2 wt.% BZT could already transmit 90 % of visible light. After compounding, the extruded melt was cooled in a water bath and cut into pellets using a Dr. Collin CSG171 (Germany) strand pelletizer. The throughput of the compound was 1.5 kg/hr.

A Dr. Collin E20T (Germany) single screw extruder was used to extrude HDPE films as shown in ***Figure 4.1(a)***. A melt pump was used to control the throughput. The single screw extruder was operated at 45 rpm while the temperature of the slot die was around 200 °C. The extruded films were cooled by an X'plore (Netherlands) air knife before being collected using a flat-film take-off unit (Dr. Collin CR72T, Germany). The width and thickness of the slot die was 10 cm and 0.30−0.45 mm, respectively. The winding speed of the collector was about 0.6 m/min. The average thickness (t) of the extruded films was calculated using the following equation:

$$t\ (\mu m) = \frac{\rho_l (dtex)}{\rho (g/cm^3) \times w\ (cm) \times 100} \tag{4.1}$$

where ρ_l is the linear density of the extruded films, which is measured by weighing a certain length of film, ρ is the density of the films (0.958 g/cm^3 for neat HDPE and 0.962 g/cm^3 for HDPE + 2 wt.% BZT) and w is the width of the films.

An initial drawing process often called draw down which predominantly occurs in the melt will take place during cast film extrusion[178-179]. The draw down or pre-orientation ratio (λ_{pre}), was calculated as a geometric draw ratio using the following equation:

$$\lambda_{pre} = \frac{w_{slot} \times t_{slot}}{w_{extruded} \times t_{extruded}} \tag{4.2}$$

where w_{slot}, t_{slot}, $w_{extruded}$ and $t_{extruded}$ denote the width or thickness of the slot die or extruded films, respectively. The obtained thickness of as-extruded cast films after draw down (λ_{pre} = 4) was generally in the range of 100−200 μm.

The as-extruded HDPE films with and without BZT additives were subsequently drawn in the solid-state using a Dr. Collin MDO-A & MDO-B (Germany) uniaxial stretching line as shown in ***Figure 4.1(b)***. Based on the research in Chapter 3, the solid-state drawing

temperature was chosen at 105 °C in order to achieve highly transparent high strength HDPE films without the need to incorporate additives. The rotating speed of the rollers in part I and part II depended on the requested draw ratio, usually 0.10−0.20 m/min and 1.0−2.2 m/min, respectively. The machine direction (MD) corresponds to the drawing direction.

The average thickness (t) of the drawn films was also calculated using Equation (4.1), usually about 20−40 μm on the basis of the solid-state draw ratio (λ), which was calculated using the following equation:

$$\lambda = \frac{w_{extruded} \times t_{extruded}}{w_{drawn} \times t_{drawn}} \tag{4.3}$$

where $w_{extruded}$, $t_{extruded}$, w_{drawn} and t_{drawn} are the width or thickness of extruded films or drawn films, respectively.

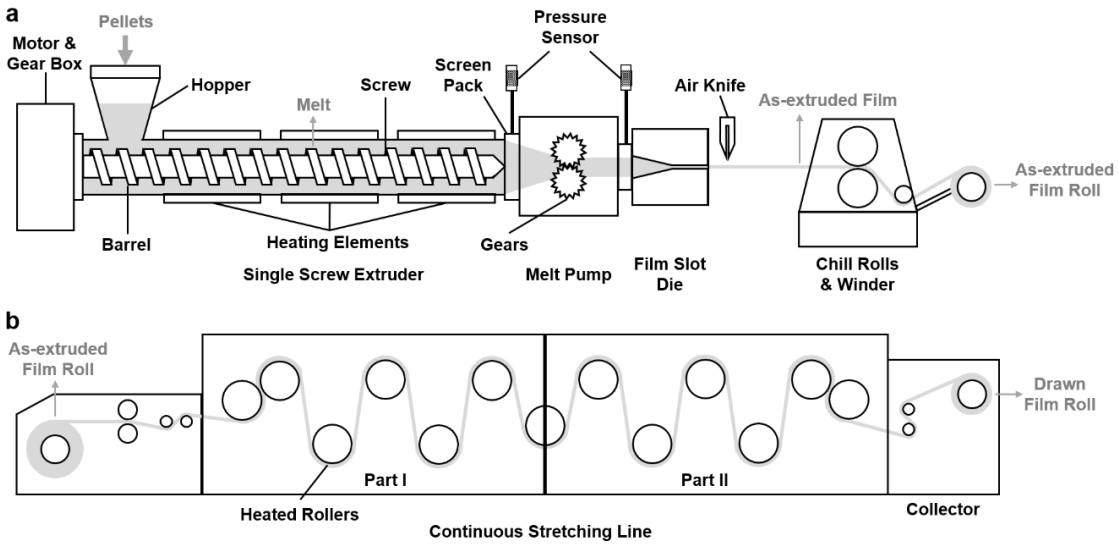

Figure 4.1 *Schematic diagram of (a) cast film extrusion and (b) solid-state drawing.*

In case of two-step drawing, the extruded films were drawn twice in the solid-state. For instance, films were first drawn to a draw ratio of 5 followed by a draw ratio of 2, making

a total $\lambda = 10$. The draw ratios of the 1st and 2nd drawing are called λ_1 and λ_2, respectively, that is $\lambda_1 = 5$ and $\lambda_2 = 2$ as in the above case. The drawing temperature in this multi-stage drawing process was again kept constant at 105 °C.

For purposes of comparison, isotropic compression moulded HDPE films ($\lambda_{pre} = 1$ and $\lambda = 1$) with a thickness of ~ 100 μm were prepared using a Dr. Collin P300E (Germany) hot press at 160 °C for 3 min and then cooled down to RT.

In order to eliminate light scattering from surface roughness effects[75], HDPE films with and without additives were sandwiched between two glass slides using TPU films as interlayers when testing optical performance. Compression moulding of these laminated structures was carried out in a Rondol (UK) hot press at 100 °C, 3 bar for 5−10 min.

4.2.3 Characterization

Transmittance spectra of laminates based on drawn HDPE films with and without additives were acquired using a PerkinElmer Lambda 950 (USA) UV-vis spectrometer in the wavelength regime of 400−700 nm at an interval of 1 nm. A sample-to-detector distance of 40 cm was used in order to obtain transmittance values in the far field rather than near field, which as mentioned in Chapter 3 is of greater practical importance for potential applications like glazing or windows. Transmittance measurements were carried out at least three times for each film.

Small-angle light scattering (SALS) of the laminated samples was carried out using a JDS Uniphase (USA) 15 mW helium-neon gas laser at a steady intensity with a wavelength of 633 nm as a light source. The sample-to-screen distance was fixed at 15.5 cm. The tested range of scattering vector (q) was 0.6−6 μm^{-1}, and therefore the corresponding detectable

microvoid size is around 3−25 μm[180]. V_v polarization patterns were obtained with the polarizer and the analyser set parallel to each other. The laminated samples were placed between polarizers with the MD of the oriented films perpendicular to the polarizers. The scattering vector (q) is calculated using the following equation:

$$q = \frac{4\pi \times \sin\theta}{\lambda} \tag{4.4}$$

where 2θ is the scattering angle and λ is the wavelength.

Young's modulus and tensile strength of the films were measured using an Instron 5566 (UK) universal tensile tester with manual wedge action grips at RT according to ASTM D882-18 standard. Rectangular test specimens with gauge dimensions of 100 mm × 10 mm were carefully cut from the films. The tensile tests were carried out at a pre-load of 0.2 N and at a crosshead speed of 50 mm/min, corresponding to a strain rate of 0.5 min^{-1}. Young's modulus was calculated from the tangent of the engineering stress-strain curve at a strain < 0.5 %. The average Young's modulus and tensile strength as well as their standard deviation were calculated using a minimum of five specimens in most cases, while in the case of the drawn HDPE films with λ = 13 and 19, the values were calculated from only three or four specimens due to the lack of samples.

Scanning electron microscopy (SEM) of HDPE films was carried out using a FEI Inspect F (Netherlands) at an acceleration voltage of 5 kV. Energy-dispersive X-ray spectroscopy (EDS) was measured using spot scan mode in combination with SEM. Wide-angle X-ray scattering (WAXS) and small-angle X-ray scattering (SAXS) were all carried out using a SAXSLAB Ganesha 300XL instrument (Denmark) with a Genix-Cu ultralow divergence source, which could emit X-ray photons with a wavelength of 1.54 Å at a flux of 10^8 photons per second. Diffraction patterns of the films were collected on a Dectris Pilatus

300K silicon pixel detector with 487 × 619 pixels. The detector possessed three plates with a total area of 172 μm^2 and intervals between each of the plate was 17 pixels, leading to two straight dark bands in the diffraction pattern. The sample-to-detector distance was 91 mm for WAXS and 1491 mm for SAXS, respectively. The q range of SAXS tests was 0.006−0.1 Å^{-1}, which corresponds to a detectable nanovoids' dimension (d) of less than 105 nm as estimated by equation $d = 2\pi/q$[181-182]. The beam centre and the scattering vector (q) of the WAXS and SAXS images were calibrated using the diffraction peaks of a silver behenate (AgBeh) standard in SAXSGUI software, while the q value was calculated using Equation (4.4).

Crystallinity (X_c) could be calculated from the WAXS data using the following equation[75]:

$$X_c = \frac{I_{110}+1.46I_{200}}{I_{110}+0.75I_a+1.46I_{200}} \times 100\% \quad (4.5)$$

where I_{110}, I_a and I_{200} denote the integrated areas of the (110), amorphous and (200) peak of polyethylene, respectively.

Hermans' orientation factor (f_c) is usually used to quantify the degree of the orientation of drawn polymeric samples[183-184]. For uniaxial orientation along the MD, f_c was calculated from the WAXS data using the following equation:

$$f_c = \frac{3<\cos^2\beta_c>-1}{2} \quad (4.6)$$

where β_c is the angle between the chain axis and the MD. For polyethylene, $<cos^2\beta_c>$ equals to[184]:

$$<\cos^2\beta_c> = 1 - 0.565 <\cos^2\beta_{200}> - 1.435 <\cos^2\beta_{110}> \quad (4.7)$$

where β_{110} and β_{200} are the angles between the MD and (110) or (200) peak, and $<cos^2\beta_x>$ is defined by the following equation:

$$< \cos^2 \beta_x >= \frac{\int_0^{\frac{\pi}{2}} I(\beta_x) \cos^2 \beta_x \sin \beta_x d\beta_x}{\int_0^{\frac{\pi}{2}} I(\beta_x) \sin \beta_x d\beta_x} \tag{4.8}$$

where x represents (110) or (200) peak, and $I(\beta_x)$ is the scattering intensity along the angle β_{110} or β_{200}.

The long period (L_p) in HDPE films was calculated using the Bragg equation[185]:

$$L_p = \frac{2\pi}{q_{max}} \tag{4.9}$$

where q_{max} is the peak value of the scattering vector (q) in the Lorentz-corrected intensity (I) versus scattering vector curve.

Lamellar thickness (L_c) could be estimated from the long period according to a two-phase model using the following equation[186]:

$$L_c = L_p \times X_c \tag{4.10}$$

where X_c is the crystallinity of the HDPE films measured by WAXS.

4.3 Results and discussion

4.3.1 The effect of additive and additive-free technology on properties and structures of continuously extruded and drawn HDPE films

The appearance of the as-extruded HDPE films with and without BZT additive at a draw down or pre-orientation ratio (λ_{pre}) of 4 is milky and opaque as shown in ***Figure 4.2(a)***, whereas after solid-state drawing at 105 °C to a draw ratio (λ) of 10, the films have quite a clear appearance (***Figure 4.2(b)***).

It should be noted that the fluctuations in film thickness along both widthwise and lengthwise directions always exist in the extruded as well as the solid-state drawn HDPE films no matter with or without BZT. Along the widthwise direction, the edges are usually thicker and have a higher molecular chain orientation compared to the middle part of the extruded films due to a higher shear stress at the edges. This effect results in the thickness fluctuations in the following solid-state drawn films, which possibly leads to the fibrillation and the split along the MD especially when drawn to a high draw ratio (> 22). The lengthwise thickness fluctuations can be attributed to the unstable pressure during extrusion. In practice, these thickness fluctuations will result in the different optical and mechanical properties regarding to the positions of the films. Here, the properties mentioned in this Chapter are all referred to the average properties of the films.

Figure 4.2(c) shows that the transmittance of the HDPE films in the visible light wavelength regime significantly increases after solid-state drawing. Moreover, both solid-state drawn HDPE films with and without BZT additive show similar transmittance values at a wavelength of 550 nm at equal draw ratios (***Figure 4.2(d)***). It is noteworthy that a transmittance value of nearly 91 % can be achieved for both types of films at high

draw ratios ($\lambda \geq 10$) even in the far field, which is close to glass (~ 92 %). This means that solid-state drawing of HDPE films carried out at a temperature of 105 °C and of films with BZT additive in both cases leads to highly transparent HDPE films after drawing.

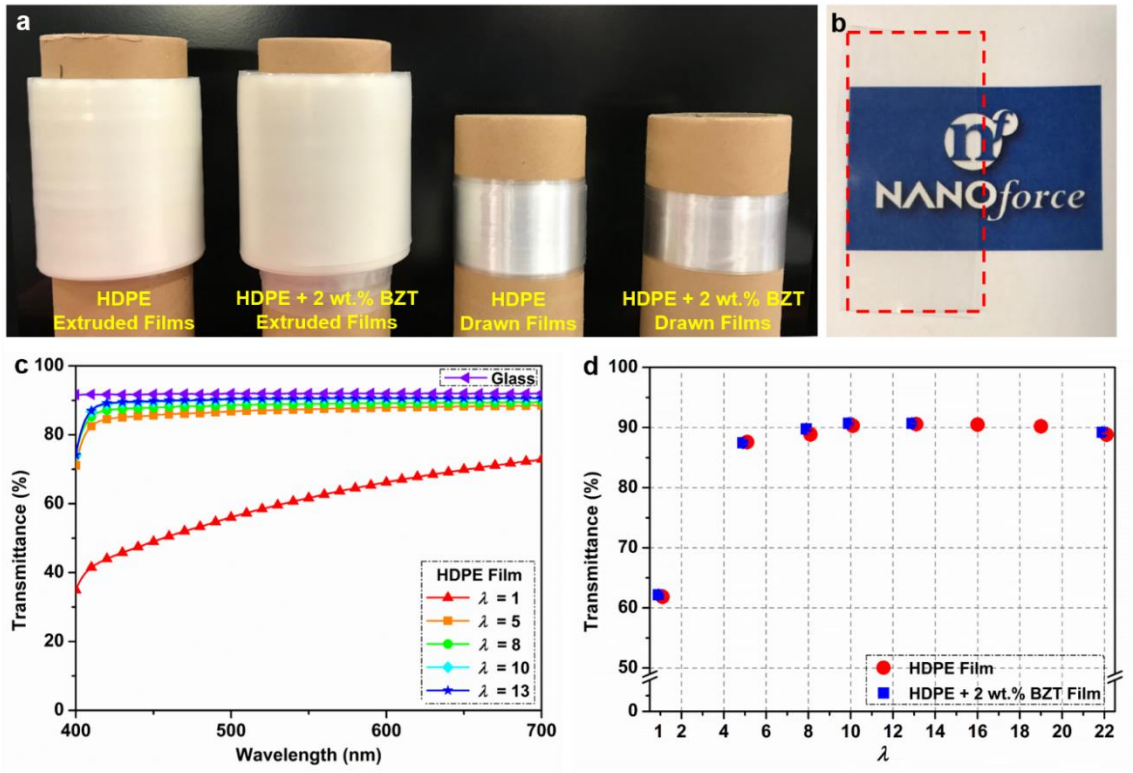

Figure 4.2 *(a) Photographs of as-extruded (λ_{pre} = 4) and drawn (λ = 10) HDPE film rolls with and without BZT additives and (b) the appearance of drawn HDPE films with λ_{pre} = 4 and λ = 10 (marked and located between the dashed red lines), showing a high transparency after solid-state drawing. (c) Transmittance of HDPE films in the visible spectrum range and (d) transmittance of HDPE and HDPE + 2 wt.% BZT films (λ_{pre} = 4) drawn at 105 °C to different draw ratios at a wavelength of 550 nm and a 40 cm sample-to-detector distance (far field), illustrating similar optical performance of films with and without additives when drawn at 105 °C. For transmittance test, the films were sandwiched between TPU interlayers and glass to eliminate surface light scattering effects.*

As Chapter 3 already showed, a relatively high drawing temperature facilitates greater chain mobility and the formation of less interfibrillar defects, leading to a reduction in the formation of microvoids in the bulk or on the surface of the films. Suitable additives like BZT, having a similar refractive index to HDPE, can fill such voids and reduce the mismatch of refractive indices between HDPE and the voids[75]. What's more, it was observed that these films reached an optimum transmittance value at λ = 13−16. This phenomenon can be explained by the formation of microvoids and microcracks parallel or perpendicular to the machine direction (MD) at higher draw ratios (λ > 16) as described in Chapter 3.

Figure 4.3 shows the Young's modulus and the tensile strength of solid-state drawn HDPE films with and without BZT additives along the MD as a function of draw ratio. Both modulus and strength increase with draw ratio for both types of HDPE films. The stress-strain curves of ultra-drawn HDPE films with λ = 22 both with and without BZT additive (see ***Figure 4.4***) illustrate that the films fail at an elongation (ε) of 8−9 % and possess a maximum attainable modulus of ~ 33 GPa and a maximum tensile strength of ~ 900 MPa along the MD. These moduli and strength values are similar to those of unidirectional glass fibre reinforced plastics but at about half the density. The maximum achievable modulus and strength exceeds nearly 15 times that of common transparent polymeric materials like PC and PMMA. Moreover, on a weight basis these polymeric films even outperform a lightweight engineering materials like aluminium with a specific modulus and tensile strength of, respectively 34 GPa/(g·cm^{-3}) and 940 MPa/(g·cm^{-3}) for HDPE (along the MD) versus 26 GPa/(g·cm^{-3}) and 125 MPa/(g·cm^{-3}) for aluminium. Mechanical properties of uniaxially stretched polyethylene films along the transverse direction (TD) are however usually much lower, with typical moduli and strengths of ~ 2 GPa and ~ 15 MPa according to the previous study[176].

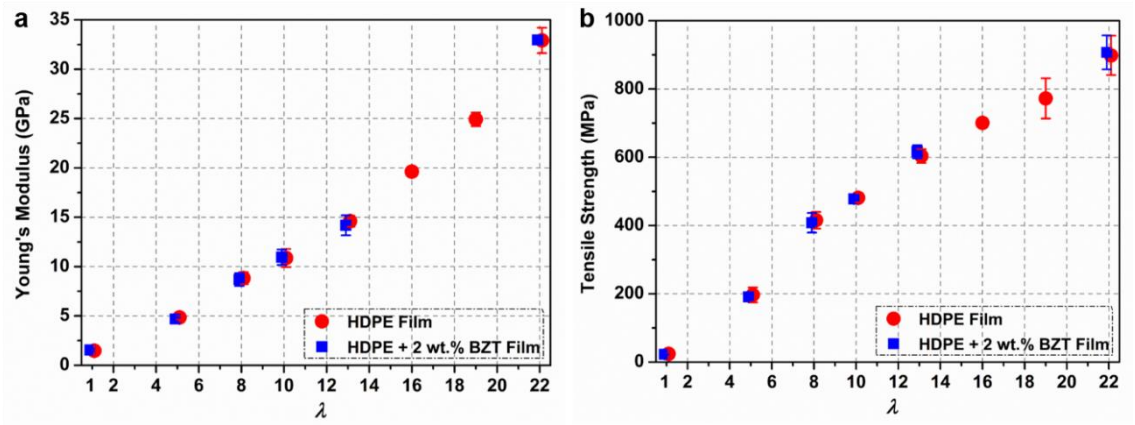

Figure 4.3 *(a) Young's modulus and (b) tensile strength of HDPE films with and without BZT additives (λ_{pre} = 4) along the MD as a function of draw ratio, indicating similar mechanical properties for HDPE films with and without additives when drawn at 105 °C.*

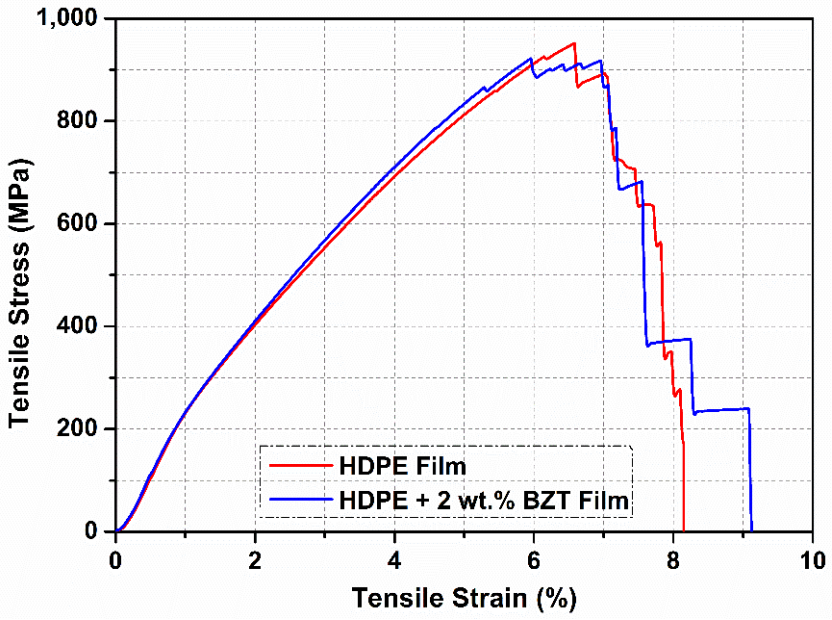

Figure 4.4 *Stress-strain curve of HDPE films (λ_{pre} = 4) with a draw ratio of 22 with and without BZT additives.*

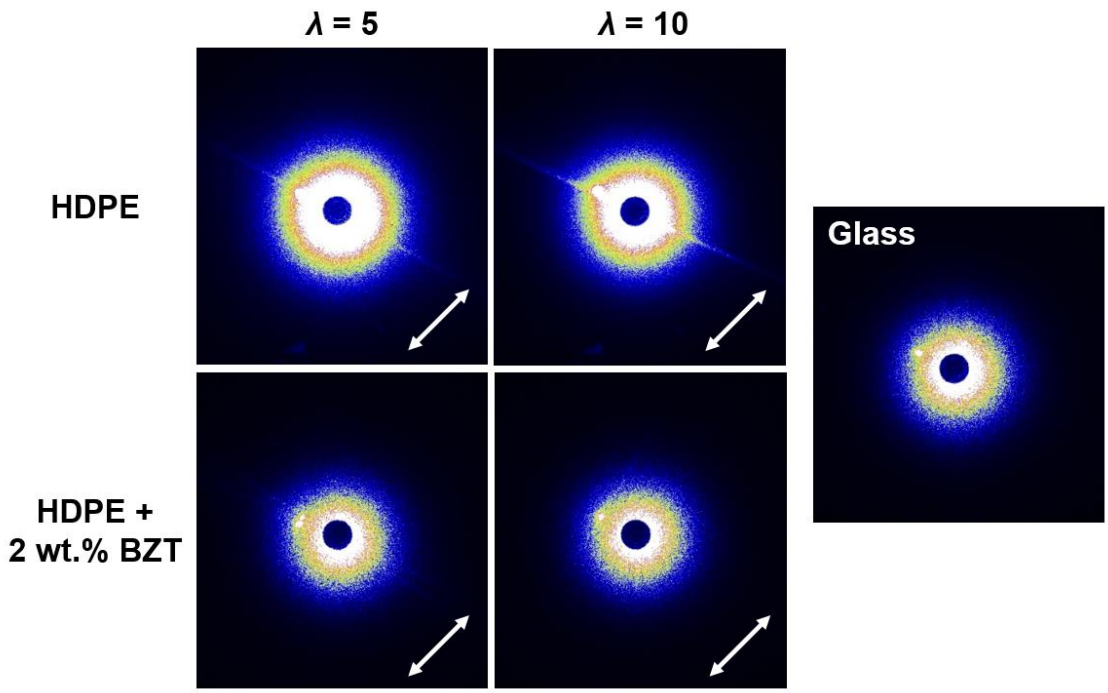

Figure 4.5 *SALS images of glass, drawn HDPE films with and without BZT additives (λ_{pre} = 4) at λ = 5 and λ = 10, indicating negligible light scattering from remaining microvoids for both types of films. The films were sandwiched between glass and TPU interlayer to eliminate surface light scattering effects, and the arrows show the MD of the films.*

SALS under V_v polarization mode is generally carried out to detect light scattering from a perspective of density fluctuations[187]. In ***Figure 4.5***, relatively weak light scattering can be seen in the drawn HDPE films, indicating that only a small amount of microvoids exist in these films along the MD. The crystalline phase of HDPE can undergo plastic flow[188]. Quenching results in a weaker crystalline phase which can undergo plastic flow and crystalline block slip[189-190]. Moreover, drawing at temperatures well above the α-relaxation temperature of polyethylene, which is expected to be around 80 °C, results in greater chain transport and mobility in the crystalline phase and less cavitation[191-192]. Chain transport avoids the build-up of triaxial stresses between crystals. These stresses are responsible for cavitation and void formation during drawing, leading to light

scattering and an opaque appearance of the films. Drawing at temperatures well above the α-relaxation temperature lowers these stresses, leading to highly transparent HDPE films even without the use of additives (***Figure 4.2(b)***). HDPE films with BZT additives show even less scattering after drawing with patterns similar to glass. However, the small amount of light scattering still present in the films without BZT hardly affects the transparency of these films (***Figure 4.2(d)***). Clearly it is the small number of remaining (unfilled) microvoids in both types of HDPE films that is responsible for the high clarity of both films after drawing.

Although nano-sized defect structures that are smaller than the wavelength of visible light in principle may not contribute to light scattering, these nanovoids might aggregate and develop into microvoids[193]. In the insets of ***Figure 4.6***, the 2D-SAXS images of extruded HDPE films with and without additives ($\lambda_{pre} = 4$, $\lambda = 1$) show tear-drop shaped meridional lobes parallel to the MD. This SAXS pattern can be interpreted in terms of a two-phase system of lamellae and amorphous regions, where the stacks of lamellae are slightly oriented perpendicular to the MD in the extrusion process[184]. After solid-state drawing to $\lambda = 10$, the 2D-SAXS pattern increases in intensity to a two-point layer-like pattern with two sharp meridional spots situated on each side of the beam stop, illustrating that a highly-aligned lamellar structure is generated[70]. Moreover, a streak-like scattering across the beam stop (indicated by the yellow solid single-headed arrow in the insets of ***Figure 4.6***) perpendicular to the MD is observed for the drawn films as a result of differences in electron density between polymer and voids together with the formation of a fibrillar structure along the MD after solid-state drawing[194-195]. The morphology of the extruded HDPE films ($\lambda = 1$) with and without BZT additives (shown in ***Figure 4.7***) does not show a surface structure after pre-orientation, whereas the drawn HDPE films ($\lambda = 10$) show a highly fibrillar surface structure after solid-state drawing. Since the fibrillar structure of

the drawn HDPE films is similar for the same solid-state draw ratio, the differences in the streak intensity at identical draw ratios is expected to come from the presence of voids parallel to the MD[77]. The scattering vector (q) range of SAXS test was 0.006−0.1 Å^{-1}, corresponding to a detectable nanovoids' dimension (d) of less than 105 nm as estimated from equation $d = 2\pi/q$[181-182]. In the corresponding 1D-SAXS curves (***Figure 4.6***), the 1D scattering intensity (I) at low q value corresponds to the intensity of the streak. It demonstrates that the scattering intensity of the streak is similar for HDPE films with and without BZT additives at equal draw ratios. This outcome suggests that the lateral and longitudinal dimensions of voids inside both types of films are similar, explaining the high transparency of both solid-state drawn films after drawing at a temperature of 105 °C.

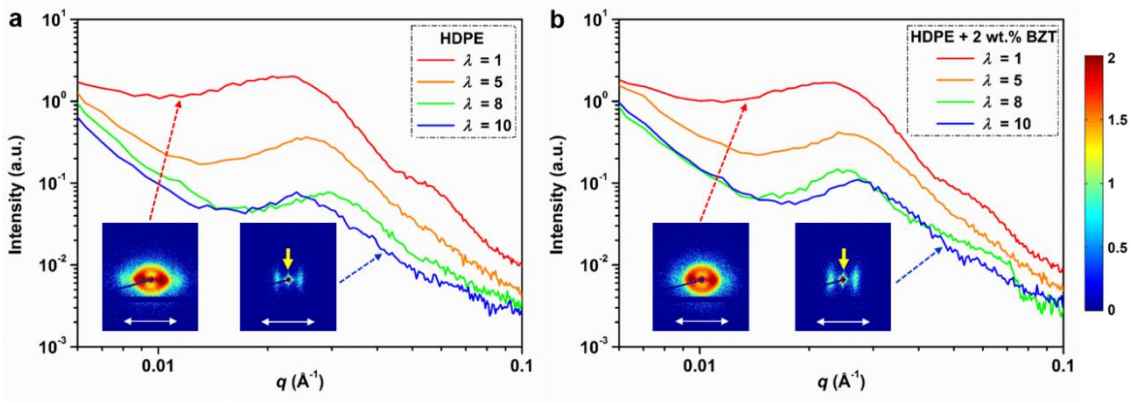

Figure 4.6 *1D-SAXS curves of scattering intensity in HDPE films (a) with and (b) without BZT additives (λ_{pre} = 4) at different draw ratios as a function of scattering vector, suggesting the presence of only a small amount of nanovoids in both films. The insets are the corresponding 2D-SAXS patterns of films at λ = 1 and λ = 10, the yellow solid single arrows indicate the streak-like scattering while the white double arrows represent the MD.*

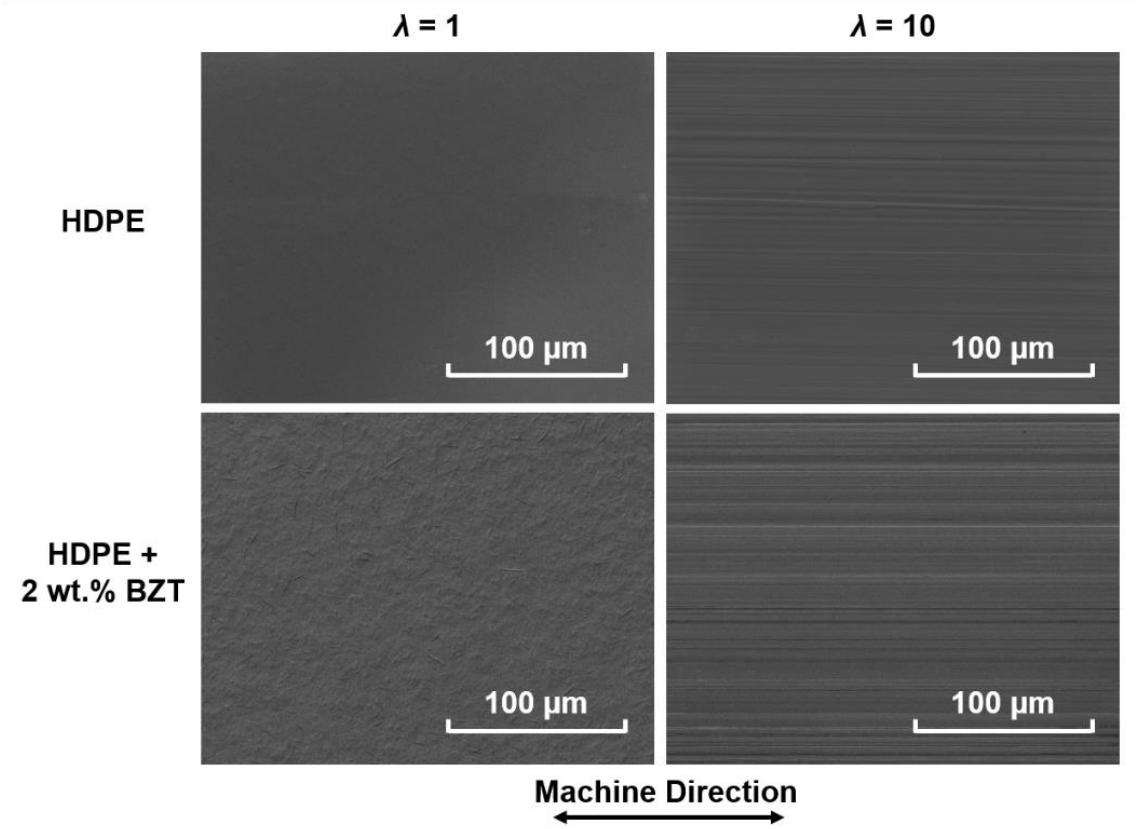

Figure 4.7 *SEM images of the extruded (λ = 1) and drawn (λ = 10) HDPE films with and without BZT additives (λ_{pre} = 4), showing the formation of a fibrillar structure after solid-state drawing.*

With increasing draw ratio, typical (110) and (200) reflections of the orthorhombic polyethylene unit cell in the WAXS patterns become more apparent and more oriented as shown in ***Figure 4.8***. At λ = 1 the WAXS pattern shows a fairly diffuse ring typical for an isotropic semi-crystalline polymer, suggesting negligible molecular orientation, while the film drawn to λ = 10 shows sharp spotty reflections, revealing high chain orientation along the MD for this sample. The Hermans' orientation factor (f_c) in ***Table 4.1*** increases rapidly at relatively low draw ratios ($\leq$ 5), suggesting higher crystal alignment and chain orientation along the MD with solid-state drawing[184, 196]. Hermans' orientation factor saturates at higher draw ratios, meaning that there is no major increase in the molecular orientation and crystal orientation remains more or less constant at draw ratios above 8.

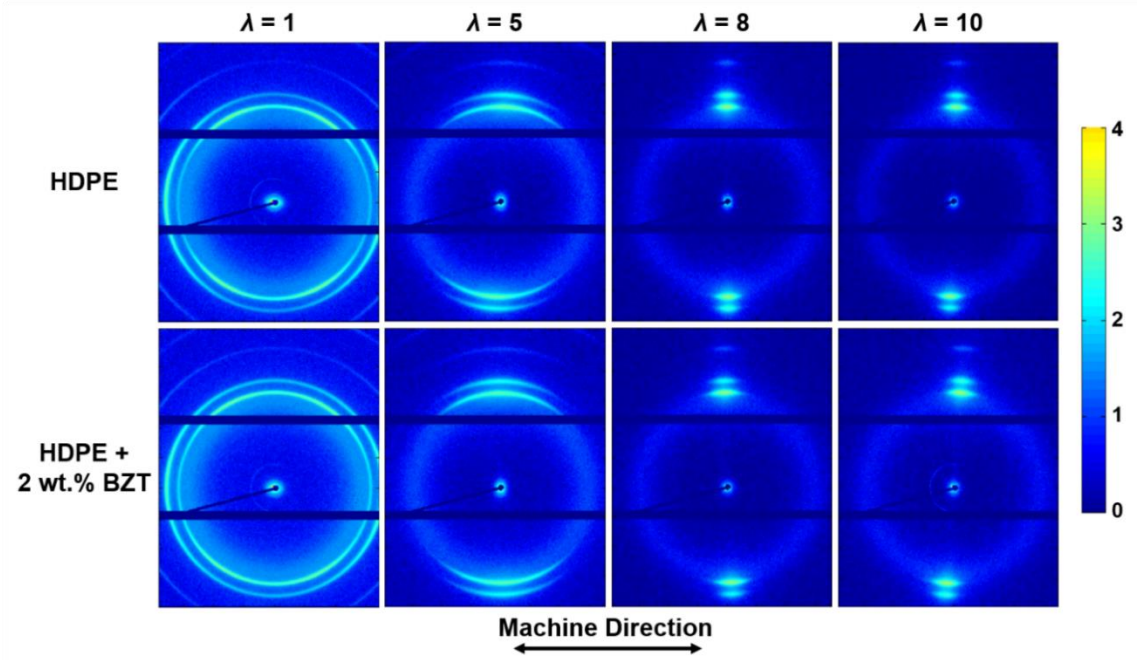

Figure 4.8 *WAXS images of HDPE films with and without BZT additives (λ_{pre} = 4) drawn at 105 °C to different draw ratios, showing a similar transition from isotropic to oriented structure with draw ratio for both types of films.*

Crystallinity (X_c) partially declines at low draw ratios ($\lambda \leq 5$) which is related to the breakup of lamellar crystallites at the early stages of drawing[118]. Then X_c increases with further drawing because of the transformation from microfibrils to chain-extended and highly-aligned structures during deformation, leading to a reduction in amorphous regions and therefore an increase in overall crystallinity[197]. However, X_c only goes up slightly at higher draw ratios. This effect results from the increased continuity of the lamellar blocks according to Peterlin's molecular deformation model as mentioned in Section 2.4[116-117], and these loading blocks contribute to a high modulus and strength at a high draw ratio after solid-state drawing as shown in ***Figure 4.3***. Furthermore, it should be noted that WAXS patterns, X_c, f_c, L_p and L_c of HDPE films with and without BZT additives are similar for each draw ratio (***Figure 4.8*** and ***Table 4.1***). This means there is little difference in microstructure of both types of HDPE films.

Table 4.1 *Crystallinity (X_c), Hermans' orientation factor (f_c), long period (L_p) and lamellar thickness (L_c) of HDPE films drawn at 105 °C with and without BZT additives with different pre-orientation ratios (λ_{pre}) and draw ratios (λ) from the WAXS and SAXS data.*

HDPE Films	λ_{pre}	λ_1	λ_2	X_c [%]	f_c	L_p [nm]	L_c [nm]
Neat HDPE	4			65.8	/	30.3	19.9
	4	5		62.7	0.805	25.1	15.8
	4	8		63.8	0.896	22.9	14.6
	4	10		65.6	0.911	26.7	17.5
	4	5	2	65.9	0.907	27.5	18.1
	4	19		67.7	0.926	26.7	18.1
	18			68.4	/	29.0	19.8
	18	5		63.0	0.874	26.2	16.5
HDPE +	4			64.1	/	30.0	19.2
2 wt.% BZT	4	5		62.5	0.803	25.2	15.8
	4	8		64.4	0.894	25.6	16.5
	4	10		65.9	0.907	23.6	15.6

It is noteworthy that in the case of HDPE + 2 wt.% BZT, some powders started to appear on the surface of the drawn films after 6 months storage in a sealed box at RT as shown in ***Figure 4.9(a)*** and ***Figure 4.9(b)***. SEM images in combination with EDS analysis corroborated that BZT particles were present on the surface of these HDPE films. As a result, transmittance values of the films dropped by 1−5 % compared to corresponding freshly drawn films (see ***Table 4.2***). However, the presence of these powders on the HDPE film surface did not significantly affect the clarity of the final laminates when these films were sandwiched between glass slides and TPU interlayers. Freshly drawn HDPE + 2 wt.%

BZT films showed that hardly any BZT particles were present on the surface of these films (***Figure 4.9(c)***) while drawn HDPE films without additives maintained their highly transparent character even after long-term storage (over 6 months) in a sealed box at RT (***Figure 4.9(d)***). This phenomenon of BZT powders migrating to the surface of the films after long periods of time implies that BZT is not all that stable and compatible with HDPE. Clearly this is a disadvantage of the BZT-based technology, while an additional compounding step before film extrusion is also necessary when using such additives, adding costs compared to a methodology which is merely based on an optimized drawing temperature and draw ratio. In addition, the cost of such additives is usually high. On the whole, it can therefore be concluded that solid-state drawing at an optimal drawing temperature of 105 °C without additives is therefore the preferred method to achieve cost-effective highly transparent HDPE films with excellent mechanical performance.

Table 4.2 *Transmittance values of HDPE + 2 wt.% BZT films (λ_{pre} = 4) with λ = 5 and λ = 10 at different wavelengths. Freshly drawn and after 6 months storage in a sealed box at RT.*

HDPE Films	**700 nm**	**550 nm**	**400 nm**
Freshly drawn (λ = 5)	88.8 ± 0.2 %	87.5 ± 0.4 %	67.0 ± 0.8 %
After 6 months (λ = 5)	87.5 ± 0.6 %	85.7 ± 1.0 %	61.5 ± 2.1 %
Freshly drawn (λ = 10)	90.9 ± 0.1 %	90.7 ± 0.1 %	73.5 ± 0.3 %
After 6 months (λ = 10)	89.7 ± 0.3 %	89.3 ± 0.2 %	70.2 ± 0.3 %

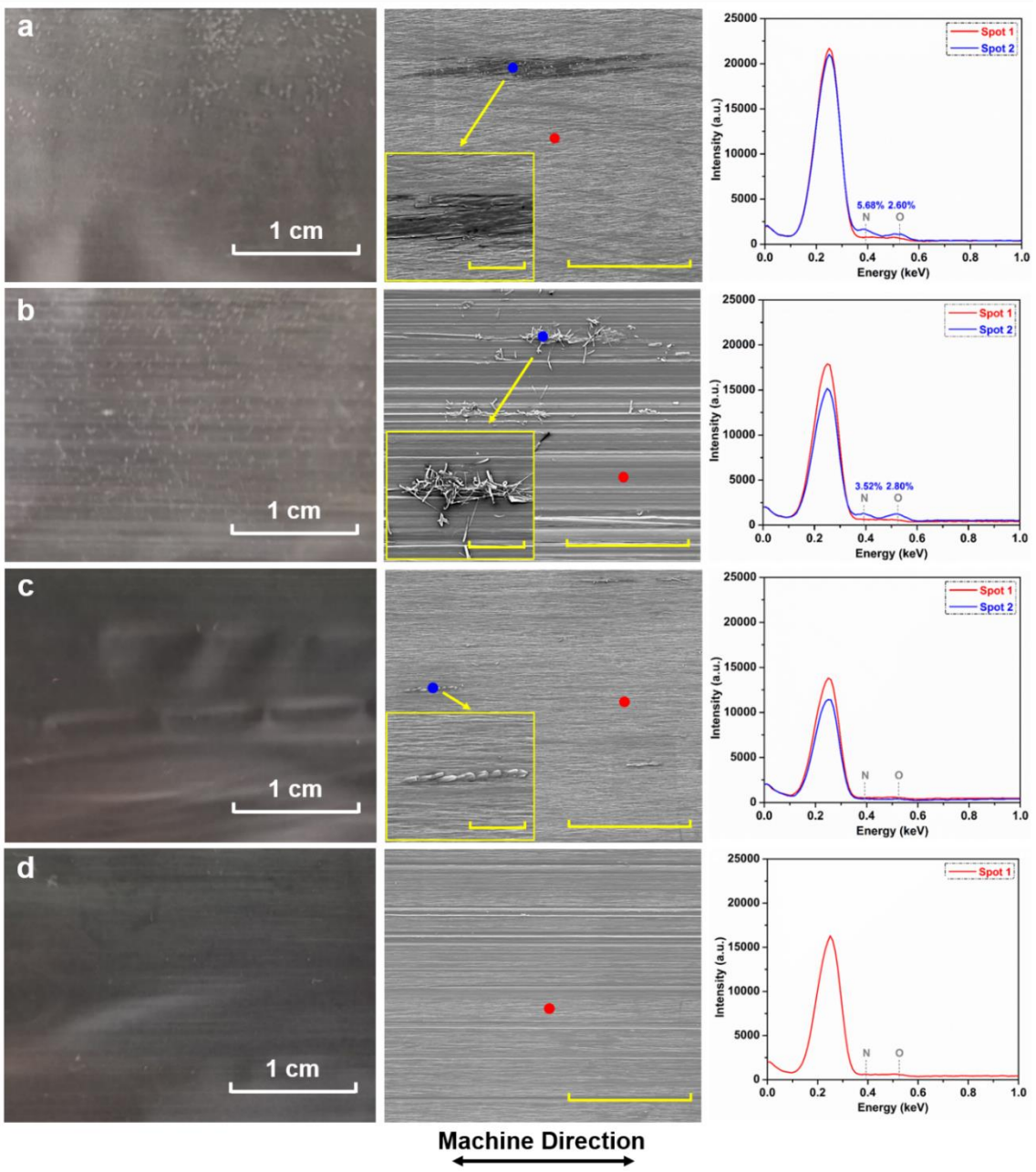

Figure 4.9 *Appearance, SEM images and EDS analysis of drawn HDPE + 2 wt.% BZT at (a) λ = 5 and (b) λ = 10 after 6 months storage in a sealed box at RT, (c) freshly drawn HDPE + 2 wt.% BZT films with λ = 8 and (d) drawn HDPE films (λ = 10) after 6 months storage in a sealed box at RT, showing some BZT powders on the surface of the films. The scale bar for the SEM images and the inlets are 100 μm and 20 μm, respectively.*

4.3.2 The influence of pre-orientation and draw down on properties and structure of continuously extruded and drawn HDPE films

Figure 4.10 shows that the draw down or pre-orientation ratio (λ_{pre}) has a significant effect on mechanical properties of the films after solid-state drawing. Here, the pre-orientation ratio is defined as a geometric pre-orientation draw ratio. When λ_{pre} is increased, the slope of the modulus and strength versus draw ratio curves becomes significantly steeper (***Figure 4.10(a)*** and ***Figure 4.10(b)***). A more than 55 % increase in Young's modulus and tensile strength of HDPE films at λ = 5 can be observed when λ_{pre} is increased from 4 to 18. WAXS patterns shown in ***Figure 4.11*** and f_c listed in ***Table 4.1*** show a higher degree of chain orientation in the drawn HDPE films with λ_{pre} = 18. Moreover, due to some induced chain pre-orientation during draw down of the melt in cast film extrusion, the strength of these extruded and drawn films is higher than batch-wise processed films as reported in Chapter 3 and previous studies[75]. More importantly, the transmittance values of the solid-state drawn HDPE films with different λ_{pre} still remain high (~ 90 %) and barely change with draw ratio as shown in ***Table 4.3***. Nevertheless, a high geometric pre-orientation draw ratio usually does not result in significant structure changes at the molecular level in the pre-oriented HDPE films drawn in the melt state due to a high degree of chain relaxation occurred at a temperature above its melting temperature. The effective strain, which leads to the changes of internal structures and properties, is limited when stretched in the melt state.

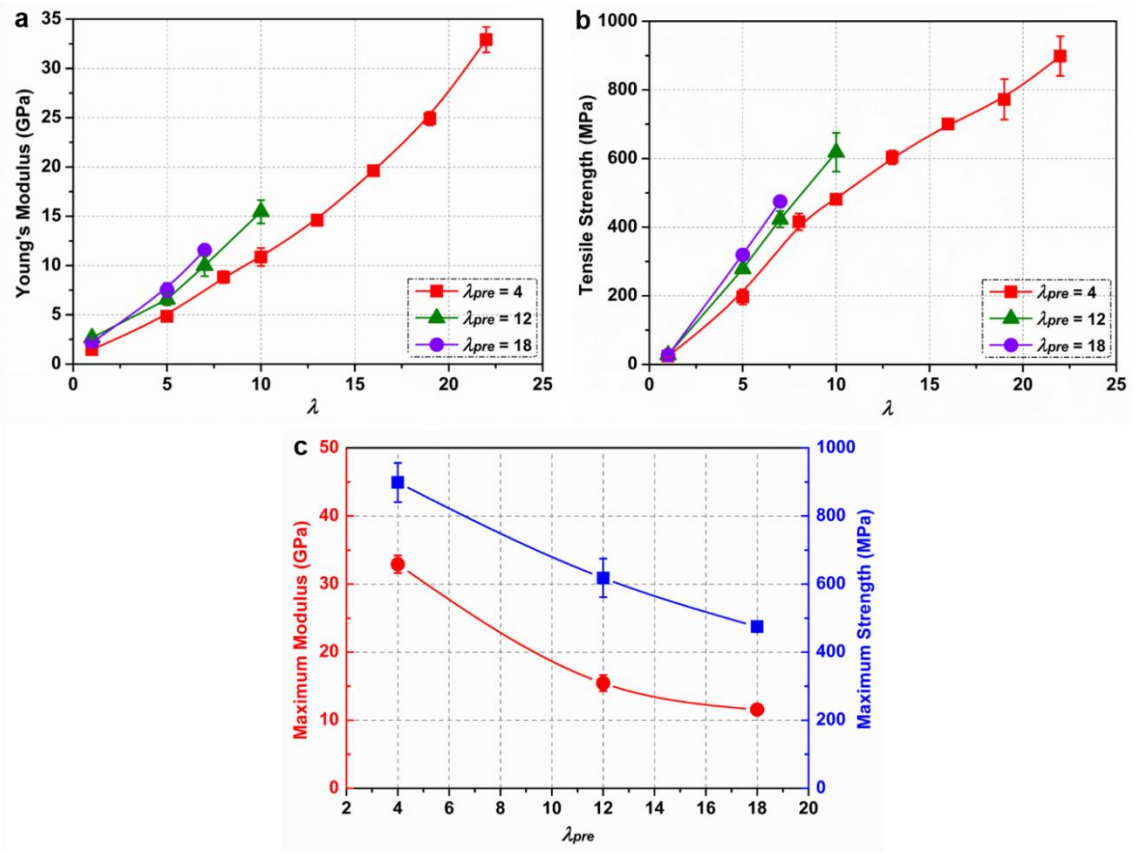

Figure 4.10 *(a) Young's modulus and (b) tensile strength of solid-state drawn HDPE films versus draw ratio with different pre-orientation ratios and (c) maximum modulus and strength of drawn HDPE films as a function of pre-orientation ratio. These results indicate that a high* λ_{pre} *will lead to better mechanical properties at equal draw ratios but poor ultimate mechanical properties.*

However, the maximum attainable solid-state draw ratio (λ_{max}) of HDPE films is only 10 for λ_{pre} = 12 and 7 for λ_{pre} = 18, respectively. The maximum modulus and strength of the films therefore drops with increasing λ_{pre} (***Figure 4.10(c)***). This reduction in ultimate mechanical properties with increasing λ_{pre} is the result of a certain degree of chain alignment along the MD in the melt state during the film extrusion process[198-199]. Thus, the draw down or pre-orientation ratio ought not to be chosen too high for the purpose of achieving a high ultimate mechanical performance.

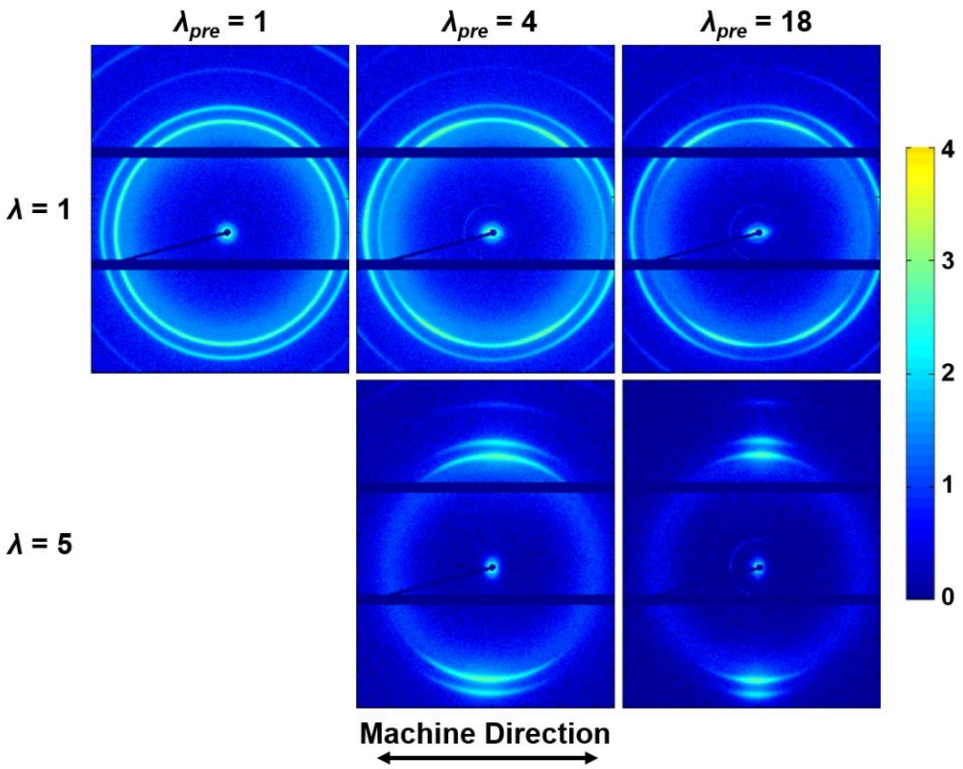

Figure 4.11 *2D-WAXS patterns of HDPE films with different pre-orientation ratios and draw ratios, showing higher orientation along the MD with increasing λ_{pre} at the same λ.*

Table 4.3 *Transmittance at 550 nm of HDPE films with different pre-orientation (λ_{pre}) and draw ratios (λ).*

HDPE Films	λ_{pre} = 4	λ_{pre} = 12	λ_{pre} = 18
λ = 5	87.6 ± 0.5 %	89.7 ± 0.1 %	89.3 ± 0.4 %
λ = 7	88.6 ± 0.3 %	90.0 ± 0.2 %	90.0 ± 0.3 %
λ = 10	90.3 ± 0.2 %	90.4 ± 0.1 %	/

4.3.3 The influence of two-step drawing on properties and structure of continuously extruded and drawn HDPE films

As for the importance of two-step drawing, the transmittance, Young's modulus and tensile strength of films fabricated by such a two-step drawing process were all very

similar to those made using a one-step drawing process (***Table 4.4***). Previous work on poly(oxymethylene) (POM) which has similar drawing behaviour as LPE and PP also suggested that there is no significant advantage of using a two-step drawing process instead of a one-step drawing process in terms of achieving ultimate mechanical properties[200]. The SEM images, WAXS patterns, X_c, f_c, L_p and L_c from ***Table 4.1*** and ***Figure 4.12*** show great similarities between them. These results suggest that a two-step drawing process did not significantly alter film morphology, crystallinity, degree of orientation or optical and mechanical properties.

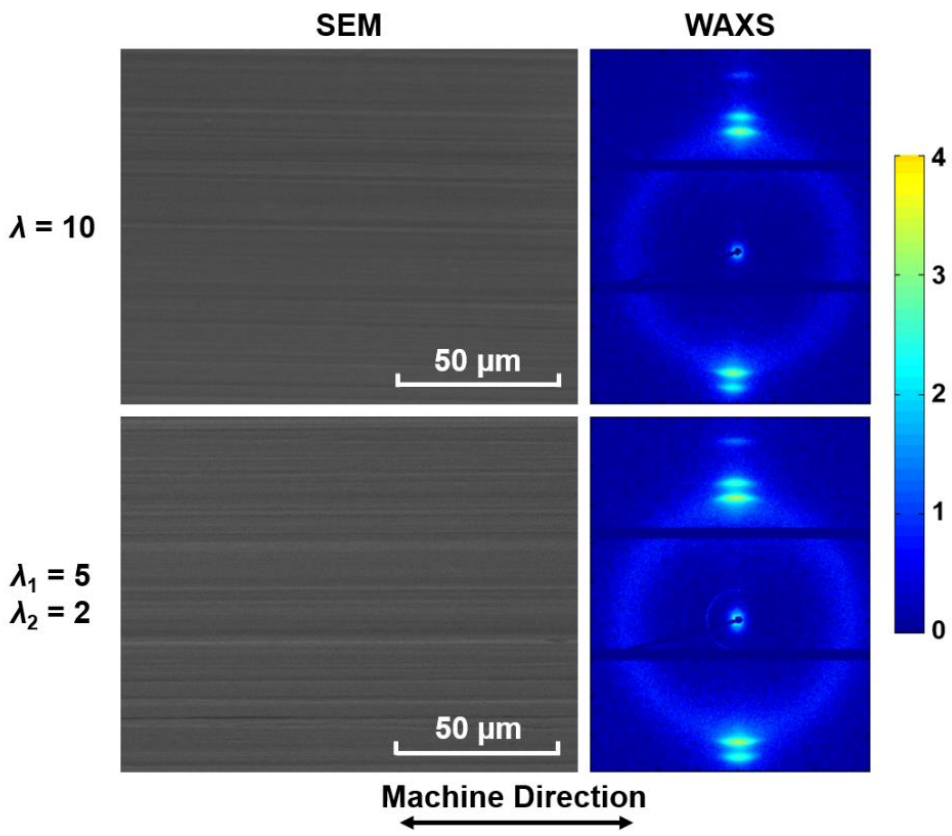

Figure 4.12 *SEM and WAXS images of HDPE films (λ_{pre} = 4) after one-step and two-step drawing, indicating similar surface morphologies and polymer orientation.*

Table 4.4 *Transmittance at 550 nm and mechanical properties of drawn HDPE films (λ_{pre} = 4 and λ = 10) by one-step and two-step drawing process.*

HDPE Films	Transmittance [%]	Modulus [GPa]	Strength [MPa]
One-step Drawing	90.3 ± 0.2	10.87 ± 0.92	481 ± 14
Two-step Drawing	90.0 ± 0.2	10.76 ± 0.75	483 ± 34

4.3.4 The influence of molecular weight on properties of continuously extruded and drawn HDPE films

It is widely acknowledged that the molecular weight and the molecular weight distribution have a significant influence on the drawing behaviour and ultimate mechanical performance of LPE products[110, 112, 123], whereas its effect on optical transparency was only partially studied. As mentioned in Section 2.3.3, it was previously discovered that LPE films with a relatively high $\overline{M_w}$ (~ 400 kg/mol) or a high MWD (> 20) possess good optical transparency after solid-state drawn to a relatively low draw ratio (~ 10) without adding additives[77, 95]. However, solid-state drawn LPE films with $\overline{M_w}$ < 140 kg/mol and MWD < 10 were normally opaque. Here, two grades of HDPE within this molecular weight range were chosen and their optical as well as mechanical properties were measured and compared. HDPE 1 refers to Borealis VS4580 with a $\overline{M_n}$ of 37 kg/mol, a $\overline{M_w}$ of 134 kg/mol and a MWD of 3.6, and HDPE 2 with a lower number-average and weight-average molecular weight refers to Total M5510EP (having a $\overline{M_n}$ of 28 kg/mol, a $\overline{M_w}$ of 77 kg/mol and a MWD of 2.7).

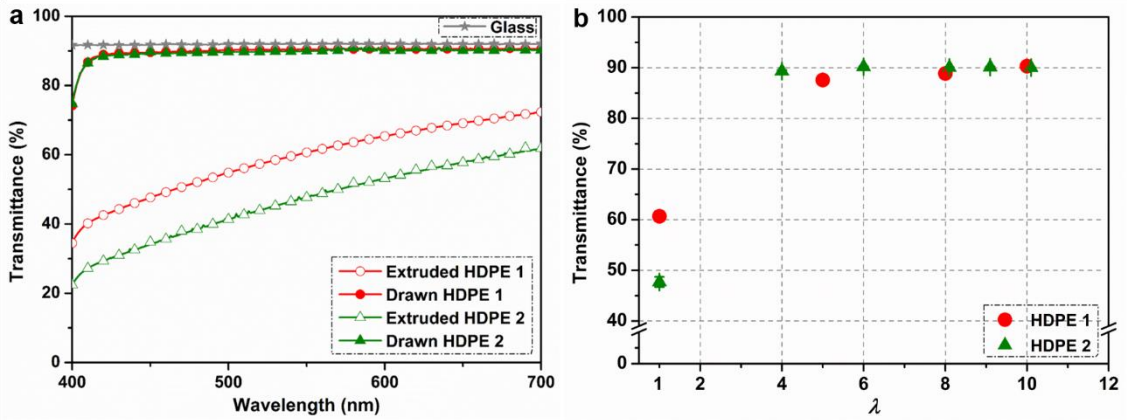

Figure 4.13 *(a) Transmittance of as-extruded (λ_{pre} = 4) and drawn (λ = 10) HDPE 1 and HDPE 2 films in the visible spectrum range and (b) transmittance of HDPE 1 and HDPE 2 films (λ_{pre} = 4) drawn at 105 °C to different draw ratios measured at a wavelength of 550 nm and a 40 cm sample-to-detector distance, illustrating similar optical performance of both kinds of drawn HDPE films. The films were sandwiched between TPU interlayers and glass to eliminate surface light scattering effects.*

Figure 4.13 shows that although as-extruded HDPE 2 films have a lower transmittance (~ 48 % at 500 nm), the solid-state drawn HDPE 2 films with a draw ratio of 4−10 possess similarly high optical transmittance of around 90 % in the visible light wavelength range as HDPE 1 films, with only about 2 % lower transmittance of both kinds of HDPE compared to that of inorganic sheet glass (~ 92 %). This indicates that the method of tuning drawing temperatures during solid-state drawing process to achieve optical transparency of the films seems to be applicable to the HDPE with the above mentioned molecular weight ranges ($\overline{M_w}$ < 140 kg/mol and MWD < 10).

The mechanical performance of two grades of HDPE indicates that both types of HDPE have a similar trend of Young's modulus as a function of draw ratio as shown in ***Figure 4.14(a)***, but HDPE 1 with a higher molecular weight possesses a steeper slope of the fitting curve of tensile strength versus modulus (dashed red line) in ***Figure 4.14(b)***

compared to that of HDPE 2 (dashed green line) and hence a higher strength at similar modulus value is achieved in HDPE 1. Generally, the tensile strength of LPE is more sensitive to the molecular weight and its distribution in contrast to Young's modulus. According to Wu and Black[112], the number-average molecular weight ($\overline{M_n}$) is the predominant factor in determining the tensile strength of melt-spun and ultra-drawn LPE fibres since there are more interchain interactions (mainly van der Waals force) in chain-extended polymers with a high $\overline{M_n}$. Usually, $\overline{M_n}$ should be higher than 22 kg/mol in order to obtain a high strength for LPE. However, if the molecular weight is too high ($\overline{M_w}$ > 400 kg/mol), it becomes more difficult to produce fibres, tapes or films from melt-crystalline LPE[95]. Thus, it can be concluded that a relatively higher molecular weight contributes to superior mechanical properties of HDPE films in terms of tensile strength while still maintains a high optical transparency (~ 90 %).

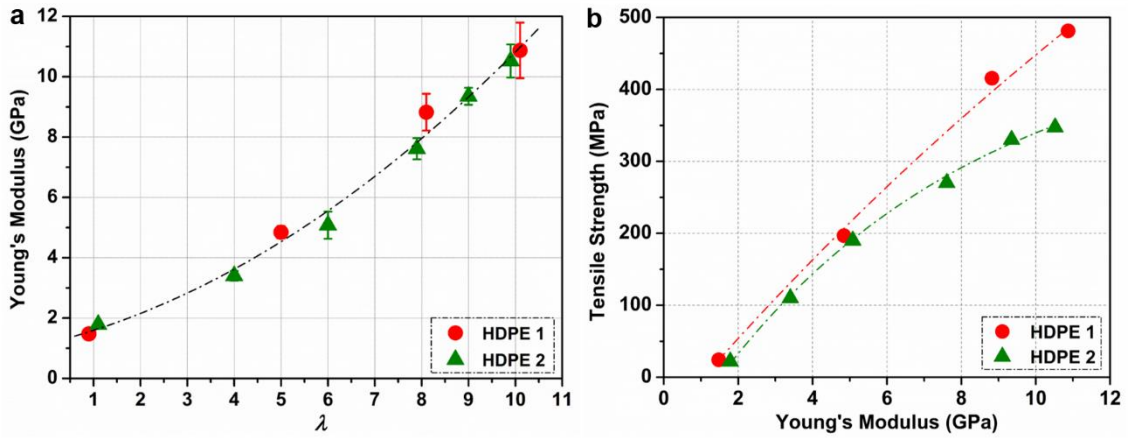

Figure 4.14 *(a) Young's modulus versus draw ratio and (b) tensile strength versus Young's modulus of HDPE 1 and HDPE 2 films (λ_{pre} = 4) along the MD, indicating a similar modulus but superior tensile strength of HDPE 1 compared to HDPE 2 at similar draw ratio. The dashed line indicates the fitting curves.*

4.4 Conclusions

This chapter successfully demonstrated the potential of a continuous extrusion and solid-state drawing process for the low-cost production of lightweight, transparent, high strength HDPE films and tapes. Two approaches based on solid-state drawing at a temperature of 105 °C with and without the incorporation of BZT as an additive into these oriented HDPE films were used and compared. It was shown that optical and mechanical properties, void content, crystallinity as well as the degree of molecular orientation were similar for both types of HDPE films at equal draw ratios. Both methods resulted in a negligible amount of micro- or nano-voiding after drawing which limited the amount of potential light scattering by such voids, hence leading to films possessing a high transparency of almost 91 % even in the far field within the visible light spectrum. Moreover, these highly drawn films possessed a high maximum Young's modulus of ~ 33 GPa and tensile strength of ~ 900 MPa, which are nearly 15 times higher than those of PC and PMMA and on a weight basis even outperforms structural materials like aluminium or glass fibre reinforced plastics. The use of a two-step drawing process did not significantly improve the optical and mechanical properties of the films. A high draw down or pre-orientation ratio was, however, beneficial in enhancing modulus and strength at the same draw ratio, but would also lead to a reduction in ultimate mechanical properties of the films. Besides, a relatively high molecular weight facilitates the achievement of a higher tensile strength as well as preserving a high optical transparency of around 90 %. This chapter showed that, for the studied draw ratios, the use of BZT as an additive to induce transparency in drawn HDPE films is not necessary when drawing is performed at a temperature of 105 °C. In fact, the BZT-free technology will be the preferred technology from a perspective of long-term stability, low cost, easy processing and convenience.

Chapter 5

High performance transparent composite laminates based on highly oriented HDPE films

This chapter is partially reproduced from: Y. Lin, J. Cao, M. Zhu, E. Bilotti, H. Zhang, C. W. M. Bastiaansen, T. Peijs, *ACS Applied Polymer Materials* **2020**, *2* (6), 2458-2468.

5.1 Introduction

Advanced composites reinforced by high performance fibres like carbon, glass, aramids or UHMWPE, are widely used as lightweight materials in the fields of aerospace, sports, defence and protection owing to their high specific modulus and strength. However, most of today's high performance fibre-reinforced composites are opaque because of severe light scattering resulting from the large surface area of reinforcing fibres, light absorption by the fibres and differences in refractive indices between fibre and matrix.

Common transparent materials consisting of inorganic glass and amorphous polymers can be used in areas requiring high clarity, whilst their mechanical performance is rather limited. Although some efforts have been made to enhance the mechanical performance of these materials by laminating glass, PC and/or PMMA with other transparent polymeric interlayers such as PVB, EVA or TPU, limited improvements have been achieved so far[3-5].

In Chapter 4, ultra-drawn HDPE films possessing a high strength and high stiffness in combination with high optical clarity were successfully produced by a cast film extrusion process followed by solid-state drawing. These transparent high strength HDPE films can be used as the reinforcing phase in laminated composites, opening new avenues towards the development of high performance transparent composites.

In this chapter, highly oriented transparent HDPE films with unidirectional (UD) or bidirectional (BD) orientations were used as the reinforcing phase in composite laminates with either glass or PC as outer layers. The study also involved the selection of an appropriate interlayer material that ensures high optical clarity together with good adhesive bonding. The optical performance of HDPE laminates with glass or PC as outer layers was studied for both UD and BD laminates with different numbers of HDPE layers in the far field. Moreover, the mechanical behaviour of these laminates was explored by tensile tests for both UD and BD laminates and quasi-static dart penetration tests for BD laminates.

5.2 Experimental

5.2.1 Materials

The used HDPE was again Borealis VS4580 (Borealis AG, Austria). As an outer layer material, D 263® T eco, a borosilicate glass with a thickness of 210 μm was used which was supplied by Schott AG (USA). PC 801E films with a thickness of 25 μm were provided by Sichuan Longhua Film Co., Ltd. (China) and RS Pro Clear PC sheets with a thickness of 1 mm were purchased from RS Components (UK). As an adhesive interlayer material, TPU ST-6050 sheets were used which were provided by Schweitzer-Mauduit

International, Inc. (USA). EVAevguard® Clear sheets and PVB Everlam™ Clear sheets were purchased from Qdel laminating solutions (Netherlands). 2-Butanone (99.5 %, GC) and ethylene glycol (99.8 %) were purchased from Sigma-Aldrich (USA).

5.2.2 Preparation of specimens

Highly oriented solid-state drawn transparent HDPE films were manufactured using continuous cast film extrusion and solid-state drawing process using a Collin E20T (Germany) single screw extruder and a Collin MDO-A & MDO-B (Germany) uniaxial stretching line, as described in Chapter 4. These oriented films possess a pre-orientation ratio (draw down) of ~ 4, a solid-state draw ratio of ~ 15 and a final average thickness of around 30 μm. The mechanical properties of these uniaxial films are as follows: the films have a Young's modulus of approximately 12 GPa, a tensile strength of 440 MPa and a strain-at-break of 25 % in the drawing direction. The transverse properties of these highly anisotropic PE films are significantly lower: a Young's modulus of ~ 2 GPa and tensile strength of ~ 15 MPa[176] (see ***Table 5.1***).

Table 5.1 *Mechanical properties of the laminate constituent materials.*

Material		**Thickness [μm]**	**Modulus [GPa]**	**Strength [MPa]**	**Strain-at-break [%]**
HDPE	**Longitudinal**	30	12	440	25
	Transverse[176]	30	~ 2	~ 15	-
TPU		10 − 20	0.15	3.0	500
Glass*		210	70	-	-
PC		25	2.9	60	90

* The data of glass are from the corresponding datasheet provided by suppliers.

Clearly, orientation of the uniaxial HDPE films within the laminate has a great influence on the mechanical properties of the composites. Unidirectional (UD) laminates will be very stiff and strong along the drawing or 0° direction of the film, whereas they will be weak in the transverse 90° direction. Such laminates will deliver ultimate mechanical performance, albeit only when loaded uniaxially in tension. Bidirectional (BD) composites with a 0°/90° lay-up are more applicable for most multi-axially loaded engineering applications[201-202]. Here, we evaluated both UD and BD laminate configurations but these uniaxially oriented HDPE films allow for a multitude of laminate designs, including quasi-isotropic lay-ups like 0°/60°/-60° or 0°/45°/-45°/90°.

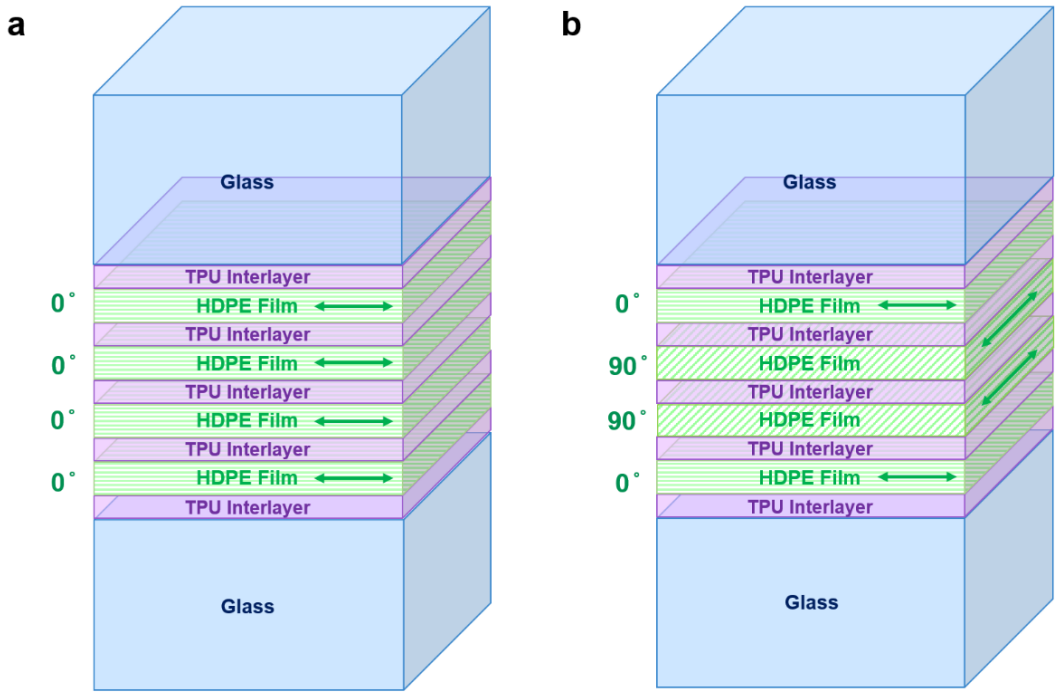

Figure 5.1 *Schematic diagram of different HDPE laminate designs with sheet glass (210 µm) as outer layers: (a) unidirectional (UD) and (b) bidirectional (BD) stacking of oriented HDPE films with TPU coatings as interlayers. PC is also be used as outer layers but has a much lower thickness (25 µm) than glass, similar to HDPE (30 µm). Relative thickness of the different layers drawn to scale.*

In order to cover a wide spectrum of properties and applications, UD and BD laminate lay-ups were manufactured and evaluated in this study: (i) UD laminates with four layers of unidirectionally stacked HDPE films with a $[0]_4$ stacking sequence (***Figure 5.1(a)***), and (ii) BD laminates with four layers of cross-plied HDPE films with a $[0,90]_S$ stacking sequence sandwiched between either glass (***Figure 5.1(b)***) or PC.

The selection of TPU as interlayers in the laminates will be discussed in detail with regards to optical, thermal and adhesive properties in Section 5.3.1. In order to obtain thin TPU interlayers for bonding glass or PC outer layers to HDPE film or between HDPE films, TPU sheets (360 μm) were cut into pieces and dissolved at 5 wt.% in 2-butanone at 80 °C for 2 h until the solution became homogeneous and clear. Next, 1 mL of this 5 wt.% TPU/2-butanone solution was dip-coated at RT onto both sides of the oriented HDPE films with a surface area of about 25 cm^2. After evaporation of the solvent in a fume hood at 60 °C overnight, HDPE films with a thin (~ 10 μm) TPU coating on both sides were obtained. Subsequently, these TPU-coated HDPE films were stacked together with sheet glass (210 μm) or PC sheets (25 μm) as outer layers in a lay-up sequence as indicated in ***Figure 5.1***. The interlayer thickness between HDPE and glass or PC was around 10 μm and doubled to around 20 μm between the dip-coated HDPE films. The corresponding laminates were compression moulded using a Rondol (UK) hot press at 100 °C, 20 bar for 10 min, i.e. well below the melting temperature of the HDPE (134 °C) to prevent chain relaxation and loss of mechanical properties of the oriented HDPE films.

5.2.3 Characterization

The contact angles between a liquid droplet and layer materials were measured using a KRÜSS DSA100 (Germany) drop shape analyser. A 5 μL sessile droplet of distilled water

or ethylene glycol was dropped onto the surface of the solid layer and the contact angle was measured using Drop Shape Analysis software. The surface free energy (or surface tension) was calculated to obtain information on the wettability between layers and interlayers using the Owens-Wendt-Rabel-Kaelble (OWRK) model[203], which is suitable for most of materials, including polymers like PC and TPU. In this theory, the surface free energy of a solid material is assumed to be composed of two components: (1) a dispersive part originating from van der Waals and other apolar interactions; (2) a polar part originating from hydrogen bonding, dipole-dipole, dipole-induced dipole and other secondary interactions. This model is mainly based on the Young's equation (Equation (5.1)) and Good's equation (Equation (5.2))[204-205]:

$$\gamma_s = \gamma_{sl} + \gamma_l \cos\theta \tag{5.1}$$

$$\gamma_{sl} = \gamma_s + \gamma_l - 2\sqrt{\gamma_s^d \gamma_l^d} - 2\sqrt{\gamma_s^p \gamma_l^p} \tag{5.2}$$

where γ_{sl} is the interfacial free energy between a solid and a liquid; γ_s and γ_l are the surface free energy of the solid or the liquid; θ is the contact angle between the solid and the liquid; γ_s^d, γ_l^d, γ_s^p, γ_l^p are the dispersive (*d*) or polar (*p*) component of the surface free energy of the solid (*s*) and the liquid (*l*), respectively.

Combining Equation (5.1) and (5.2) leads to the following equation:

$$\frac{\gamma_l(\cos\theta+1)}{2\sqrt{\gamma_l^d}} = \sqrt{\gamma_s^p}\frac{\sqrt{\gamma_l^p}}{\sqrt{\gamma_l^d}} + \sqrt{\gamma_s^d} \tag{5.3}$$

Equation (5.3) is equivalent to a linear equation $y = ax + b$, where:

$$y = \frac{\gamma_l(\cos\theta+1)}{2\sqrt{\gamma_l^d}}; \quad a = \sqrt{\gamma_s^p}; \quad x = \frac{\sqrt{\gamma_l^p}}{\sqrt{\gamma_l^d}}; \quad b = \sqrt{\gamma_s^d} \tag{5.4}$$

Thus, the overall, dispersive part and polar part of the surface free energy of a solid material can be obtained by fitting a linear equation to the contact angle data for at least two types of liquid on a solid. The interfacial free energy between two solid or semi-solid materials, like two viscoelastic polymers, can also be calculated using Equation (5.2) from the solid surface free energy of these two materials[206].

Transmission spectra of the laminates were measured using a PerkinElmer Lambda 950 (USA) UV-vis spectrometer in the wavelength range of 300−700 nm at an interval of 1 nm. A sample-to-detector distance of 40 cm was used to obtain transmittance values in the far field rather than in the near field, which is of greater practical importance for applications like windows or visors as stated in Chapter 3. Transmission spectra were measured in triplicate for each laminate type. Optical micrographs were recorded on an Olympus BX60 (USA) microscope in transmission-mode between crossed polarizers.

Differential scanning calorimetry (DSC) was used to examine the thermal behaviour of different materials using a TA Instruments DSC25 (UK). 5−10 mg specimens were placed in aluminium pans with a single heating-cooling cycle carried out under a flow of nitrogen gas at a constant heating rate of 10 °C/min. At least three specimens were tested for each material.

T-peel tests, tensile tests and quasi-static penetration tests were all carried out in an Instron 5566 (UK) universal tensile tester at RT. T-peel tests were carried out to evaluate interlaminar bonding at a constant crosshead speed of 254 mm/min in accordance with ASTM 1876-08[207]. For T-peel test specimens, the interlayer material was sandwiched

between two oriented HDPE films as shown in ***Figure 5.4(a)*** in Section 5.3.1 and then compression moulded using a Collin P300E (Germany) hot press at a pressure of 20 bar. Different temperatures were used for each type of interlayer (100 °C for TPU, 90 °C for EVA and 120 °C for PVB) and these temperatures were selected based on their thermal properties (see Section 5.3.1). T-peel specimens were used with a width of 25 mm, a bond length of 241 mm and an unbonded length of 76 mm (for clamping inside the pneumatic side action grips). The normalised peel force (N/mm) was defined as the force per unit width of the specimen required to produce progressive separation of the two bonded films. The average normalised peel force for crack propagation was calculated over the extension range of 150−400 mm by integrating the area below the normalised peel force-extension curves and dividing this by the extension range (250 mm). At least five specimens were measured to ensure reproducibility.

For tensile tests, rectangular-shaped laminates with a dimension of 100 mm × 10 mm were prepared by compression moulding. In order to avoid stress concentration at the clamps, tapered end-taps of PC sheets with a thickness of 1 mm and a tab length of 25 mm were bonded to the laminates using TPU as an adhesive, as shown in ***Figure 5.9(a)*** in Section 5.3.5. Samples were clamped in manual wedge action grips and tests were carried out at a constant crosshead speed of 2 mm/min according to ASTM D3039-17[208], which corresponds to a strain rate of 0.04 min^{-1}. The Young's modulus was calculated from the tangent of the engineering stress-strain curve at a strain below 0.5 %. The average Young's moduli and tensile strengths in combination with their standard deviation were calculated from at least five repeats.

For the quasi-static penetration tests, square-shaped laminates with a dimension of 50 mm × 50 mm were clamped between two steel plates, which had an internal circular opening

with a diameter of 30 mm. A hemispherical dart with a diameter of 10 mm was used and a constant dart speed of 1.25 mm/min was employed during these quasi-static dart penetration tests in accordance with ASTM D6264-17[209]. Only BD laminates were tested considering the multi-directional loading nature of this test. Energy absorption required for full penetration was obtained by integrating the area under the force-displacement curve during the penetration process. The contact force, absorbed energy and peak force were all normalised by specimen thickness.

5.3 Results and discussion

5.3.1 Interlayer selection

To ensure a high optical transparency together with a high mechanical performance, interlayer materials with a refractive index close to the other materials and good adhesive bonding to the reinforcing HDPE phase are required. Therefore, a systematic study was performed to evaluate some common interlayer materials prior to transparent composite fabrication.

For laminated glass with high clarity, commonly used polymeric interlayers include PVB, EVA and TPU. All these three interlayer materials are employed here to assess their performance in current HDPE transparent composites. Here, the TPU interlayer used in this Chapter was chosen based on the criteria for making transparent TPU products as stated in Section 2.2.5. ***Table 5.2*** shows that the use of TPU results in a slightly higher transmission at a wavelength of 550 nm than EVA and PVB for both types of laminates, as a result of the smaller refractive index mismatch between TPU and the glass or PC. In comparison to EVA and PVB, the refractive index of TPU (n = 1.50) is closer to glass (n

= 1.50−1.52)[1], PC (*n* = 1.58−1.60)[210] and the birefringent HDPE films (with an average refractive index of 1.54)[7]. As a consequence, the extent of light reflection at each interface decreases and therefore more light is transmitted through the laminates using TPU as interlayers.

Table 5.2 *Comparison among TPU, EVA and PVB interlayers with respect to compression moulding temperature, refractive index, transmittance at a wavelength of 550 nm when sandwiched between glass or PC tested at a 40 cm sample-to-detector distance and average peel force from T-peel tests.*

Material	Lamination Temperature [°C]	Refractive Index	Transmittance between Glass [%]	Transmittance between PC [%]	Average Normalised Peel Force [N/mm]
TPU	100	1.50	91.6 ± 0.2	89.9 ± 0.3	0.150 ± 0.061
EVA	90	1.48−1.49	91.4 ± 0.1	89.4 ± 0.2	0.080 ± 0.013
PVB	120	1.48	91.0 ± 0.1	88.8 ± 0.2	0.043 ± 0.008

Figure 5.2 shows the transmittance spectra of the three interlayer materials sandwiched between glass or PC. Since the refractive index differences between PC and interlayers are larger than for glass and interlayers, the differences in transmittance values when sandwiched between PC (***Figure 5.2(b)***) are higher than for glass (***Figure 5.2(a)***).

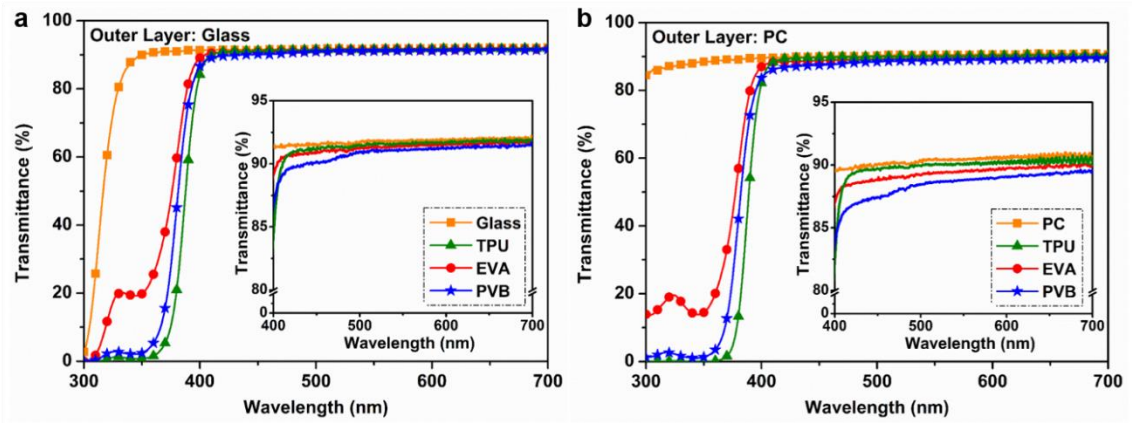

Figure 5.2 *Transmittance spectra of pure glass, pure PC, different interlayers between (a) glass or (b) PC in a wavelength range of 300−700 nm measured at a 40 cm sample-to-detector distance, showing that specimens with TPU interlayers possess slightly higher transmittance values among them. The interlayers were sandwiched between sheet glass or PC sheets and compression moulded at the temperatures listed in Table 5.2.*

DSC curves revealing the thermal properties of each material including the three interlayer materials are shown in ***Figure 5.3***. EVA shows two significant melting endotherm peaks in the temperature range of 25−87 °C, corresponding to melting of less perfect crystals at a low temperature and more perfect organized crystals at higher temperature[211]. Hence, 90 °C was chosen for lamination using EVA interlayers. TPU has a melting endotherm peak between 60−95 °C, and therefore for this interlayer system a lamination temperature of 100 °C was used. PVB exhibits a glass transition temperature (T_g) at ~ 16 °C[212]. Through actual compression moulding trials, it was found that PVB did not melt or flow until 120 °C. Since the lamination temperature cannot be too close to the melting point of HDPE (T_m ~ 134 °C), as this will result in loss of molecular orientation due to chain relaxation or even melting, PVB was compression moulded at a maximum temperature of 120 °C. In terms of outer layers, PC and sheet glass have both thermal stabilities well above the moulding temperature range of 90−120 °C.

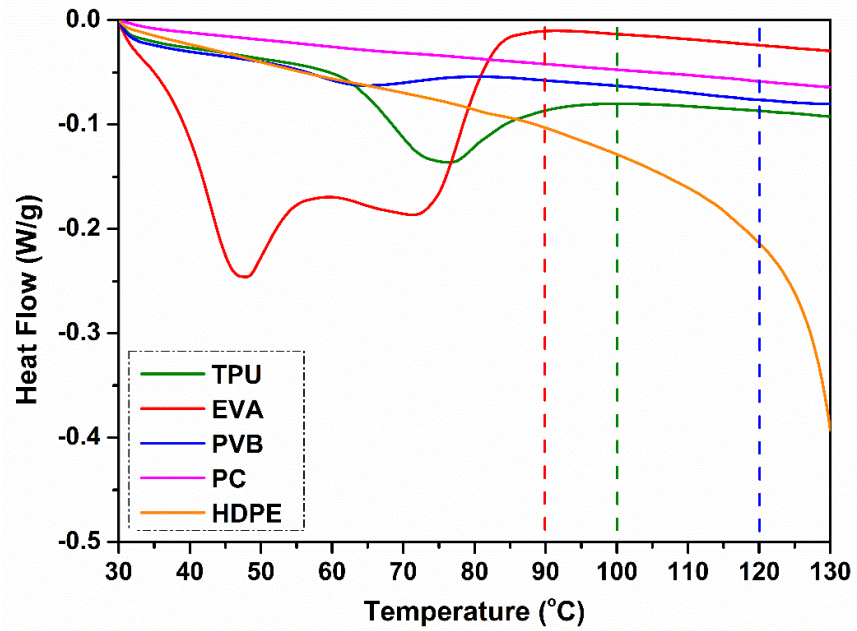

Figure 5.3 *DSC curves of the first heating cycle for each material used in the laminates.*

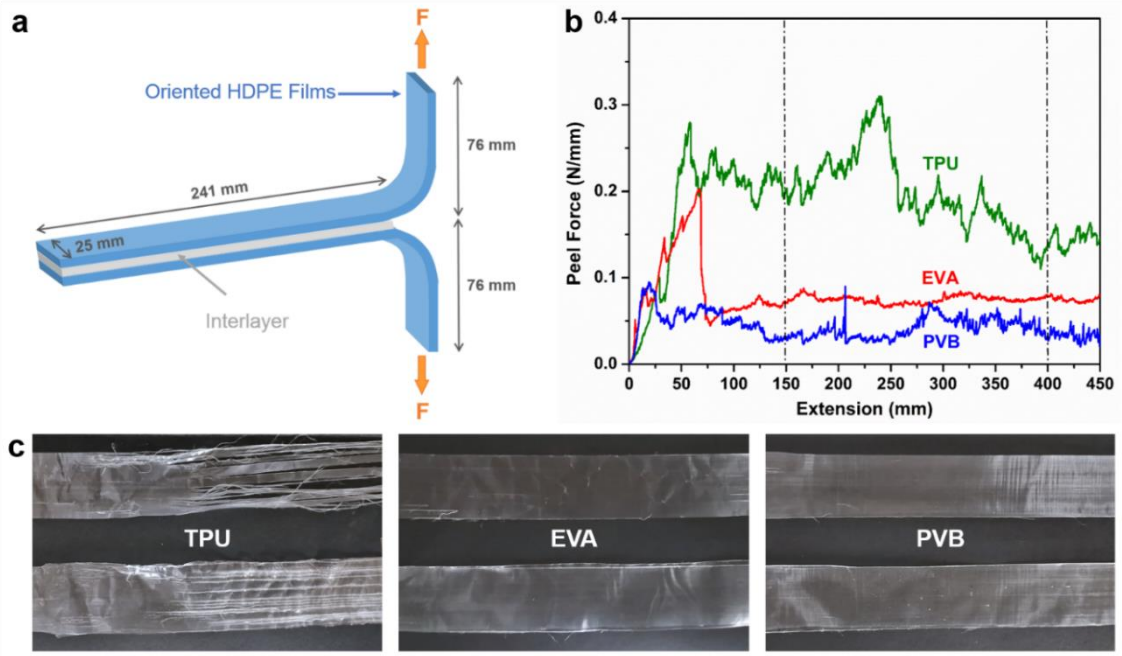

Figure 5.4 *(a) Schematic diagram of T-peel test sample, (b) peel force versus extension curves from T-peel tests of different interlayers between two oriented HDPE films after lamination by hot pressing and (c) appearance of T-peel specimens with different interlayers after testing, showing HDPE fibrillation in the case of TPU interlayer indicative of strong adhesive bonding.*

Interfacial bonding was investigated by T-peel tests, which examined the resistance to Mode-I peeling failure between different layers for all three interlayer materials. In ***Table 5.2*** and ***Figure 5.4(b)***, it is shown that the average peel force required to separate two oriented HDPE films adhesively bonded together by a TPU interlayer is nearly twice and 3.5 times than that of EVA or PVB, respectively. In all cases, after T-peel testing the interlayers only adhered to one of the two films, indicating interfacial adhesive failure between interlayer and HDPE film for all three interlayer materials. However, obvious splitting of the oriented HDPE films is observed in the case of TPU as shown in ***Figure 5.4(c)***, which suggests good load transfer between TPU and HDPE and which is in clear contrast to the smooth fracture surface with PVB or EVA. With regard to tensile properties, all three interlayer materials exhibit a high elongation (> 250 %) and a relatively low tensile strength as shown in ***Figure 5.5*** and ***Table 5.3***.

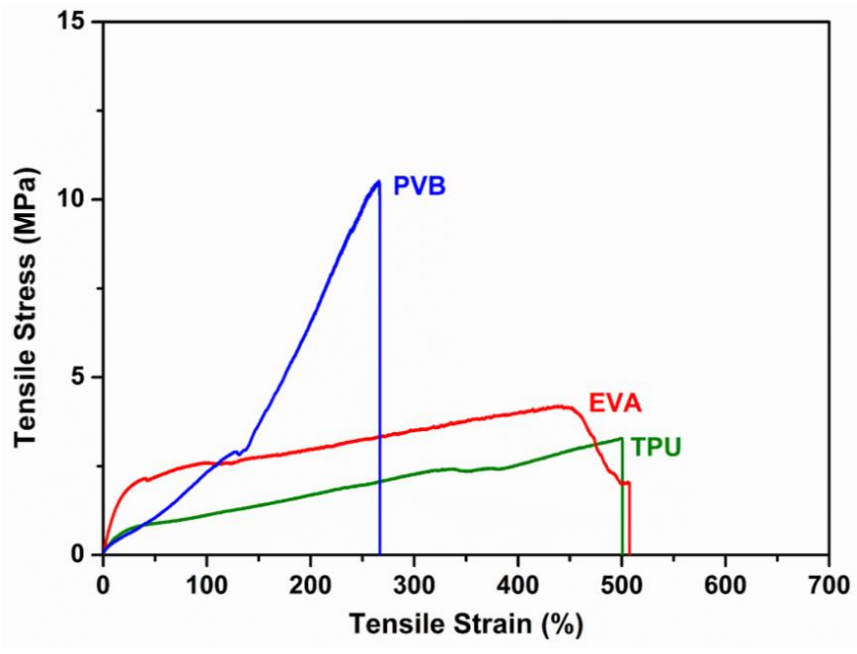

Figure 5.5 *Stress-strain curves of TPU, EVA and PVB.*

***Table 5.3** Mechanical properties of TPU, EVA and PVB.*

Material	Young's Modulus [GPa]	Tensile Strength [MPa]	Strain-at-break [%]	Work-to-break [J/m^3]
TPU	0.15 ± 0.01	3.0 ± 0.6	501 ± 75	7.9 ± 1.6
EVA	0.17 ± 0.02	4.4 ± 0.4	606 ± 100	20.0 ± 5.0
PVB	0.15 ± 0.02	10.5 ± 0.6	299 ± 21	13.1 ± 1.3

Because of the brittleness of the thin sheet glass, the adhesion properties between glass and the adhesives interlayer materials are difficult to determine by T-peel tests. Instead, contact angles of outer layer materials (glass and PC), reinforcing phase (oriented HDPE) and interlayer materials (TPU, EVA and PVB) and corresponding solid surface free energies were measured and calculated (see ***Table 5.4***). Improved wetting is expected by a lower contact angle and higher solid surface free energy[203]. On the basis of the solid surface free energies, the corresponding interfacial free energies between different adjacent layers used in the laminates were calculated using Equation (5.2) and are listed in ***Table 5.5***. The interfacial free energy between glass and HDPE is 68.8 ± 1.04 mN/m, which is the highest among all values in ***Table 5.5***, indicating the weakest interfacial interaction between them among all interfaces. In fact, glass and the HDPE film will not stick to each other at all unless the HDPE is melted, which is why an adhesive interlayer is needed to bond them together in a laminate. After incorporating polymeric interlayers between the glass and HDPE, the interfacial free energies at these new interfaces are significantly reduced. PVB possesses the lowest interfacial free energy when in contact with glass, which is why PVB is widely used in commercial laminated glass, while TPU had again a lower interfacial free energy compared to EVA. However, TPU and EVA have a lower interfacial free energy than PVB when in contact with PC or HDPE. Since a lower interfacial free energy is desirable for better wetting and adhesive bonding[203], it can be

concluded that TPU provides the best overall balance in wetting and interfacial bonding with glass, PC and HDPE in comparison to EVA and PVB. It should be noted that surface modifications like corona or plasma treatments could be used to modify the surface of HDPE films by introducing some functional groups and improved adhesive bonding[176], but such surface treatments may result in a worse optical transparency.

Table 5.4 *Contact angles and solid surface free energies of different layer materials in laminates.*

Material	Contact Angle θ [deg]		Surface Free Energy [mN/m]		
	Water	Ethylene Glycol	γ	γ^d	γ^p
Glass	49.8 ± 0.9	52.8 ± 1.4	58.1 ± 0.7	1.8 ± 0.1	56.3 ± 0.6
PC	88.3 ± 1.0	61.3 ± 1.0	27.4 ± 0.5	23.0 ± 0.4	4.5 ± 0.1
HDPE	95.8 ± 0.8	59.3 ± 3.7	36.3 ± 1.6	35.9 ± 1.5	0.4 ± 0.1
TPU	92.4 ± 1.4	72.8 ± 1.5	20.1 ± 0.6	14.3 ± 0.4	5.8 ± 0.2
EVA	107 ± 0.9	86.1 ± 0.8	15.2 ± 0.3	13.9 ± 0.2	1.4 ± 0.1
PVB	73.6 ± 2.2	60.2 ± 1.4	29.9 ± 0.9	9.6 ± 0.4	20.4 ± 0.5

Table 5.5 *Interfacial free energy (mN/m) calculated between adjacent layers in laminates.*

Material	Glass	PC	HDPE
TPU	31.8 ± 0.16	1.10 ± 0.01	7.94 ± 0.35
EVA	45.8 ± 0.26	2.06 ± 0.03	5.40 ± 0.56
PVB	12.0 ± 0.05	8.61 ± 0.12	23.2 ± 0.52

From the above analysis of optical properties, average peel force and interfacial free energy, TPU was selected as the interlayer of choice for the current transparent HDPE laminates.

5.3.2 Optical properties of HDPE laminates with glass as outer layers

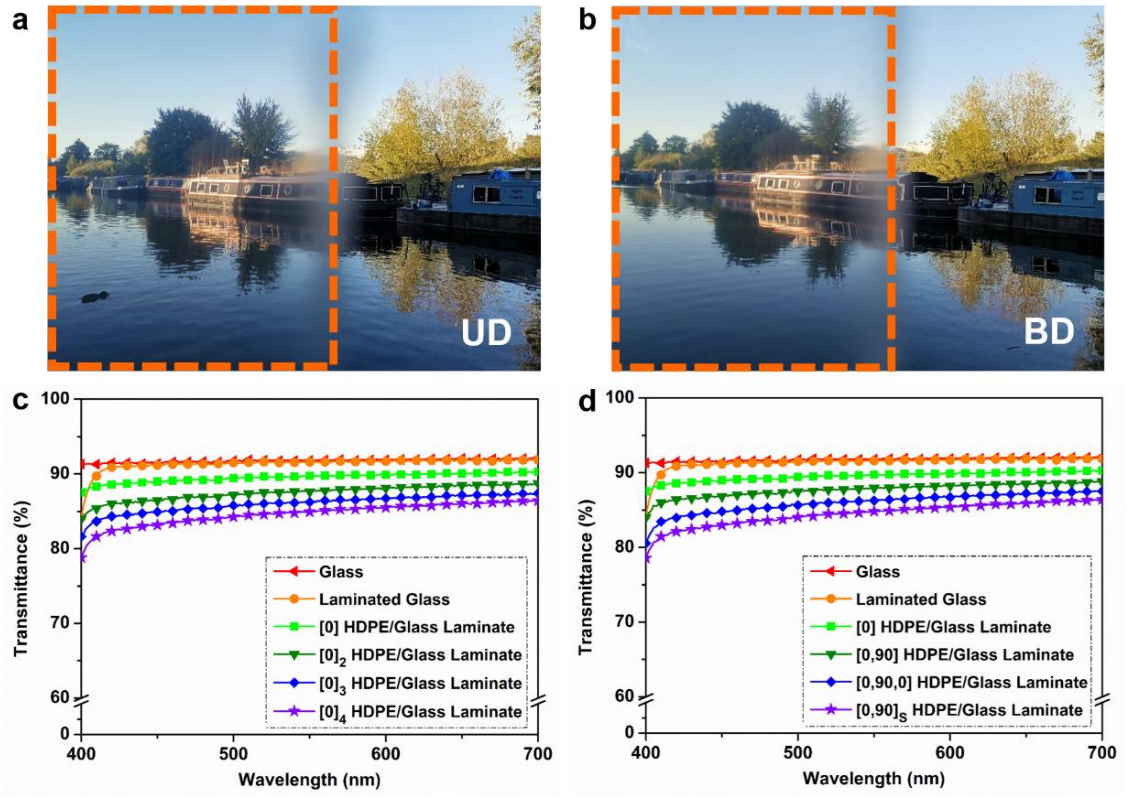

Figure 5.6 *Optical appearance of (a) $[0]_4$ and (b) $[0,90]_S$ HDPE laminates with glass as outer layers when positioned in front of a distant scenery, showing a clear appearance for both UD and BD HDPE/glass laminates in the far field. For clarity, the dashed box sections in (a) and (b) mark the position of the laminates in front of the image. Transmittance spectra of (c) UD and (d) BD HDPE/glass laminates with different numbers (1, 2, 3, 4) of oriented HDPE layers measured at a sample-to-detector distance of 40 cm in the visible wavelength range, indicating a reduction in transmittance in the far field of around 1−2 % with every additional layer of TPU-coated HDPE.*

In most studies claiming optical transparency, the "transparent" specimen is positioned close to or directly on top of a background image or at a very short distance from an object[213-214], which is usually considered as optical transparency in the near field. However, actual transmittance generally refers to the ability of an observer to a non-

distorted view through a relatively distant sample and object which is far away (ASTM D1746-15)[215], in a similar way as one observes a distant scenery through a window as stated in Chapter 3. Therefore, here the optical appearance of the UD and BD HDPE composite laminates with glass as outer layers is examined when the laminates are positioned in front of a distant scenery as shown in ***Figure 5.6(a)-(b)***, representing the appearance of the laminates in the so-called far field. The fuzzy area between the laminate covered and uncovered sections in the middle of ***Figure 5.6(a)-(b)*** results from the edge of the laminate because the focus of the camera is on the distant scenery so that the laminate edge is out of the focal plane. It is shown that both UD and BD laminates have a highly transparent appearance and the distant scenery can be clearly seen with only minor differences between the laminate covered section (left) and the uncovered section (right). Clearly, both $[0]_4$ and $[0,90]_S$ TPU-coated HDPE laminates possess a high optical transparency when sandwiched between glass, even at a distance from the object.

To study the effect of the number of reinforcing HDPE layers on the optical transmittance of the resulting composite laminates, laminates with different numbers of TPU-coated HDPE films were analysed by UV-vis transmittance spectra using a sample-to-detector distance of 40 cm to mimic the far field. The transmittance of HDPE laminates with glass as outer layers in the visible light wavelength regime is presented in ***Figure 5.6(c)-(d)*** and ***Table 5.6***. It is shown that UD and BD HDPE/glass laminates with an identical number of HDPE layers have similar transmittance values. In addition, it is found that introducing an additional layer of TPU-coated HDPE to the laminates will lead to a transmittance drop of around 1−2 % in the visible light range. The drop in transparency at 550 nm as measured with the UV-vis might seem surprising especially in view of the photographs presented in ***Figure 5.6(a)-(b)***.

Table 5.6 *Transmittance values of UD and BD HDPE laminates with glass as outer layers and TPU as interlayer materials with different numbers of HDPE layers (1, 2, 3, 4) measured at a sample-to-detector distance of 40 cm at a wavelength of 700 nm, 550 nm and 400 nm.*

Material	**Transmittance [%]**		
	700 nm	**550 nm**	**400 nm**
Glass	92.1 ± 0.1	91.8 ± 0.1	91.3 ± 0.2
Laminated Glass	91.8 ± 0.2	91.6 ± 0.2	84.1 ± 0.2
[0] HDPE/Glass Laminate	90.3 ± 0.1	89.7 ± 0.2	87.7 ± 0.1
$[0]_2$ HDPE/Glass Laminate	88.6 ± 0.1	87.6 ± 0.1	83.9 ± 0.1
$[0]_3$ HDPE/Glass Laminate	87.3 ± 0.2	86.1 ± 0.2	81.8 ± 0.3
$[0]_4$ HDPE/Glass Laminate	86.6 ± 0.2	85.0 ± 0.2	79.0 ± 0.2
[0,90] HDPE/Glass Laminate	88.7 ± 0.1	88.0 ± 0.1	83.9 ± 0.2
[0,90,0] HDPE/Glass Laminate	87.4 ± 0.1	86.2 ± 0.1	80.6 ± 0.1
$[0,90]_S$ HDPE/Glass Laminate	86.3 ± 0.1	84.7 ± 0.1	78.5 ± 0.2

Laminates with a single layer of oriented HDPE possess a transmittance value of ~ 90 % at 550 nm, while for four layers of HDPE, the transmittance values of UD and BD HDPE/glass laminates are around 85 %. It is believed that this transmittance loss with increasing numbers of HDPE layers is mainly the result of the increasing number of interfaces between HDPE films and TPU interlayers. At these interfaces, increased light reflection is to be expected due to the, albeit small, refractive index difference between the birefringent and solid-state stretched HDPE[216-217] and the optically isotropic TPU. In other words, anisotropic adhesive layers need to be identified to generate refractive index matching in three dimensions if this drop in transmittance is to be avoided or reduced. Additional light scattering can also contribute to the transmittance drop as a result of increased defects, impurities and dust in or between the layers. At the moment, however,

we believe that this is a minor effect which can be resolved by working in a clean environment with more or less standard precautions for dust control, etc.

5.3.3 Penetration resistance of HDPE laminates with glass as outer layers

The penetration resistance of HDPE laminates with glass as outer layers was studied by quasi-static dart penetration tests. Since failure of UD laminates during such a test will merely lead to transverse splitting of the highly anisotropic films and brittle fracture with limited energy absorption[218], only BD laminates were considered to evaluate the penetration resistance of these transparent HDPE/glass laminates.

Figure 5.7(a) shows the normalised contact force as a function of indenter displacement for sheet glass, laminated glass with TPU interlayers, and BD $[0,90]_S$ HDPE laminate with glass as outer layers. For both sheet glass and laminated glass specimens, the contact force dropped to zero at a low displacement (< 2 mm) due to the inherent brittle nature of glass. On the other hand, although a clear drop was also observed at a similar low displacement for the BD HDPE/glass laminate as a result of fracture of the glass outer layers, these laminates showed pseudo-ductile behaviour with the contact force increasing again with further displacement, until final fracture of the laminate at around 20 mm displacement.

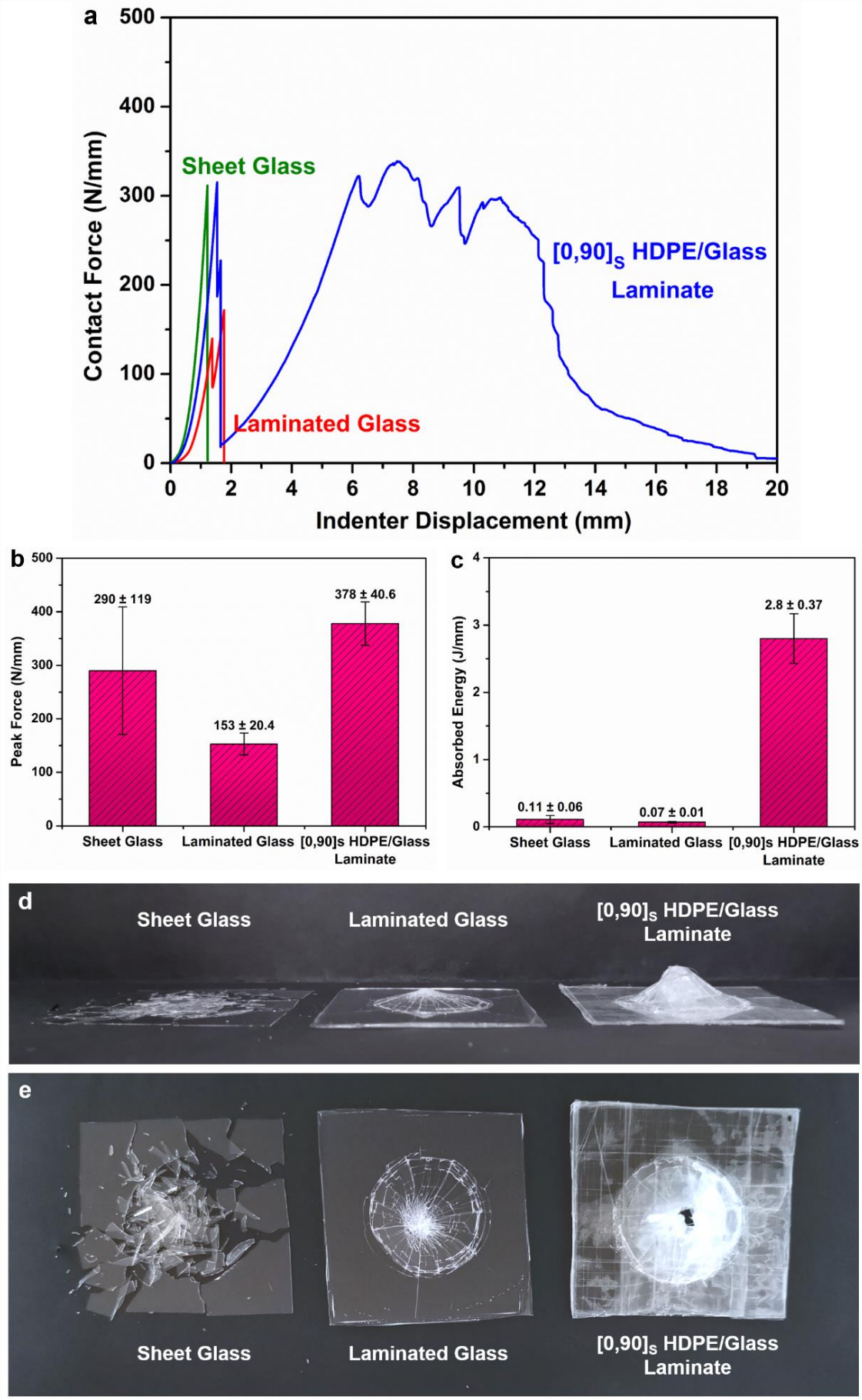
a
Contact Force (N/mm)
Indenter Displacement (mm)
Sheet Glass
Laminated Glass
[0,90]S HDPE/Glass Laminate
b
Peak Force (N/mm)
290 ± 119
153 ± 20.4
378 ± 40.6
Sheet Glass
Laminated Glass
[0,90]s HDPE/Glass Laminate
c
Absorbed Energy (J/mm)
0.11 ± 0.06
0.07 ± 0.01
2.8 ± 0.37
Sheet Glass
Laminated Glass
[0,90]s HDPE/Glass Laminate
d
Sheet Glass
Laminated Glass
[0,90]S HDPE/Glass Laminate
e
Sheet Glass
Laminated Glass
[0,90]S HDPE/Glass Laminate

Figure 5.7 *(a) Contact force versus indenter displacement, (b) peak force and (c) absorbed energy of sheet glass, laminated glass and* $[0,90]_S$ *HDPE laminates with glass as outer layers. It shows that the BD HDPE/glass laminate can absorb more than 25 times the energy of sheet glass or laminated glass. (d) Edge-side view of tested laminates with large out-of-plane deformation in the case of BD HDPE laminate sandwiched between glass and (e) bottom-side view of penetration damage of sheet glass, laminated glass and BD HDPE/glass laminate, indicating significant energy absorption by delamination and improved structural integrity after full penetration for the latter. Contact force, absorbed energy and peak force are all normalised by specimen thickness to enable a fair comparison.*

The average peak force normalised by specimen thickness (~ 210 mm for sheet glass and ~ 650 mm for laminated glass as well as $[0,90]_S$ HDPE/glass laminate) for the BD HDPE/ glass laminate reached 378 N/mm, higher than for both sheet glass (290 N/mm) and laminated glass with a TPU interlayer (153 N/mm) as shown in ***Figure 5.7(b)***. This can be attributed to the reinforcing HDPE phase, providing increased strength together with good load transfer between the layers due to the adhesive TPU interlayers. Interestingly, because of the increased thickness of laminated glass and the intrinsic low energy absorption capability of the TPU interlayer, the normalised peak force and normalised absorbed energy of laminated glass actually reduced compared to plain sheet glass.

The appearance of the specimens after quasi-static penetration is presented in ***Figure 5.7(d)-(e)***. In contrast to the complete shattering of sheet glass, the BD HDPE/glass laminate still maintained some level of integrity even after full penetration, greatly improving the safety and security aspects for impact resistant glazing applications. Furthermore, the BD HDPE/glass laminate shows much greater out-of-plane deformation

than sheet glass and laminated glass (see ***Figure 5.7(d)***). The normalised energy absorbed under low velocity penetration by the HDPE-reinforced laminate is more than 25 times higher than that of sheet glass or laminated glass, with 2.8 J/mm compared to 0.11 J/mm for sheet glass and 0.07 J/mm for laminated glass (see ***Figure 5.7(c)***). Delamination between HDPE layers is observed in the test region as well as in the surrounding areas (as shown in ***Figure 5.7(e)***). This extended delaminated area in BD HDPE/glass laminates contributes greatly to the higher overall energy absorption capability and greater penetration resistance. This increase in toughness can be attributed to the increased surfaces generated during delamination and tape pull-out, together with transverse splitting and fibrillation of the tapes. Hereinto, the fibrillation of the oriented HDPE tapes occurs due to their highly anisotropic structures during the fracture process, which can absorb a certain amount of energy upon impact and improve fracture toughness of the material, while the fibrillation may also lead to whitening and thus a decrease in optical transparency of the sample. These fracture mechanisms together with crack deflection at the glass/TPU/HDPE interface may contribute to synergistic effects in energy absorption of the composites during penetration, which means that the work-of-fracture of the laminates can be higher than the cumulative fracture energies of the individual constituents[219].

It is also noteworthy that unlike the non-visible or barely-visible impact damage commonly observed in high performance composites like carbon fibre reinforced plastics (CFRPs) and some glass fibre reinforced plastics (GFRPs) under low-energy impact[220], the internal damage in the current HDPE/glass laminates can be observed by simple visual inspection, leading to a much more efficient quality control and condition-based maintenance of the resulting composite component.

5.3.4 Optical properties of HDPE laminates with PC as outer layers

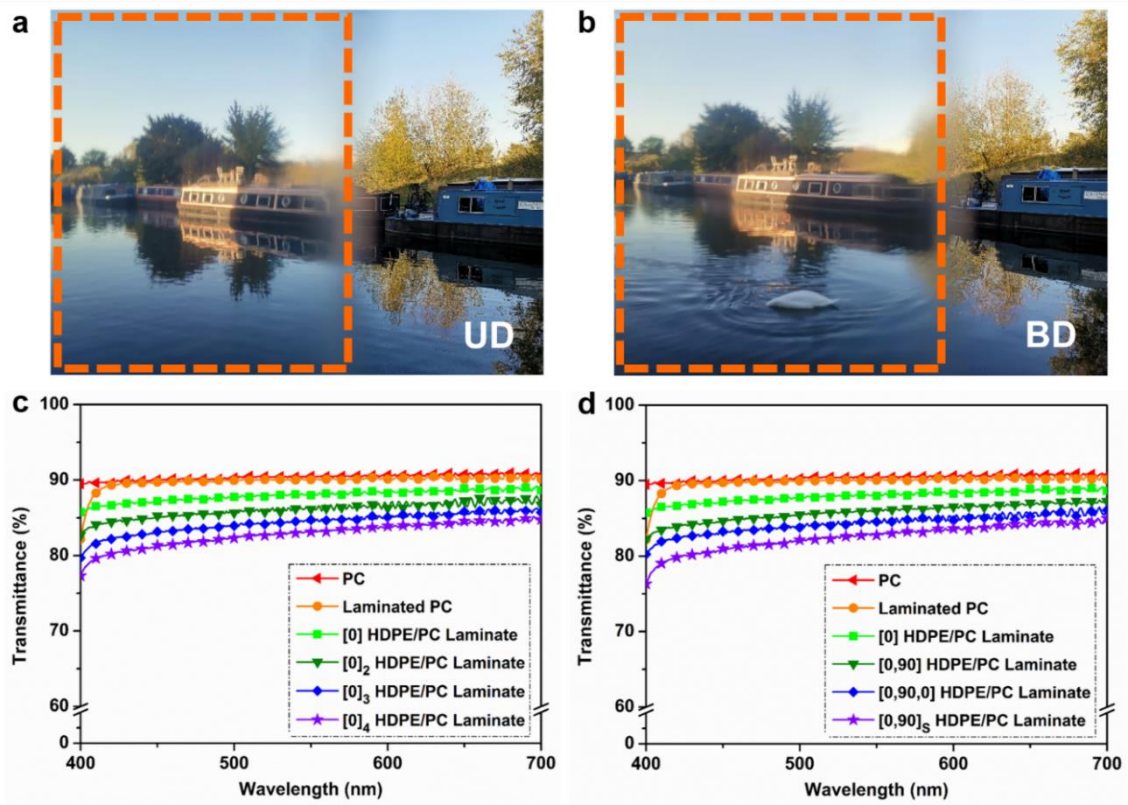

Figure 5.8 *Optical appearance of (a) $[0]_4$ and (b) $[0,90]_S$ HDPE laminates with PC as outer layers when positioned in front of a distant scenery, revealing a transparent appearance for both UD and BD HDPE/PC laminates in the far field. For clarity, the dashed box sections in (a) and (b) mark the position of the laminates in front of the image. Transmittance spectra of (c) UD and (d) BD HDPE/PC laminates with different numbers (1, 2, 3, 4) of oriented HDPE layers measured at a sample-to-detector distance of 40 cm in the visible light range, showing a decrease in transmittance of about 1−2 % with every additional layer of TPU-coated HDPE in the far field.*

In the case of HDPE laminates with PC as the outer layers, the transmittance values at 550 nm are about 88 % for a single UD [0] HDPE/PC laminate, and about 83 % for 4-ply UD $[0]_4$ HDPE/PC laminate or BD $[0,90]_S$ HDPE/PC laminate, as shown in ***Figure***

5.8(c)-(d) and ***Table 5.7***. The optical properties of these HDPE/PC laminates also follow the trend that transmittance values reduced by 1−2 % for every additional layer of TPU-coated HDPE, regardless of its UD or BD structure. This additional drop in transmittance has the same physical origin as for laminates sandwiched between glass (see Section 5.3.2). Due to the larger refractive index difference between PC (n = 1.58−1.60)[210] and air ($n \approx 1$) compared to that of glass and air, a higher reflectance and hence slightly lower transmittance can be expected. As a result, UD $[0]_4$ HDPE and BD $[0,90]_S$ HDPE laminates with PC as outer layers exhibit a slightly lower transparency (~ 2 % lower transmittance in ***Figure 5.8(a)-(b)***) as those sandwiched between glass.

Table 5.7 *Transmittance values of UD and BD HDPE laminates with PC as outer layers and TPU as interlayer materials with different numbers of HDPE layers (1, 2, 3, 4) measured at a sample-to-detector distance of 40 cm at a wavelength of 700 nm, 550 nm and 400 nm.*

Material	**Transmittance [%]**		
	700 nm	**550 nm**	**400 nm**
PC	90.3 ~ 90.9	90.4 ± 0.2	89.5 ± 0.2
Laminated PC	90.2 ~ 90.5	89.9 ± 0.3	82.4 ± 0.3
[0] HDPE/PC Laminate	88.4 ~ 89.2	88.0 ± 0.1	85.6 ± 0.2
$[0]_2$ HDPE/PC Laminate	86.9 ~ 87.9	86.2 ± 0.1	82.5 ± 0.3
$[0]_3$ HDPE/PC Laminate	85.8 ~ 86.3	84.7 ± 0.2	79.8 ± 0.2
$[0]_4$ HDPE/PC Laminate	84.5 ~ 85.1	83.1 ± 0.2	77.4 ± 0.4
[0,90] HDPE/PC Laminate	87.1 ~ 87.3	86.0 ± 0.1	82.2 ± 0.1
[0,90,0] HDPE/PC Laminate	85.7 ~ 86.4	84.8 ± 0.3	80.3 ± 0.4
$[0,90]_S$ HDPE/PC Laminate	84.1 ~ 84.9	82.8 ± 0.1	76.5 ± 0.1

5.3.5 Tensile properties of HDPE laminates with PC as outer layers

Tensile tests were performed to obtain the Young's modulus, tensile strength, and strain at break for all specimens and the HDPE reinforcing efficiency was also evaluated by comparing experimental laminate data with theoretical data (see ***Table 5.8***) based on the generalized Rule of mixtures (RoM) (Equation (5.5) and (5.6))[221]. In our case, oriented HDPE films are regarded as the reinforcing phase and PC together with TPU are considered as the matrix.

$$E_c = k\, E_{HDPE} V_{HDPE} + E_{PC} V_{PC} + E_{TPU} V_{TPU} \tag{5.5}$$

$$\sigma_c = k\, \sigma_{HDPE} V_{HDPE} + \sigma_{PC} V_{PC} + \sigma_{TPU} V_{TPU} \tag{5.6}$$

where E_c represents the Young's modulus of the composite laminate, σ_c represents the tensile strength of the composite. V_{HDPE}, V_{PC} and V_{TPU} are the volume fraction of the reinforcing HDPE phase, the PC and the TPU, respectively. E_{HDPE}, E_{PC} and E_{TPU} are the Young's modulus of the HDPE film (12 GPa), the PC (2.9 GPa) and the TPU (0.15 GPa). σ_{HDPE} is the uniaxial tensile strength of the HDPE film (440 MPa) and σ_{PC} and σ_{TPU} are the stress in PC and TPU at the onset of HDPE failure (around 60 MPa for PC and 0.5 MPa for TPU). In the generalized RoM, k is the efficiency parameter. Based on our previous studies, uniaxially oriented polyethylene films typically have a transverse Young's modulus of about 2 GPa together with a transverse tensile strength of around 15 MPa, i.e. perpendicular to the machine direction[176], and hence these values are here used for theoretical calculations and prediction of composite properties.

Table 5.8 *Tensile properties of UD [0]$_4$ HDPE and BD [0,90]$_S$ HDPE laminates with PC as outer layers.*

Sample	Young's Modulus [GPa]	Theoretical Modulus [GPa]	Modulus Efficiency [%]	Tensile Strength [MPa]	Theoretical Strength [MPa]	Strength Efficiency [%]	Work-to-break × 10^6 [J/m^3]
Laminated PC	0.58 ± 0.09	0.66	87.8	12.5 ± 0.2	12.9	96.9	13.2 ± 3.1
UD HDPE/PC Laminate	4.64 ± 0.31	5.87	79.0	196 ± 17.0	205	95.4	124 ± 28.5
BD HDPE/PC Laminate	2.98 ± 0.14	3.68	81.0	113 ± 5.8	116	97.4	27.5 ± 8.4

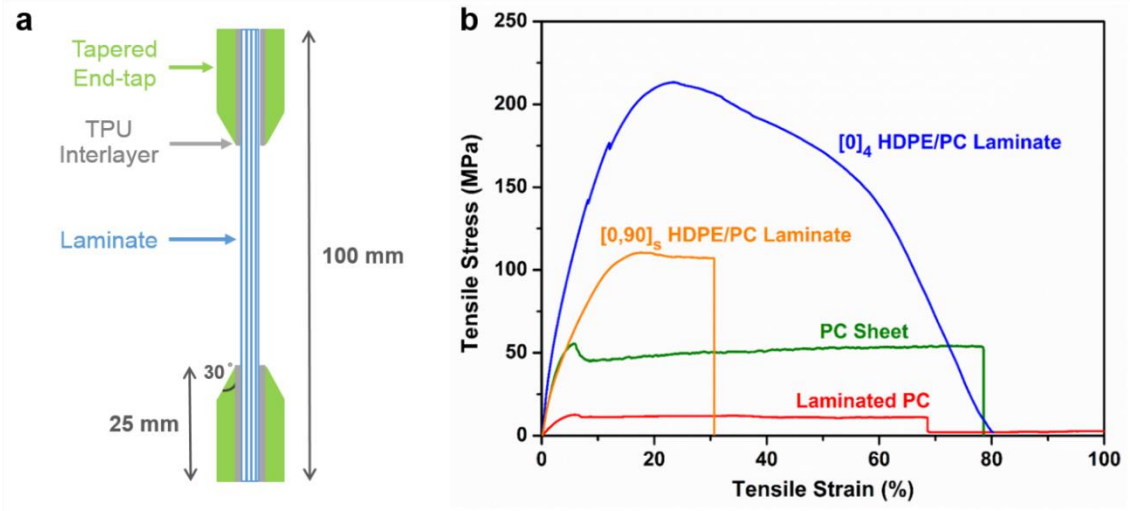

Figure 5.9 *(a) Schematic illustration of the tensile test sample with tapered end-taps and (b) stress-strain curves of PC sheet, laminated PC, UD [0]$_4$ and BD [0,90]$_S$ HDPE laminates with PC as outer layers, showing a much improved work-to-break for UD laminates incorporating HDPE reinforcements as compared to pure PC sheet.*

It is shown in ***Table 5.8*** that UD [0]$_4$ HDPE laminates with PC as outer layers have a strength of 196 MPa and a modulus of 4.6 GPa, which is nearly 16 times and 8 times that of laminated PC with TPU as interlayers at a similar thickness, and 3.3 times and 1.6 times that of pure PC sheet (see ***Table 5.1***). The 4-ply UD HDPE/PC laminates display

an almost 2 times higher work-to-break (i.e. the area below stress-strain curve) compared to PC sheet. The stress-strain curve of the UD HDPE/PC laminate as presented in ***Figure 5.9(b)*** shows an increasing stress up to an elongation of 23 %, followed by a gradual drop in stress without obvious yielding and necking until final fracture at $\varepsilon \sim 80$ %. Upon loading, the laminate delaminates first at the HDPE/TPU interface, followed by some transverse splitting of the oriented HDPE films. With further loading, the oriented HDPE films deform by yielding some plastic deformation, which is accompanied by whitening of the films before final fracture. The observed gradual drop in stress levels before final failure is attributed to the successive breakage of one or more HDPE films, as the laminate contains four layers of HDPE. As for the PC sheet and laminated PC, yielding occurs at $\varepsilon \sim 5$ % followed by some strain hardening until final fracture at $\varepsilon = 70-80$ %, with much less energy absorbed during the process compared to the UD HDPE-reinforced laminates.

With regard to BD $[0,90]_S$ HDPE laminates with PC as outer layers, a nearly doubling in tensile strength value (113 MPa) together with a similar modulus value compared to pure PC sheet was found. As expected, UD HDPE/PC laminates exhibit a higher Young's modulus and tensile strength than BD HDPE/PC laminates as all four oriented PE films are effectively loaded along its principal materials' axis. BD laminate on the other hand have only half of the oriented films effectively loaded as a result of the cross-ply structure. Hence, the Young's modulus of the BD laminate is the weighted sum of the corresponding longitudinal and transverse moduli, with the transverse modulus of these oriented PE films being much lower than the longitudinal modulus. The stress-strain curve of the BD HDPE/PC laminate showed a similar but lower trend to that for the UD laminate, except for a more sudden failure at a lower strain of around 30 %. This is mainly due to the relatively poor transverse mechanical properties of the two uniaxially drawn HDPE films oriented at 90° direction, resulting in effectively only two reinforcing HDPE layers in the

loading direction of the laminate. It is also noteworthy that the reinforcing efficiency *k* of the HDPE films is over 95 % for tensile strength, confirming the good stress transfer capability of the TPU interlayers and reinforcing effect of the oriented HDPE films in the laminates.

5.3.6 Penetration resistance of HDPE laminates with PC as outer layers

Figure 5.10(a) shows the contact force as a function of indenter displacement during the quasi-static penetration tests. PC sheet and laminated PC were directly penetrated at an indenter displacement of about 13 mm, with the load dropping instantaneously to nearly zero after the peak force was reached, indicating brittle fracture. A much lower contact force was measured for laminated PC compared to pure PC sheet due to presence of the soft TPU interlayers. With the addition of four plies of HDPE, the BD $[0,90]_S$ HDPE laminate with PC as outer layers reached a slightly higher maximum peak force of ~ 1859 N/mm at a similar indentation of around 11 mm, followed by successive drops before final penetration at an indentation of around 18.5 mm. Clearly, the BD HDPE/PC laminate was still able to withstand continued loading and deformation even after reaching the peak force, indicative of a greater damage tolerance with a gradual load drop rather than a sudden load drop and catastrophic failure. As shown in ***Figure 5.10(b)-(c)***, BD HDPE/PC laminates can absorb nearly 6 times the energy required for penetration and show a 8 times higher peak force in comparison to laminated PC without the HDPE reinforcement. It also shows an equally high penetration energy and peak force as pure PC sheet.

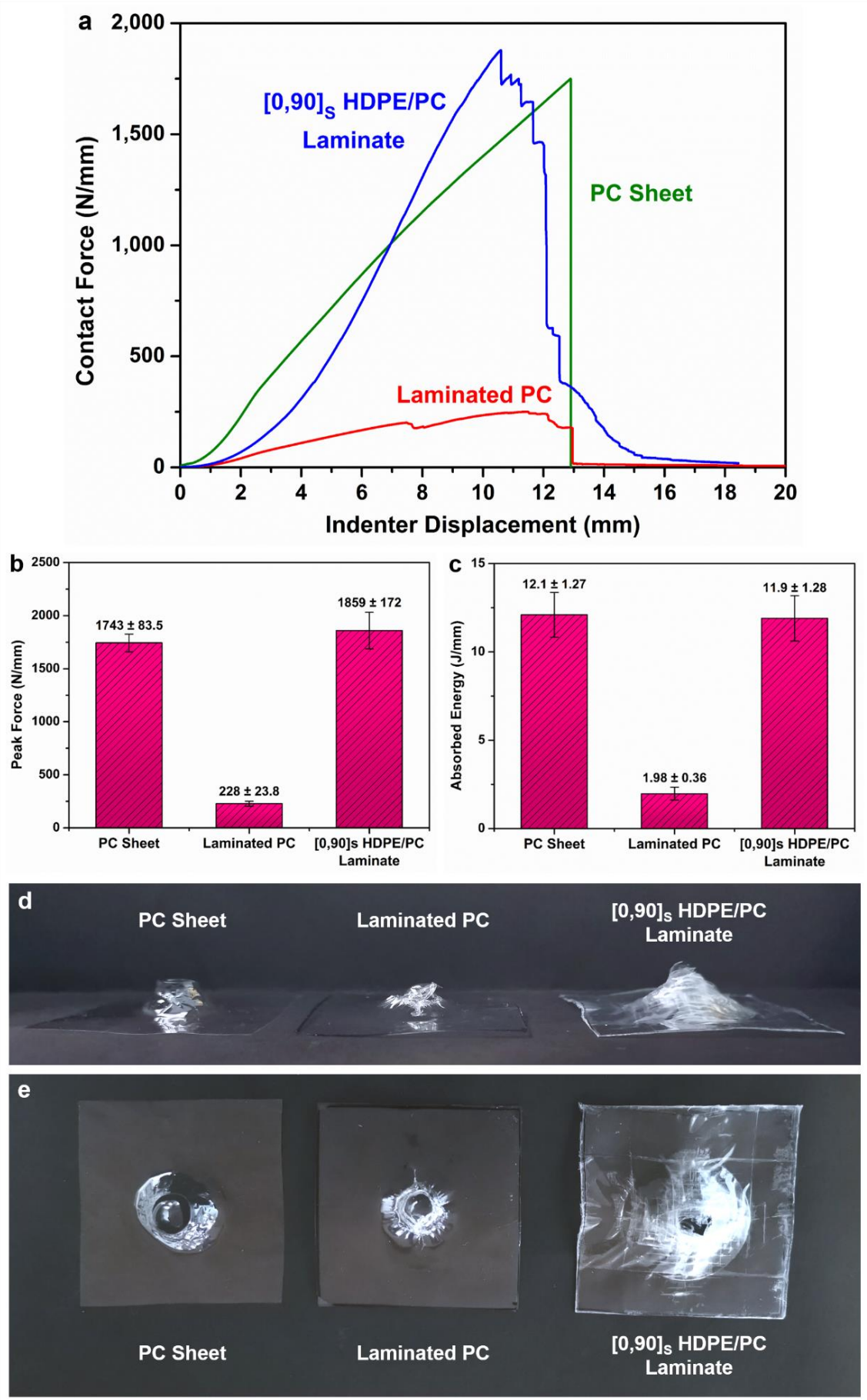
a
Contact Force (N/mm)
Indenter Displacement (mm)
[0,90]S HDPE/PC Laminate
PC Sheet
Laminated PC
b
Peak Force (N/mm)
1743 ± 83.5
228 ± 23.8
1859 ± 172
PC Sheet
Laminated PC
[0,90]s HDPE/PC Laminate
c
Absorbed Energy (J/mm)
12.1 ± 1.27
1.98 ± 0.36
11.9 ± 1.28
PC Sheet
Laminated PC
[0,90]s HDPE/PC Laminate
d
PC Sheet
Laminated PC
[0,90]S HDPE/PC Laminate
e
PC Sheet
Laminated PC
[0,90]S HDPE/PC Laminate

Figure 5.10 *The penetration resistance of BD HDPE transparent composites with PC as outer layers: (a) contact force versus indenter displacement, (b) absorbed energy and (c) peak force of PC sheet, laminated PC and BD [0,90]$_S$ HDPE/PC laminate, showing that the BD HDPE/PC laminate displays a similar performance to PC but with a much higher energy absorption and peak force compared to laminated PC. (d) Edge-side view of specimens with clear out-of-plane deformation and (e) bottom-side view after full penetration of PC sheet, laminated PC and BD [0,90]$_S$ HDPE laminate sandwiched between PC, showing the largest area of deformation for the BD HDPE/PC laminate. Contact force, absorbed energy and peak force are all normalised by specimen thickness.*

Images of fully penetrated specimens are shown in ***Figure 5.10(d)-(e)***. Pure PC sheet and laminated PC show a relatively small and localised out-of-plane deformation area with mainly yielding and plastic deformation. On the other hand, the BD [0,90]$_S$ HDPE/PC laminate consisting of four layers of oriented high performance HDPE films experienced many different stages of deformation upon loading before ultimate penetration. Failure modes range from delamination between HDPE layers, to tape fibrillation and lateral fracture of HDPE tapes. These fracture processes all contribute to the high level of energy absorption during penetration, as well as the large deformed area and out-of-plane deformation.

A few critical remarks are appropriate with respect to the results presented here. Most importantly, UD [0]$_4$ HDPE/glass laminates, as expected, exhibit birefringence between crossed polarizers (see ***Figure 5.11(a)***). Under specific illumination conditions (e.g. low incoming angle of direct sunlight), this birefringence can cause undesired optical effects such as the appearance of colours originating from polarization and wavelength dispersion effects[107]. Usually, these effects can be reduced efficiently by designing 0°/90°

cross-ply BD laminates and by compensation of the optical retardation ($d\Delta n$) in two or three dimensions. In ***Figure 5.11(b)***, it is shown that optical compensation is only partly achieved in BD $[0,90]_S$ HDPE/glass laminates which is probably related to thickness fluctuations in our stretched HDPE films and impurities like dust trapped within the laminates. It is anticipated that these technical issues can be resolved in an optimized manufacturing environment.

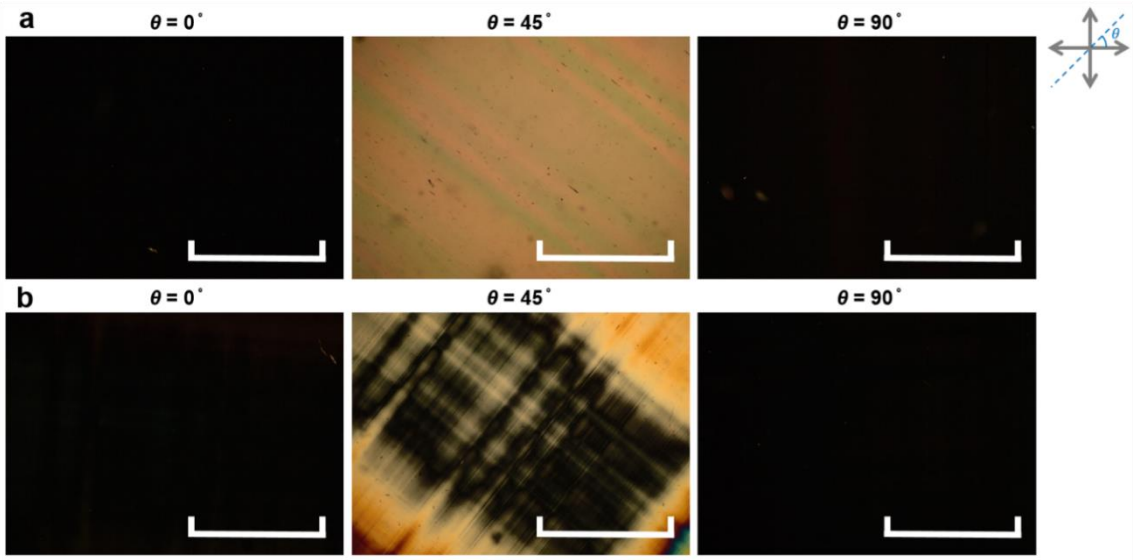

Figure 5.11 *Optical micrographs of (a) UD $[0]_4$ and (b) BD $[0,90]_S$ HDPE laminates with glass as outer layers between crossed polarizers. The direction of the crossed polarizers is horizontal and vertical. The scale bar is 500 µm.*

Although the PC outer layers exhibit a more ductile failure mode compared to laminates sandwiched between glass, the susceptibility to UV exposure and relatively low scratch resistant nature of PC may result in reduced levels of optical transmittance after long-term usage. On the other hand, the HDPE laminates with glass as outer layers may maintain their clear appearance after prolonged use especially if proper stabilizers are used in the HDPE. However, the nature of glass can lead to brittle fracture and cracking of the sheet glass in the laminates, whereas PC is more flexible and fails by yielding.

Therefore, depending on the requirements of the application, the most appropriate outer layer for these laminates should be selected. The number of reinforcing HDPE layers can also be adjusted according to the balance required between optical and mechanical properties, since an increase in number of HDPE layers for greater mechanical performance may lead to a sacrifice in optical clarity.

Due to the excellent combination of high tensile strength, penetration resistance and far field optical transparency, the fabricated HDPE laminates with either glass or PC as outer layers show great potential for replacing traditional inorganic glass or polymeric glasses like PC and PMMA for applications in structural glazing for buildings, automotive and aerospace, windshields, visors, displays, etc.

5.4 Conclusions

High performance transparent composite laminates based on highly oriented HDPE films sandwiched between either glass or PC have been successfully manufactured with a good combination of high optical transparency, good tensile properties and penetration resistance. TPU was selected as the interlayer material of choice because of its higher refractive index and better wetting and bonding properties compared to other evaluated adhesives. Far field transmittance values of around 85−90 % at 550 nm were achieved in laminates consisting of 1−4 layers of HDPE films with glass as outer layers, while about 2 % lower transmittance values were reported for corresponding specimens sandwiched between PC. It was also found that transmittance dropped by 1−2 % with every additional layer of TPU-coated HDPE due to increased reflections and light scattering at interfaces, regardless of a UD or BD lay-up within the laminates.

In terms of mechanical performance, good penetration resistance was achieved in BD $[0,90]_S$ HDPE laminates with glass as outer layers. Such laminates were able to absorb more than 25 times the energy required for full penetration compared to sheet glass or laminated glass. The high mechanical performance of these laminates was mainly attributed to the high strength and stiffness of the oriented HDPE films, together with good load transfer between layers by TPU interlayers. Apart from a high reinforcing efficiency of the HDPE films in terms of both modulus and strength, UD $[0]_4$ HDPE laminate with PC as outer layers also demonstrated a two times higher tensile strength and work-to-break compared to that of pure PC.

Chapter 6

Conclusions and future work

6.1 General discussion and conclusions

HDPE is one of the most widely used plastics with excellent processability and low cost. However, HDPE typically does not show simultaneously both high optical transparency and high mechanical performance. Existing transparent HDPE films and sheets are mostly drawn or blown in the melt state with moderate levels of molecular orientation and hence low moduli (0.6−3 GPa) and strengths (30−230 MPa)[8]. Compared to stretching in the melt, solid-state drawing is a far more effective way to increase the stiffness and tensile strength of polymers, notably polyethylenes. However, solid-state drawn HDPE fibres or films are normally opaque as a result of the large crystal sizes as well as the introduction of voids and defects during stretching.

In this work, high transparency, lightweight and high mechanical performance have been successfully combined in HDPE films as well as resulting composites. The thesis has focused on the production and characterization of these highly transparent high strength HDPE tapes or films prepared by a lab-scale and batch-wise process as well as a scalable and continuous pilot-scale extrusion process. Composite laminates based on these highly oriented transparent HDPE films have been manufactured and characterised.

First, the fabrication and properties of highly transparent high strength HDPE films made by a batch-wise process involving compression moulding and solid-state drawing at elevated temperatures was studied in Chapter 3. By tuning solid-state drawing processing parameters like drawing temperature and draw ratio, highly oriented HDPE films with a highly transparent appearance and a maximum light transmittance of ~ 90 % were achieved without the need of additives. When the drawing temperature rose to above 90 °C, the optical appearance of solid-state drawn HDPE films changed from opaque to transparent because this temperature is well above the α_c-relaxation temperature of PE which is typically around 80 °C[122]. Thus, greater mobility of chain segments in crystalline phases at high drawing temperatures are believed to be responsible for fewer defects in the bulk and on the surface of the drawn films, resulting in less light scattering and hence high clarity. This phenomenon was supported by reduced micro-voiding parallel to the drawing direction in combination with less interfibrillar defects and separation of fibrils with increasing drawing temperature after morphological observations. An optimum light transmittance of the solid-state drawn HDPE films was reached at a draw ratio of around 15, as microcracking vertical to the drawing direction was observed only for draw ratios above 20 and an increased number of micro-voiding and interfibrillar defects parallel to the drawing direction was also detected above this draw ratio.

These highly transparent HDPE films can reach a maximum Young's modulus of 27 GPa and a maximum tensile strength of 800 MPa along the drawing direction. This high modulus after solid-state drawing can be attributed to the formation of taut tie molecules, which connect crystalline regions and effectively transmit stress in the materials, induced by the orientation of polymer chains. And the high strength is related to the interchain interactions (mainly van der Waals forces) between highly oriented

chains, which can undergo a certain degree of chain slip. However, a decrease in modulus and strength at high draw ratios was observed at high drawing temperatures (T_d > 110 °C) as a result of the weak strain hardening, the relaxation of molecular deformation and orientation of the films in combination with a reduction in the number of taut tie molecules, resulting in less effective drawing at high temperatures. Besides, the microcracking perpendicular to the drawing direction occurred at high draw ratios, which is a local failure of several consecutive fibrils, also limited further orientation and deformation of polymer chains. It has been demonstrated that a wide processing window, ranging from 90 °C to 110 °C, can be used to tailor the required balance between optical and mechanical performance in order to achieve high strength transparent HDPE films.

Since the limited dimensions of the ultra-drawn HDPE films or tapes obtained by the above batch-wise process severely restricts the usage and evaluation of these films in single or multilayer laminates of larger dimensions, a continuous process was utilized to produce high strength transparent HDPE films using a cast film extrusion and solid-state drawing line (Chapter 4). The use of air knife during extrusion can decrease frost line height and hence increase cooling rate, leading to smaller sizes of crystals and improved transparency of the films. Also, it helps to get slightly wider extruded films and a higher uniformity in film thickness. Two methodologies have been explored to achieve such high strength transparent HDPE films: i) the use of BZT additives and ii) solid-state drawing at an optimal temperature of 105 °C (without additives). Both methodologies have been proven to result in highly oriented HDPE films of high transparency (nearly 91 %) in the far field as a result of a negligible amount of micro- or nano-voiding after solid-state drawing. An elevated drawing temperature facilitates the mobility of chain segments and results in reduced light scattering induced by the

voids and defects in the films as previously discussed, while the addition of BZT additives with a similar refractive index to HDPE can fill the existing voids and decrease the mismatch of refractive indices between HDPE and the voids[75]. Maximum attainable modulus (~ 33 GPa) and tensile strength (~ 900 MPa) of both types of drawn films are an order of magnitude higher than traditional transparent plastics such as PC and PMMA, and on a weight basis even outperforms structural materials like aluminium or glass fibre reinforced plastics. The BZT-free technology is a preferable technology from the point of low cost, easy processing and long-term stability as it was observed that BZT powders would migrate to the surface of the films after long-term storage (over 6 months) in a sealed box at RT, which indicates that BZT is not that stable and compatible with HDPE. Besides, an extra compounding step is needed before film extrusion and such additives are typically expensive in the BZT-based technology.

It has been confirmed that a high pre-orientation ratio is beneficial in improving mechanical properties of the films in a certain degree at equal draw ratios, whereas it also lowers the maximum attainable draw ratio and as such the ultimate modulus and tensile strength of the films. A high geometric pre-orientation ratio may not contribute to significant structure changes at the molecular level in pre-oriented HDPE films extruded in the melt state since a high degree of chain relaxation occurs above its melting temperature. A two-step drawing process does not notably alter the optical and mechanical performance of the films. In addition, a relatively high molecular weight gives rise to an excellent optical transparency of ~ 90 % in combination with a higher tensile strength of the drawn HDPE films as tensile strength is more sensitive to the molecular weight and its distribution in contrast to Young's modulus in terms of LPE.

Based on these continuous highly oriented transparent HDPE films as reinforcing phase, high performance transparent composite laminates have been successfully manufactured with a good combination of optical transparency and mechanical properties in Chapter 5. High optical transparency was achieved even in the far field, together with good tensile properties and penetration resistance in laminates sandwiched between glass or PC sheets. The selection of interlayer materials between the reinforcing HDPE layers was systematically studied in order to achieve efficient adhesion, load transfer in combination with optical clarity. Transparent TPU interlayer was chosen as a result of the matching refractive index to glass, PC as well as the oriented HDPE films in combination with its good wetting and bonding properties compared to EVA and PVB. Good optical transparency was achieved by fabricating composite laminates consisting of one to four layers of reinforcing HDPE films, showing a far field transmittance of around 90 % to 85 % at 550 nm with glass as outer layers, respectively. Slightly lower transmittance values (from 85 % to 83 %) were obtained for specimens sandwiched between PC because of a larger refractive index difference between PC and air compared to that of glass and air, thus leading to a higher reflectance. It was also found that with every additional layer of HDPE, the transmittance values dropped by 1−2 % as a result of more reflection at interfaces due to the refractive index difference between the solid-state drawn, birefringent HDPE and the optically isotropic TPU together with more light scattering induced by more defects, impurities and dust in or between layers with increasing numbers of HDPE layers, regardless of a UD or BD lay-up within the laminates.

Apart from a high reinforcing efficiency of the HDPE films in terms of both modulus and strength, good penetration resistance was achieved with BD HDPE $[0,90]_S$ laminates with glass as outer layers which were able to absorb more than 25 times the energy required for full penetration compared to that of sheet glass. The high mechanical performance of

these laminates was mainly attributed to the high strength and stiffness of the cross-plied oriented HDPE films, together with the good load transfer between layers due to the TPU interlayers. And the improved fracture toughness upon impact might result from the increased surfaces during delamination, tape pull-out, transverse splitting in combination with fibrillation of the tapes. The UD HDPE $[0]_4$ laminate with PC as outer layers also demonstrated a two times higher tensile strength and work-to-break compared to that of pure PC.

In short, optically transparent highly oriented polyethylene films and corresponding composites have been developed with excellent mechanical performance. These films and composites successfully fill the gap of high mechanical properties together with high optical clarity, offering great potential for numerous practical applications.

6.2 Future work

6.2.1 Application to other PE grades and other semi-crystalline polymers

The effects of drawing parameters including drawing temperature, draw ratio and drawing speed on optical and mechanical behaviour of drawn HDPE films was systematically investigated in Chapter 3. Some other factors such as molecular weight, molecular weight distribution and long chain branching may also have a remarkable influence on transparency, drawing behaviour and ultimate mechanical performance of the drawn HDPE films[13, 110, 123, 169]. In our current study, only two types of HDPE grade (Borealis VS4580 with a $\overline{M_w}$ of 134 kg/mol and a MWD of 3.6 as well as Total M5510EP with a $\overline{M_w}$ of 77 kg/mol and a MWD of 2.7) was researched. These grades were selected based

on earlier studies about the effect of polymer grade on drawability and ultimate mechanical properties of polyethylene fibres[77, 110, 112]. According to previous researches[77, 95], it was reported that drawn melt-crystallized linear polyethylene (LPE) films with a relatively high weight-average molecular weight ($\overline{M_w}$ ~ 408 kg/mol) or a high molecular weight distribution (MWD > 20) revealed a high transparency (~ 90 %) even without incorporating any additives at low draw ratios (λ ~ 10). On the other hand, solid-state drawn LPE films with $\overline{M_w}$ < 140 kg/mol or MWD < 10 were always opaque due to the microvoid-induced light scattering. In this thesis, only two grades of HDPE conforming to this range were checked. More studies on different PE grades with different molecular weights and molecular weight distributions within this range (opaque solid-state drawn films) should be carried out to observe whether the method of regulating drawing parameters like drawing temperature is also applicable to more polyethylene with different molecular weights and distributions. If this universality in LPE is confirmed, a relationship between the solid-state drawing temperature range for highly oriented transparent LPE films and molecular weight as well as its distribution could be further explored.

Since solution processed UHMWPE can reach much higher draw ratios (λ > 70) than melt-crystalized HDPE, it is worthwhile to investigate whether adjusting drawing temperature during solid-state drawing is also suitable to achieve transparent UHMWPE films or products after solution casting or other techniques so as to get higher mechanical properties including modulus, strength and impact resistance together with optical clarity.

Furthermore, as mentioned in Section 2.3.3.3, some other semi-crystalline polymers such as PP and PLA can possess some levels of transparency after solid-state drawing

at proper drawing temperatures and below certain draw ratios[103, 105]. However, few studies have systematically explored the influence of solid-state drawing temperature on the optical transparency of these polymers. The universality and regularity of tuning solid-state drawing temperature and draw ratio to fabricate transparent polymer films can be further examined in other semi-crystalline polymers to verify whether this approach is a general methodology to produce high mechanical performance transparent polymer products.

6.2.2 The challenge of manufacturing ultra-drawn transparent HDPE films at an industrial scale

In Chapter 4, an industrially relevant process including a cast film extrusion and solid-state in-line stretching line was carried out at pilot-scale. Although the use of conventional polymer processing equipment allows a direct implementation of this processing method into an industrial environment, some potential problems may emerge during practical industrial production, such as the inhomogeneity in film thickness, surface texturing, instabilities and discontinuity of the solid-state drawing process, etc.

The unevenness of film thickness at greater widths after drawing and thickness fluctuations along the lengths during extrusion may result in some issues including but not limited to: (i) transverse splitting of oriented films before reaching a high draw ratio during solid-state in-line stretching; (ii) different degrees of birefringence effects, which may lead to undesired optical effects like colours, affecting their application in optics.

Surface texture or roughness is primarily affected by extrusion and stretching conditions including the rheological behaviour of the melt, the crystal morphology and the degree of

crystallinity[222]. It has an impact on light transmission and the gloss of the products as light scattering due to surface roughness is a main cause of transparency loss especially in the far field.

The continuous solid-state drawing of films may also become unstable or even disrupted if improper drawing parameters are set, for instance in case a too high drawing velocity is used when aiming to achieve high draw ratios ($\lambda > 22$).

In future research, more emphasis should therefore be placed on how to solve these latent problems when this processing approach is actually transferred to industry.

6.2.3 High speed impact testing and theoretical impact models for HDPE based laminates

In Chapter 5, quasi-static penetration tests of the composite laminates based on cross-plied highly oriented transparent HDPE films were carried out at very low speed (1.25 mm/min). Penetration or impact tests under higher velocities such as in the case of falling dart impact testing (> 1 m/s) or anti-ballistic impact testing (> 100 m/s) should be carried out to explore the high speed impact resistance and damage behaviour of these laminates.

Moreover, theoretical impact models can be used to explore and predict the anti-ballistic performance of composite laminates based on these HDPE films. According to van der Werff *et al.*[223-224], a composite laminate conforms the following equation under textile based units:

$$\sqrt[3]{\Omega} = 171 \times \frac{\sigma_t^{2/3}}{E^{1/6}} \tag{6.1}$$

where Ω represents the velocity of sound in the fibres (m^3/s^3), σ_t and E are the strength (cN/dtex) and modulus (N/tex) of the fibres, respectively.

After rearranging Equation (6.1), the modulus can be represented as a function of tensile strength and speed:

$$E = \frac{171^6 \times \sigma_t^4}{(\sqrt[3]{\Omega})^6} \tag{6.2}$$

Equation (6.2) denotes the relationship between modulus and strength when Ω is a constant. In ***Figure 6.1***, the specific modulus is plotted versus specific strength for common transparent materials including our transparent oriented HDPE films. Here, the dash lines are the lines with constant cubic root of Ω ($\sqrt[3]{\Omega}$, m/s) according to Equation (6.2). Points connected by such lines are basically points with equal theoretical ballistic performance[224] and the speeds of different vehicles, projectiles or bullets are indicated here. If a material is positioned on the right-hand side of the line representing a certain speed, it denotes that this material can theoretically sustain this impact under this particular speed. Generally, the higher the value of Ω, the better the ballistic performance. This relationship can be used to predict the ballistic performance of HDPE or UHMWPE fibre reinforced composites for applications in safety and security products like safety glass, transparent armour, riot shields and automotive windshields. Using this model, the ballistic performance of our HDPE tape reinforced laminates or future UHMWPE tape reinforced laminates can be predicted and compared to the existing transparent products.

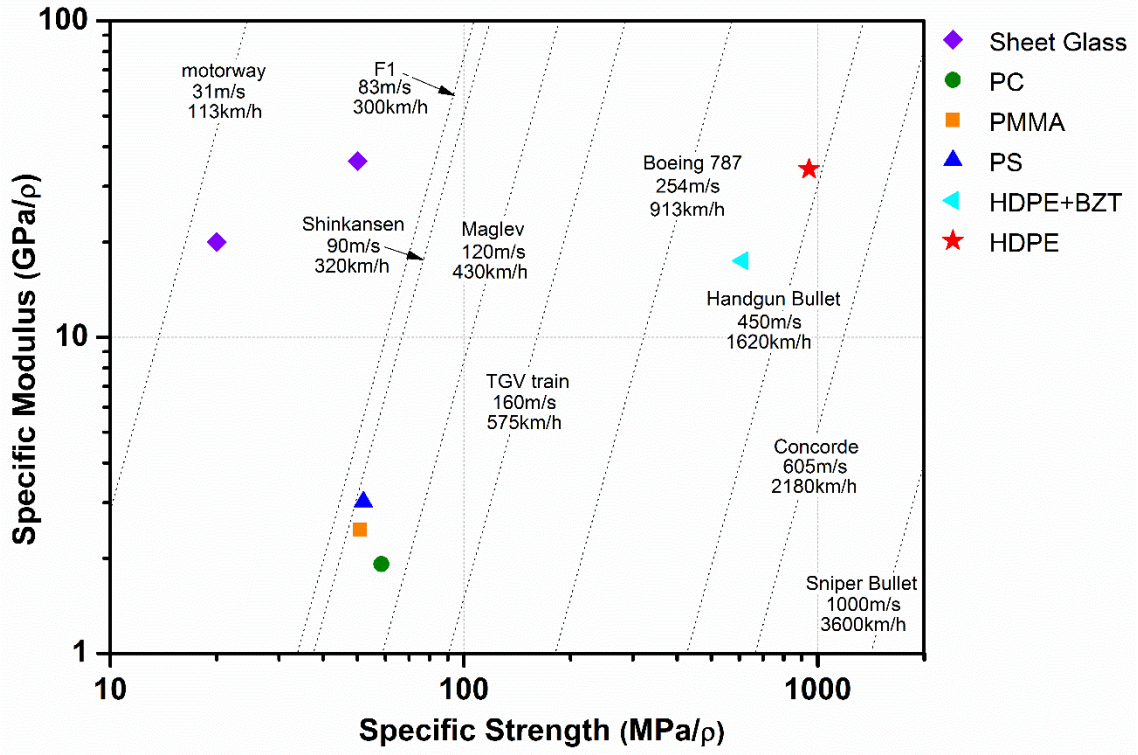

Figure 6.1 *Specific modulus versus specific strength of common transparent materials, previous transparent HDPE films with BZT additives*[75] *and our solid-state oriented HDPE films along the drawing direction, together with the corresponding sustainable speeds showing theoretical ballistic performance according to theoretical impact model.*

6.2.4 Other fabrication methods for HDPE-reinforced laminates and the design of transparent all-PE laminates

With regard to the fabrication of HDPE-reinforced laminates, only limited dimensions of laminate specimens could be obtained with a long production cycle when using compression moulding as stated in Chapter 5. In order to realize their industrial production for practical use, some other laminated glazing or composite manufacturing methods like autoclave moulding could be used and further investigated.

Additionally, transparent all-PE multilayer laminates based on uniaxially oriented transparent HDPE films can be designed and fabricated, aiming for recyclable, flexible and lightweight packaging applications such as pouches, liners and wraps. Hereinto, the barrier properties (barrier to humidity, aromas or gases) of highly oriented transparent HDPE films should be investigated and optimized in order to replace PET as a barrier layer in common PE/PET/PE laminates. Besides, the production of monomaterial laminates may impose higher demands on sealing technology to stick layers together, for instance resulting in a smaller heat sealing window in terms of temperature, pressure and time especially for heat-sensitive monomaterials as well as difficulties in achieving high sealing speeds, which should also be concerned in the future research.

Apart from the above, the high-temperature stability of the oriented transparent HDPE films ought to be researched since a relatively high temperature is needed in the lamination and/or sealing process when producing transparent all-PE laminates, which may affect the properties especially mechanical behaviours of the oriented films. Besides, in some certain applications, for instance being used as a reinforcing layer in an automotive windshield, the oriented HDPE films should withstand high temperature and maintain good dimensional stability without significant changes in optical and mechanical performance when the car is driven on a hot summer day or even in the desert.

6.2.5 Introducing multi-functionality in highly oriented transparent HDPE films

Apart from optical and mechanical properties, other functionalities can be added to highly oriented transparent HDPE films. For instance, blending of a small amount of carbon nanotubes (CNTs) or graphene with HDPE prior to solid-state drawing or spray coating

these nanocarbons on the surface of such films may achieve a certain degree of electrical and/or thermal (anisotropic) conductivity. Previous work done by Grieg *et al.* regarding low-temperature thermal conductivity of oriented polymers showed a highly anisotropic behaviour of thermal conductivity, i.e. the oriented polymer is a good conductor along the drawing direction but a thermal insulator transversely[225-226]. It has been reported that transparent drawn UHMWPE fibres, tapes and films with a high thermal conductivity (up to 104 and 65 W/m·K for fibres and films, respectively) can be achieved by transmitting lattice vibration in combination with engineering non-crystalline chains in amorphous phase through disentanglement and alignment[227-230]. Their thermal conductivity exceeds that of typical polymers (usually ~ 0.1 W/m·K) as well as many metals and ceramics, facilitating their use in applications where dissipation of heat is required, like electrically insulating thermal conductors.

Moreover, our research team also discovered that the incorporation of photo-responsive dyes or additives (like azobenzene or BZT) to oriented transparent HDPE or UHMWPE films can induce thermal heating and entropic actuation[231-233]. Such films with high stiffness (~ 80 GPa) can generate a rapid and reversible photo-mechanical response with a record high actuation stress (~ 70 MPa) at low strains (< 0.1 %) under UV light radiation, which may be used as flexible, lightweight polymeric actuators with physical values approaching metals or ceramics. Resulting products with different functionalities may be applied in sensors, actuators, thermal conductors or automotive rear windows with deicing and defogging function. For this direction of research, the main focal point should be on how to reduce transmittance loss in order to maintain a transparent appearance in combination with introducing new functionalities.

6.3 Potential applications

A major advantage of polyethylene over most other solid materials is the low density ($\rho \approx 1$ g/cm^3), which leads to high values of specific strength (tensile strength divided by density) and specific modulus (elastic modulus divided by density) of the ultra-drawn polyethylene fibres and films.

The specific strength and modulus of common transparent materials like sheet glass, PMMA, PC, PS and BOPET films, drawn HDPE films with BZT additives previously produced by Shen *et al.*[75], our current highly oriented transparent HDPE films along the drawing direction together with UD and BD HDPE-reinforced laminates with PC as outer layers are shown in ***Figure 6.2***. Sheet glass including laminated glass, tempered glass or toughened glass like Gorilla® glass has a relatively low specific strength due to its high density ($\rho \approx 2.5$ g/cm^3). In comparison, polymers usually have lower densities around 1−1.5 g/cm^3. Commercial transparent polymeric materials such as PMMA, PC and PS typically possess specific moduli of around 2−3 GPa/(g·cm^{-3}) and specific strengths of 40−60 MPa/(g·cm^{-3}), and transparent BOPET films widely used in packaging have a specific modulus and strength of about 3.3 GPa/(g·cm^{-3}) and 145 MPa/(g·cm^{-3}) in both MD and TD. However, the specific strength and modulus of our highly transparent solid-state drawn HDPE films along the drawing direction can reach values as high as 940 MPa/(g·cm^{-3}) and 34 GPa/(g·cm^{-3}), which is similar to that of high strength glass fibres. The specific strength of these oriented HDPE films is more than 15 times higher than both traditional sheet glass and traditional transparent polymeric materials, over 5 times higher than transparent BOPET films, and also about 45 % higher than previous drawn HDPE films where transparency was induced through the addition of additives like BZT. The specific modulus of these transparent films is also similar to classic engineering materials

like aluminium and steel, while its specific strength is over 9 times that of aluminium alloy and 12 times that of high strength steel. Composite laminates based on these highly oriented transparent HDPE films as the reinforcing phase and PC as the outer layers with either UD or BD lay-ups also exhibit higher specific strengths compared to conventional glass and other transparent plastics. Hence, our optimized solid-state drawn HDPE films and corresponding UD and BD HDPE reinforced composite laminates successfully combine high transparency with lightweight, high strength and high stiffness.

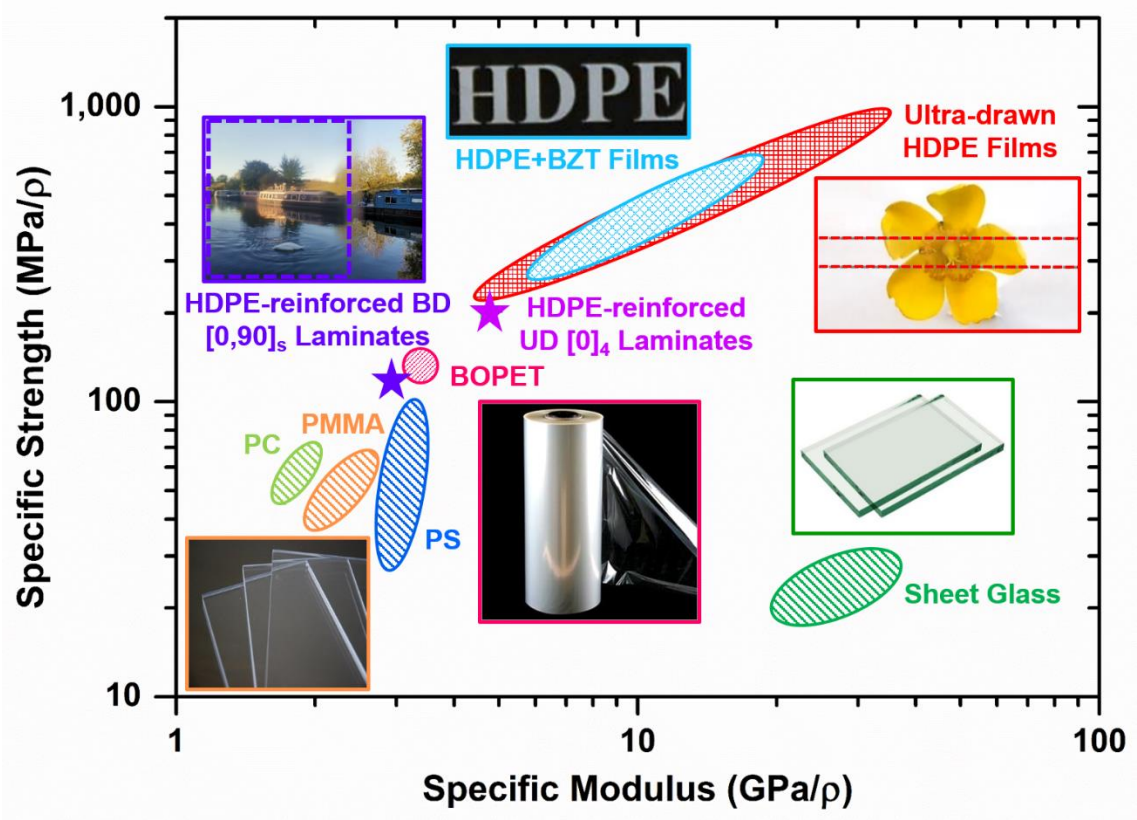

Figure 6.2 *Comparison of specific strength, specific modulus and the appearance of common transparent materials, previous transparent HDPE films with BZT additives*[75]*, our solid-state oriented HDPE films along the drawing direction and UD and BD HDPE-reinforced composite laminates with PC as outer layers.*

In terms of potential applications, they can be expected when subject to the successful completion of the future work as stated in Section 6.2. Firstly, the produced highly transparent, high strength ultra-drawn polyethylene films and tapes can act as reinforcing layers in transparent composite laminates or laminated glazing as reported in Chapter 5. Another important application area for such films could be in fully recyclable "all-PE" multilayer packaging films with good barrier properties. Currently, plastic packaging consists of multilayers like PE/PET/PE laminates, where PET with excellent barrier properties is sandwiched between low cost PE. These multi-material laminates are typically not transparent and are difficult to recycle due to the need to separate the different film layers. Machine direction orientation (MDO) processing technology like uniaxial solid-state drawing as performed in this thesis is routinely used by industry and can result in high-quality films with excellent stiffness and toughness in combination with great clarity. According to previous studies[234-235], uniaxial drawing can notably improve the barrier properties of HDPE films as a result of increased crystallinity, restricting the transmission of small molecules like water and oxygen through the films. However, uniaxially drawn PE films showed a minimum moisture and oxygen transmission rate at draw ratios of around 6−8. Interestingly, at higher draw ratios, voiding significantly lowered their barrier properties. As the HDPE films developed in this thesis revealed few micro- and nanovoids even at high draw ratios of around 15, these films may combine high mechanical properties with excellent barrier properties and transparency, all favourable characteristic for lightweight packaging. Such MDO polyethylene films have therefore the potential to replace PET as barrier layer in all-PE laminates for flexible packaging applications like pouches, sachets, bags, liners and wraps. Since the use of monomaterials in packaging makes collection, sorting and recycling more efficient, monomaterial structures are more favourable in terms of easy processibility, recyclability

and sustainability as a result of the ongoing drive towards zero-plastic waste and a circular economy. Finally, following the successful development of self-reinforced polypropylene (SRPP) materials like Curv® or PURE®, these transparent MDO polyethylene films could also form the basis for a whole new range of transparent self-reinforced "all-polymer" composites[202, 236-238]. However, the successful production and the attainable properties of the transparent self-reinforced all-PE laminates or composites will be a major challenge before they can be actually used in practical applications as stated in Section 6.2.4.

The realization of a continuous cast film extrusion and solid-state drawing process for these transparent polyethylene films makes application of these MDO films and corresponding composites in fields of packaging, transportation and life protection possible, which includes but is not limited to flexible plastic packaging, glazing for buildings, automotive vehicles or aircraft, automotive windshields, transparent armour, protective windows, visors, safety glass or displays for electronic devices. Due to their lightweight, high mechanical performance and ease of production at relatively low cost, these polyethylene films and their composite laminates have great potential as replacements for traditional inorganic glazing and commercial transparent polymeric materials like PC or PMMA.

References

1. Haldimann, M.; Luible, A.; Overend, M. *Structural Use of Glass*, IABSE: Zürich, 2008; Vol. 10.

2. Harper, C. A.; Petrie, E. M. *Plastics Materials and Processes: A Concise Encyclopedia*, Wiley: Chichester, 2003.

3. Vedrtnam, A.; Pawar, S. J. Laminated plate theories and fracture of laminated glass plate – A review. *Eng. Fract. Mech.* **2017,** *186*, 316-330.

4. Abid, H. M.; Shah, Q. H.; Ibrahim, M. S. Perforation of Polycarbonate Sheet When Subjected to Impact Test–A Review. *Int. J. Appl. Eng. Res.* **2017,** *12* (24), 14514-14522.

5. Rühl, A.; Kolling, S.; Schneider, J. Characterization and modeling of poly(methyl methacrylate) and thermoplastic polyurethane for the application in laminated setups. *Mech. Mater.* **2017,** *113*, 102-111.

6. Kristiansen, M.; Werner, M.; Tervoort, T.; Smith, P.; Blomenhofer, M.; Schmidt, H.-W. The binary system isotactic polypropylene/bis(3,4-dimethylbenzylidene)sorbitol: phase behavior, nucleation, and optical properties. *Macromolecules* **2003,** *36* (14), 5150-5156.

7. Vasile, C.; Pascu, M. *Practical Guide to Polyethylene*, iSmithers Rapra Publishing: Shropshire, 2005.

8. Johnson, M. B.; Wilkes, G. L.; Sukhadia, A. M.; Rohlfing, D. C. Optical properties of blown and cast polyethylene films: Surface versus bulk structural considerations. *J. Appl. Polym. Sci.* **2000,** *77* (13), 2845-2864.

9. Williams Jr, R. F.; Jenks, R. H. Transparent polyolefin films of high modulus and clarity. US3503843, 1970.

10. Breese, D. R. Preparation of polyethylene films. US7011892, 2006.

11. Ward, I. M.; Coates, P. D.; Dumoulin, M. M. *Solid phase processing of polymers*, Hanser Publishers: Munich, 2000.

12. Stein, R. S.; Prud'Homme, R. Origin of polyethylene transparency. *J. Polym. Sci., Part B: Polym. Lett.* **1971,** *9* (8), 595-598.

13. Jarecki, L.; Meier, D. J. Ultrahigh modulus polyethylene. II. Effect of drawing temperature on void formation and modulus. *J. Polym. Sci., Part B: Polym. Phys.* **1979,** *17* (9), 1611-1621.

14. Peijs, T.; Venderbosch, R. W.; Lemstra, P. J. Hybrid composites based on polyethylene and carbon fibres Part 3: Impact resistant structural composites through damage management. *Composites* **1990,** *21* (6), 522-530.

15. Li, H.; Richards, C.; Watson, J. High-Performance Glass Fiber Development for Composite Applications. *Int. J. Appl. Glass Sci.* **2014,** *5* (1), 65-81.

16. Tabiei, A.; Nilakantan, G. Ballistic Impact of Dry Woven Fabric Composites: A Review. *Appl. Mech. Rev.* **2008,** *61* (1), 010801.

17. Peijs, T. High performance polyethylene fibers. In *Comprehensive Composite Materials II*; Beaumont, P. W. R.; Zweben, C. H., Eds.; Elsevier: Oxford, 2018; Chapter 1.5, pp 86-126.

18. Krug Iii, D. J.; Asuncion, M. Z.; Popova, V.; Laine, R. M. Transparent fiber glass reinforced composites. *Compos. Sci. Technol.* **2013,** *77*, 95-100.

19. Menta, V. G. K.; Vuppalapati, R. R.; Chandrashekhara, K.; Schuman, T. Manufacturing of Transparent Composites Using Vacuum Infusion Process. *Polym. Polym. Compos.* **2014,** *22* (9), 843-850.

20. Bergshoef, M. M.; Vancso, G. J. Transparent Nanocomposites with Ultrathin, Electrospun Nylon-4,6 Fiber Reinforcement. *Adv. Mater.* **1999,** *11* (16), 1362-1365.

21. Krauthauser, C.; Deitzel, J. M.; O'Brien, D.; Hrycushko, J. Optical Properties of Transparent Resins with Electrospun Polymer Nanofibers. In *Polymeric Nanofibers*; American Chemical Society: Washington, DC, 2006; Chapter 25, pp 353-369.

22. O'Brien, D. J.; Parquette, B.; Hoey, M. L.; Perry, J. The design and performance of a polymer ribbon-reinforced transparent composite material. *Polym. Compos.* **2018,** *39* (7), 2523-2534.

23. Lokensgard, E. *Industrial Plastics: Theory and Applications*, Cengage Learning: Boston, 2016.

24. Skaar, J. Fresnel equations and the refractive index of active media. *Phys. Rev. E* **2006,** *73* (2), 026605.

25. AMIRAN® glass. http://www.schott.com/architecture/english/products/anti-reflective-glass/amiran-showcases.html (accessed January 9, 2020).

26. De Jong, B. H. W. S.; Beerkens, R. G. C.; van Nijnatten, P. A.; Le Bourhis, E. Glass, 1. Fundamentals. In *Ullmann's Encyclopedia of Industrial Chemistry*; Wiley: Chichester, 2000.

27. Onbaşlı, M. C.; Tandia, A.; Mauro, J. C. Mechanical and Compositional Design of High-Strength Corning Gorilla® Glass. In *Handbook of Materials Modeling: Applications: Current and Emerging Materials*; Andreoni, W.; Yip, S., Eds.; Springer International Publishing: Cham, 2020; pp 1997-2019.

28. Grattan, K. T.; Meggitt, B. T. *Optical Fiber Sensor Technology*, Springer: London, 1999.

29. Yin, S.; Ruffin, P. Fiber optic sensors. In *Wiley Encyclopedia of Biomedical Engineering*; Wiley: Chichester, 2006.

30. Campbell, F. C. *Fatigue and Fracture: Understanding the Basics*, ASM International: Ohio, 2012.

31. Rosato, D. V.; Rosato, D. V.; Rosato, M. V. 2 - PLASTIC PROPERTY. In *Plastic Product Material and Process Selection Handbook*; Rosato, D. V.; Rosato, D. V.; Rosato, M. V., Eds.; Elsevier: Oxford, 2004; pp 40-129.

32. Ashby, M. F.; Johnson, K. *Materials and Design: The Art and Science of Material Selection in Product Design*, Elsevier: Oxford, 2013.

33. McKeen, L. W. Styrenic Plastics. In *The Effect of Creep and Other Time Related Factors on Plastics and Elastomers (Third Edition)*; McKeen, L. W., Ed.; William Andrew Publishing: Boston, 2015; Chapter 2, pp 43-95.

34. Gao, R.; He, X.; Shao, Y.; Hu, Y.; Zhang, H.; Liu, Z.; Liu, B. Effects of Branch Content and Branch Length on Polyethylene Crystallization: Molecular Dynamics Simulation. *Macromol. Theory Simul.* **2016,** *25* (3), 303-311.

35. Pai, C.-L.; Boyce, M. C.; Rutledge, G. C. Mechanical properties of individual electrospun PA 6(3)T fibers and their variation with fiber diameter. *Polymer* **2011,** *52* (10), 2295-2301.

36. Hoffmann, K.; Huber, G.; Mäder, D. Nucleating and clarifying agents for polyolefins. *Macromol. Symp.* **2001,** *176* (1), 83-92.

37. Hamada, K.; Uchiyama, H. Polyolefin plastic compositions. US4016118, 1977.

38. Tenma, M.; Mieda, N.; Takamatsu, S.; Yamaguchi, M. Structure and properties for transparent polypropylene containing sorbitol-based clarifier. *J. Polym. Sci., Part B: Polym. Phys.* **2008,** *46* (1), 41-47.

39. Rekers, J. W. Bis(3,4-dialkylbenzylidene) sorbitol acetals and compositions containing same. US5049605A, 1991.

40. Wang, H.; Li, C.-C.; Ke, Y.-C.; Zhang, D.; Li, Z.-Y. Effects of rosin-type clarifying agent on the crystallization and compatibility of polypropylene and low density polyethylene. *J. Appl. Polym. Sci.* **2006,** *99* (4), 1568-1575.

41. Wang, J.; Dou, Q.; Wu, S.; Chen, X. Influence of the amount of salts of rosin acid on the nonisothermal crystallization, morphology, and properties of isotactic polypropylene. *Polym. Eng. Sci.* **2007,** *47* (6), 889-897.

42. Zhang, G. P.; Xin, Z.; Yu, J. Y.; Gui, Q. D.; Wang, S. Y. Nucleating Efficiency of Organic Phosphates in Polypropylene. *J. Macromol. Sci. B* **2003,** *42* (3-4), 467-478.

43. Kristiansen, P. M.; Gress, A.; Smith, P.; Hanft, D.; Schmidt, H.-W. Phase behavior, nucleation and optical properties of the binary system isotactic polypropylene/N,N',N''-tris-isopentyl-1,3,5-benzene-tricarboxamide. *Polymer* **2006,** *47* (1), 249-253.

44. Makarewicz, P. J.; Wilkes, G. L. Morphology studies of the liquid-induced crystallization of poly(ethylene terephthalate): Effects of polymer blending, nucleating agents, and molecular weight. *J. Appl. Polym. Sci.* **1979,** *23* (6), 1619-1638.

45. Mitra, D.; Misra, A. Study on the effect of dibenzylidene sorbitol as a nucleating agent on the crystallization and morphology of poly(ethylene terephthalate). *J. Appl. Polym. Sci.* **1988,** *36* (2), 387-402.

46. Dong, J.; Fan, Z. Nonisothermal Crystallization Behaviour of a Novel Cycloaliphatic Microcrystalline Poly(4,4'-Aminocyclohexyl Methylene Dodecanedicarboxylamide). *Polym. Polym. Compos.* **2014,** *22* (4), 401-408.

47. Gahleitner, M.; Jääskeläinen, P.; Ratajski, E.; Paulik, C.; Reussner, J.; Wolfschwenger, J.; Neißl, W. Propylene–ethylene random copolymers: Comonomer effects on crystallinity and application properties. *J. Appl. Polym. Sci.* **2005,** *95* (5), 1073-1081.

48. Gahleitner, M.; Pham, T.; Ackermans, N.; Ommundsen, E.; Grein, C.; Machl, D. Improved transparent polypropylene composition. EP1889873, 2008.

49. Mileva, D.; Androsch, R.; Radusch, H.-J. Effect of structure on light transmission in isotactic polypropylene and random propylene-1-butene copolymers. *Polym. Bull.* **2009,** *62* (4), 561-571.

50. Zhang, W.; Gui, Z.; Lu, C.; Cheng, S.; Cai, D.; Gao, Y. Improving transparency of incompatible polymer blends by reactive compatibilization. *Mater. Lett.* **2013,** *92*, 68-70.

51. Maruhashi, Y.; Iida, S. Transparency of polymer blends. *Polym. Eng. Sci.* **2001,** *41* (11), 1987-1995.

52. Hu, Y. S.; Prattipati, V.; Hiltner, A.; Baer, E.; Mehta, S. Improving transparency of stretched PET/MXD6 blends by modifying PET with isophthalate. *Polymer* **2005,** *46* (14), 5202-5210.

53. Prattipati, V.; Hu, Y. S.; Bandi, S.; Mehta, S.; Schiraldi, D. A.; Hiltner, A.; Baer, E. Improving the transparency of stretched poly(ethylene terephthalate)/polyamide blends. *J. Appl. Polym. Sci.* **2006,** *99* (1), 225-235.

54. Bühler, F. S. Colorless, highly transparent polyamide blends with improved stress cracking resistance. US6528560, 2003.

55. Lüpke, T.; Dunger, S.; Sänze, J.; Radusch, H. J. Sequential biaxial drawing of polypropylene films. *Polymer* **2004,** *45* (20), 6861-6872.

56. Masuda, J. i.; Ohkura, M. Preparation and characterization of biaxially oriented polypropylene film with high molecular orientation in the machine direction by sequential biaxial stretching. *J. Appl. Polym. Sci.* **2007,** *106* (6), 4031-4037.

57. Lin, Y. J.; Dias, P.; Chum, S.; Hiltner, A.; Baer, E. Surface roughness and light transmission of biaxially oriented polypropylene films. *Polym. Eng. Sci.* **2007,** *47* (10), 1658-1665.

58. DeMeuse, M. T. Processing and Film Properties of Polypropylene Made Using Metallocene Catalysts. *J. Plast. Film & Sheeting* **2002,** *18* (1), 17-23.

59. Menary, G. H.; Tan, C. W.; Harkin-Jones, E. M. A.; Armstrong, C. G.; Martin, P. J. Biaxial deformation and experimental study of PET at conditions applicable to stretch blow molding. *Polym. Eng. Sci.* **2012,** *52* (3), 671-688.

60. Chen, W. X.; Yu, J. S.; Chen, G. L.; Qiu, X. P.; Hu, W.; Bai, H. Y.; Shao, J. Z. Development of a novel protocol for the permanent hydrophilic modification of a BOPP film for high quality printing with water-based ink. *RSC Adv.* **2015,** *5* (107), 87963-87970.

61. Billham, M.; Clarke, A. H.; Garrett, G.; McNally, G. M.; Murphy, W. R. The Effect of Extrusion Processing Conditions on the Properties of Blown and Cast Polyolefin Packaging Films. *Dev. Chem. Eng. Min. Process* **2003,** *11* (1-2), 137-146.

62. Herman, M. *Encyclopedia of Polymer Science and Technology*, Wiley: Chichester, 2013.

63. Varma, P.; Lofgren, E. A.; Jabarin, S. A. Properties and kinetics of thermally crystallized oriented poly(ethylene terephthalate) (PET). II: Physical and optical properties. *Polym. Eng. Sci.* **1998,** *38* (2), 245-253.

64. Iler, H. D.; Rutt, E.; Althoff, S. An Introduction to Polymer Processing, Morphology, and Property Relationships through Thermal Analysis of Plastic PET Bottles. Exercises Designed to Introduce Students to Polymer Physical Properties. *J. Chem. Educ.* **2006,** *83* (3), 439.

65. Ou, X.; Cakmak, M. Influence of biaxial stretching mode on the crystalline texture in polylactic acid films. *Polymer* **2008,** *49* (24), 5344-5352.

66. Tsai, C. C.; Wu, R. J.; Cheng, H. Y.; Li, S. C.; Siao, Y. Y.; Kong, D. C.; Jang, G. W. Crystallinity and dimensional stability of biaxial oriented poly(lactic acid) films. *Polym. Degrad. Stab.* **2010,** *95* (8), 1292-1298.

67. Liu, J. G.; Ni, H. J.; Wang, Z. H.; Yang, S. Y.; Zhou, W. F. Colorless and transparent high-temperature-resistant polymer optical films–current status and potential applications in optoelectronic fabrications. In *Optoelectronics: Materials and Devices*; Pyshkin, S. L.; Ballato, J., Eds.; InTech: Rijeka, 2015; pp 57-81.

68. Cakmak, M.; Wang, Y. D.; Simhambhatla, M. Processing characteristics, structure development, and properties of uni and biaxially stretched poly(ethylene 2,6 naphthalate) (PEN) films. *Polym. Eng. Sci.* **1990,** *30* (12), 721-733.

69. Bafna, A.; Beaucage, G.; Mirabella, F.; Skillas, G.; Sukumaran, S. Optical properties and orientation in polyethylene blown films. *J. Polym. Sci., Part B: Polym. Phys.* **2001,** *39* (23), 2923-2936.

70. Jiang, Z.; Tang, Y.; Rieger, J.; Enderle, H.-F.; Lilge, D.; Roth, S. V.; Gehrke, R.; Wu, Z.; Li, Z.; Li, X.; Men, Y. Structural evolution of melt-drawn transparent high-density polyethylene during heating and annealing: Synchrotron small-angle X-ray scattering study. *Eur. Polym. J.* **2010,** *46* (9), 1866-1877.

71. Dow TF-BOPE sustainable packaging solutions and ENGAGETM PV POE Win 2018 R&D 100 Awards. In *China Chem. Rep.*, 2019; Vol. 30.

72. Lin, Y.; Xu, J.; Pan, J.; Yun, X. B.; Demirors, M., Biaxially oriented polyethylene (BOPE) films fabricated via tenter frame process and applications thereof. In *Annual Technical Conference - ANTEC, Conf. Proc.*, 2018.

73. Yao, J.; Bastiaansen, C.; Peijs, T. High strength and high modulus electrospun nanofibers. *Fibers* **2014,** *2* (2), 158.

74. Huck, N. D.; Clegg, P. L. The effect of extrusion variables on the fundamental properties of tubular polythene film. *Polym. Eng. Sci.* **1961,** *1* (3), 121-132.

75. Shen, L.; Nickmans, K.; Severn, J.; Bastiaansen, C. W. M. Improving the transparency of ultra-drawn melt-crystallized polyethylenes: toward high-modulus/high-strength window application. *ACS Appl. Mater. Interfaces* **2016,** *8* (27), 17549-17554.

76. Shen, L.; Severn, J. R.; Bastiaansen, C. W. M. Transparant drawn article. WO2017103055, 2017.

77. Shen, L.; Severn, J.; Bastiaansen, C. W. M. Improving Visible-Light Transparency of Drawn Melt-Crystallized Linear Polyethylenes: Influence of Molecular Weight Distribution. *Macromol. Mater. Eng.* **2017,** *302* (6), 1700003.

78. Pan, X.; Shen, L.; Schenning, A. P. H. J.; Bastiaansen, C. W. M. Transparent, High-Thermal-Conductivity Ultradrawn Polyethylene/Graphene Nanocomposite Films. *Adv. Mater.* **2019,** *31* (40), 1904348.

79. Shen, L.; Severn, J.; Bastiaansen, C. W. M. Drawing behavior and mechanical properties of ultra-high molecular weight polyethylene blends with a linear polyethylene wax. *Polymer* **2018,** *153*, 354-361.

80. Pan, X.; Schenning, A. H. P. J.; Shen, L.; Bastiaansen, C. W. M. The Role of Polyethylene Wax on the Thermal Conductivity of Transparent Ultradrawn Polyethylene Films. *Macromolecules* **2020,** *53* (13), 5599.

81. Erdmann, M.; Kupsch, A.; Müller, B. R.; Hentschel, M. P.; Niebergall, U.; Böhning, M.; Bruno, G. Diesel-induced transparency of plastically deformed high-density polyethylene. *J. Mater. Sci.* **2019,** *54* (17), 11739-11755.

82. Deng, H.; Reynolds, C. T.; Cabrera, N. O.; Barkoula, N. M.; Alcock, B.; Peijs, T. The water absorption behaviour of all-polypropylene composites and its effect on mechanical properties. *Compos. Part B - Eng.* **2010,** *41* (4), 268-275.

83. Nishino, T.; Arimoto, N. All-Cellulose Composite Prepared by Selective Dissolving of Fiber Surface. *Biomacromolecules* **2007,** *8* (9), 2712-2716.

84. Soykeabkaew, N.; Arimoto, N.; Nishino, T.; Peijs, T. All-cellulose composites by surface selective dissolution of aligned ligno-cellulosic fibres. *Compos. Sci. Technol.* **2008,** *68* (10), 2201-2207.

85. Yano, H.; Sugiyama, J.; Nakagaito, A. N.; Nogi, M.; Matsuura, T.; Hikita, M.; Handa, K. Optically Transparent Composites Reinforced with Networks of Bacterial Nanofibers. *Adv. Mater.* **2005,** *17* (2), 153-155.

86. Gea, S.; Bilotti, E.; Reynolds, C. T.; Soykeabkeaw, N.; Peijs, T. Bacterial cellulose–poly(vinyl alcohol) nanocomposites prepared by an in-situ process. *Mater. Lett.* **2010,** *64* (8), 901-904.

87. Moon, R. J.; Martini, A.; Nairn, J.; Simonsen, J.; Youngblood, J. Cellulose nanomaterials review: structure, properties and nanocomposites. *Chem. Soc. Rev.* **2011,** *40* (7), 3941-3994.

88. Berglund, L. A.; Peijs, T. Cellulose Biocomposites—From Bulk Moldings to Nanostructured Systems. *MRS Bull.* **2011,** *35* (3), 201-207.

89. Li, Y.; Fu, Q.; Yu, S.; Yan, M.; Berglund, L. Optically Transparent Wood from a Nanoporous Cellulosic Template: Combining Functional and Structural Performance. *Biomacromolecules* **2016,** *17* (4), 1358-1364.

90. Osaka, N.; Yanagi, K.; Saito, H. The optical transparency and structural change of quenched poly(vinylidene fluoride) caused by cold-drawing. *Polym. J.* **2013,** *45* (10), 1033-1040.

91. Southern, J. H.; Porter, R. S. The properties of polyethylene crystallized under the orientation and pressure effects of a pressure capillary viscometer. *J. Appl. Polym. Sci.* **1970,** *14* (9), 2305-2317.

92. Niikuni, T.; Porter, R. S. Preparation of ultra-oriented, high-strength filaments of polyethylene. *J. Mater. Sci.* **1974,** *9* (3), 389-397.

93. Southern, J. H.; Wilkes, G. L. Transparent high density polyethylene films crystallized under orientation and pressure. *J. Polym. Sci., Polym. Chem. Ed.* **1973,** *11* (9), 555-562.

94. Griswold, P. D.; Zachariades, A. E.; Porter, R. S. Solid state coextrusion: A new technique for ultradrawing thermoplastics illustrated with high density polyethylene. *Polym. Eng. Sci.* **1978,** *18* (11), 861-863.

95. Shen, L. Drawn melt-crystallized linear polyethylene: visible-light transparency and surface micro-patterning. Doctoral Thesis, Technische Universiteit Eindhoven, Netherlands, 2017.

96. Böhning, M.; Niebergall, U.; Adam, A.; Stark, W. Impact of biodiesel sorption on mechanical properties of polyethylene. *Polym. Test.* **2014,** *34*, 17-24.

97. Böhning, M.; Niebergall, U.; Zanotto, M.; Wachtendorf, V. Impact of biodiesel sorption on tensile properties of PE-HD for container applications. *Polym. Test.* **2016,** *50*, 315-324.

98. Erdmann, M.; Böhning, M.; Niebergall, U. Physical and chemical effects of biodiesel storage on high-density polyethylene: Evidence of co-oxidation. *Polym. Degrad. Stab.* **2019,** *161*, 139-149.

99. Rozanski, A.; Galeski, A. Controlling Cavitation of Semicrystalline Polymers during Tensile Drawing. *Macromolecules* **2011,** *44* (18), 7273-7287.

100. Coates, P. D.; Ward, I. M. Drawing of polymers through a conical die. *Polymer* **1979,** *20* (12), 1553-1560.

101. Coates, P. D.; Ward, I. M. Die drawing: Solid phase drawing of polymers through a converging die. *Polym. Eng. Sci.* **1981,** *21* (10), 612-618.

102. Pae, K. D.; Chu, H.-C.; Lee, J. K.; Kim, J.-H. Healing of stress-whitening in polyethylene and polypropylene at or below room temperature. *Polym. Eng. Sci.* **2000,** *40* (8), 1783-1795.

103. Schimanski, T.; Loos, J.; Peijs, T.; Alcock, B.; Lemstra, P. J. On the overdrawing of melt-spun isotactic polypropylene tapes. *J. Appl. Polym. Sci.* **2007,** *103* (5), 2920-2931.

104. Schimanski, T.; Peijs, T.; Lemstra, P. J.; Loos, J. Influence of Postdrawing Temperature on Mechanical Properties of Melt-Spun Isotactic Polypropylene. *Macromolecules* **2004,** *37* (5), 1810-1815.

105. Mai, F.; Tu, W.; Bilotti, E.; Peijs, T. The Influence of Solid-State Drawing on Mechanical Properties and Hydrolytic Degradation of Melt-Spun Poly(Lactic Acid) (PLA) Tapes. *Fibers* **2015,** *3* (4), 523-538.

106. Zhang, X.; Schneider, K.; Liu, G.; Chen, J.; Brüning, K.; Wang, D.; Stamm, M. Structure variation of tensile-deformed amorphous poly(l-lactic acid): Effects of deformation rate and strain. *Polymer* **2011,** *52* (18), 4141-4149.

107. Shimada, H.; Nobukawa, S.; Hattori, T.; Yamaguchi, M. Wavelength dispersion of birefringence of oriented polyethylene films. *Appl. Opt.* **2017,** *56* (13), 3806-3811.

108. Lin, X.; Caton-Rose, F.; Ren, D.; Wang, K.; Coates, P. Shear-induced crystallization morphology and mechanical property of high density polyethylene in micro-injection molding. *J. Polym. Res.* **2013,** *20* (4), 122.

109. Coates, P. D.; Caton-Rose, P.; Ward, I. M.; Thompson, G. Process structuring of polymers by solid phase orientation processing. *Sci. China Chem.* **2013,** *56* (8), 1017-1028.

110. Capaccio, G.; Ward, I. M. Preparation of ultra-high modulus linear polyethylenes; effect of molecular weight and molecular weight distribution on drawing behaviour and mechanical properties. *Polymer* **1974,** *15* (4), 233-238.

111. Capaccio, G.; Gibson, A.; Ward, I. M. *Ultra-high Modulus Polymers*, Applied Science Publishers, London: 1979.

112. Wu, W.; Black, W. B. High-strength polyethylene. *Polym. Eng. Sci.* **1979,** *19* (16), 1163-1169.

113. Smith, P.; Lemstra, P. J. Ultra-drawing of high molecular weight polyethylene cast from solution. *Colloid. Polym. Sci.* **1980,** *258* (7), 891-894.

114. Lemstra, P. J.; van Aerle, N. A. J. M.; Bastiaansen, C. W. M. Chain-extended polyethylene. *Polym. J.* **1987,** *19*, 85.

115. Rastogi, S.; Yao, Y.; Ronca, S.; Bos, J.; van der Eem, J. Unprecedented high-modulus high-strength tapes and films of ultrahigh molecular weight polyethylene via solvent-free route. *Macromolecules* **2011,** *44* (14), 5558-5568.

116. Peterlin, A. Molecular model of drawing polyethylene and polypropylene. *J. Mater. Sci.* **1971,** *6* (6), 490-508.

117. Peterlin, A. Drawing and extrusion of semi-crystalline polymers. *Colloid. Polym. Sci.* **1987,** *265* (5), 357-382.

118. Hu, W.-G.; Schmidt-Rohr, K. Polymer ultradrawability: the crucial role of α-relaxation chain mobility in the crystallites. *Acta Polym.* **1999,** *50* (8), 271-285.

119. Coates, P. D.; Ward, I. M. The plastic deformation behaviour of linear polyethylene and polyoxymethylene. *J. Mater. Sci.* **1978,** *13* (9), 1957-1970.

120. Coates, P. D.; Ward, I. M. Neck profiles in drawn linear polyethylene. *J. Mater. Sci.* **1980,** *15* (11), 2897-2914.

121. Brady, J. M.; Thomas, E. L. Conversion of single crystal mats to ultrahigh modulus polyethylene: the formation of a continuous crystalline phase. *Polymer* **1989,** *30* (9), 1615-1622.

122. Pegoretti, A.; Ashkar, M.; Migliaresi, C.; Marom, G. Relaxation processes in polyethylene fibre-reinforced polyethylene composites. *Compos. Sci. Technol.* **2000,** *60* (8), 1181-1189.

123. Capaccio, G.; Ward, I. M. Effect of molecular weight on the morphology and drawing behaviour of melt crystallized linear polyethylene. *Polymer* **1975,** *16* (4), 239-243.

124. Capaccio, G.; Crompton, T. A.; Ward, I. M. The drawing behavior of linear polyethylene. I. Rate of drawing as a function of polymer molecular weight and initial thermal treatment. *J. Polym. Sci., Part B: Polym. Phys.* **1976,** *14* (9), 1641-1658.

125. Cansfield, D. L. M.; Capaccio, G.; Ward, I. M. The preparation of ultra-high modulus polypropylene films and fibres. *Polym. Eng. Sci.* **1976,** *16* (11), 721-724.

126. Wilding, M. A.; Ward, I. M. Tensile creep and recovery in ultra-high modulus linear polyethylenes. *Polymer* **1978,** *19* (8), 969-976.

127. Gibson, A. G.; Ward, I. M.; Cole, B. N.; Parsons, B. Hydrostatic extrusion of linear polyethylene. *J. Mater. Sci.* **1974,** *9* (7), 1193-1196.

128. Coates, P. D.; Ward, I. M. Hydrostatic extrusion of polyoxymethylene. *J. Polym. Sci., Part B: Polym. Phys.* **1978,** *16* (11), 2031-2047.

129. Coates, P. D.; Gibson, A. G.; Ward, I. M. An analysis of the mechanics of solid phase extrusion of polymers. *J. Mater. Sci.* **1980,** *15* (2), 359-375.

130. Taraiya, A. K.; Nugent, M.; Sweeney, J.; Coates, P. D.; Ward, I. M. Development of continuous die drawing production process for engineered polymer cores for wire ropes. *Plast. Rubber Compos.* **2000,** *29* (1), 46-50.

131. Patterson, M. *Structural Glass Facades and Enclosures*, Wiley: Hoboken, 2011.

132. Kuntsche, J.; Schuster, M.; Schneider, J. Engineering design of laminated safety glass considering the shear coupling: a review. *Glass Structures & Engineering* **2019,** *4* (2), 209-228.

133. Martín, M.; Centelles, X.; Solé, A.; Barreneche, C.; Fernández, A. I.; Cabeza, L. F. Polymeric interlayer materials for laminated glass: A review. *Constr. Build. Mater.* **2020,** *230*, 116897.

134. Biron, M. Plastics Solutions for Practical Problems. In *Thermoplastics and Thermoplastic Composites (Third Edition)*; Biron, M., Ed.; Elsevier: Oxford, 2018; Chapter 7, pp 831-984.

135. Archer, J. S.; Lesser, A. J. Impact resistant polymeric glasses using compressive pre-stress. *J. Appl. Polym. Sci.* **2009,** *114* (6), 3704-3715.

136. Lewis, G.; Mladsi, S. Correlation between impact strength and fracture toughness of PMMA-based bone cements. *Biomaterials* **2000,** *21* (8), 775-781.

137. Hsieh, A. J.; DeSchepper, D.; Moy, P.; Dehmer, P. G.; Song, J. W. *The effects of PMMA on ballistic impact performance of hybrid hard/ductile all-plastic-and glass-plastic-based composites*; U.S. Army Research Laboratory: 2004.

138. Gunnarsson, C. A.; Weerasooriya, T.; Moy, P. Impact Response of PC/PMMA Composites. In *Dynamic Behavior of Materials, Volume 1*; Proulx, T., Ed.; Springer: New York, 2011; pp 195-209.

139. Stenzler, J. S.; Goulbourne, N. C. The effect of polyacrylate microstructure on the impact response of PMMA/PC multi-laminates. *Int. J. Impact Eng.* **2011,** *38* (7), 567-576.

140. Kerns, J.; Hsieh, A.; Hiltner, A.; Baer, E. Comparison of irreversible deformation and yielding in microlayers of polycarbonate with poly(methylmethacrylate) and poly(styrene-co-acrylonitrile). *J. Appl. Polym. Sci.* **2000,** *77* (7), 1545-1557.

141. Hsieh, A. J.; Song, J. W. Measurements of Ballistic Impact Response of Novel Coextruded PC/PMMA Multilayered-Composites. *J. Reinf. Plast. Compos.* **2001,** *20* (3), 239-254.

142. Walley, S. M.; Field, J. E.; Blair, P. W.; Milford, A. J. The effect of temperature on the impact behaviour of glass/polycarbonate laminates. *Int. J. Impact Eng.* **2004,** *30* (1), 31-53.

143. Hu, W.; Wang, Y.; Yu, J.; Yen, C.-F.; Bobaru, F. Impact damage on a thin glass plate with a thin polycarbonate backing. *Int. J. Impact Eng.* **2013,** *62*, 152-165.

144. Shim, G.-I.; Kim, S.-H.; Eom, H.-W.; Ahn, D.-L.; Park, J.-K.; Choi, S.-Y. Improvement in ballistic impact resistance of a transparent bulletproof material laminated with strengthened soda-lime silicate glass. *Compos. Part B - Eng.* **2015,** *77*, 169-178.

145. Shim, G.-I.; Kim, S.-H.; Ahn, D.-L.; Park, J.-K.; Jin, D.-H.; Chung, D.-T.; Choi, S.-Y. Experimental and numerical evaluation of transparent bulletproof material for enhanced impact-energy absorption using strengthened-glass/polymer composite. *Compos. Part B - Eng.* **2016,** *97*, 150-161.

146. Pascual, C.; de Castro, J.; Schueler, A.; Vassilopoulos, A. P.; Keller, T. Total light transmittance of glass fiber-reinforced polymer laminates for multifunctional load-bearing structures. *J. Compos. Mater.* **2014,** *48* (29), 3591-3604.

147. Pascual, C.; de Castro, J.; Kostro, A.; Schueler, A.; Vassilopoulos, A. P.; Keller, T. Optically-derived mechanical properties of glass fiber-reinforced polymer laminates for multifunctional load-bearing structures. *J. Compos. Mater.* **2015,** *49* (28), 3539-3556.

148. Velez, M.; Schuman, T.; Day, D. Optical properties of optically transparent glass-ribbon composites. *J. Compos. Mater.* **2014,** *48* (30), 3747-3754.

149. Velez, M.; Braisted, W.; Frank, G.; Phillips, P.; Day, D.; McLaughlin, M. Impact strength of optically transparent glass ribbon composites. *J. Compos. Mater.* **2012,** *46* (14), 1677-1695.

150. Lowe, J. Aerospace applications. In *Design and Manufacture of Textile Composites*; Long, A. C., Ed.; Woodhead Publishing: Cambridge, 2005; Chapter 11, pp 405-423.

151. Zhang, H.; Bilotti, E.; Peijs, T. Nano-Engineered Hierarchical Carbon Fibres and Their Composites: Preparation, Properties and Multifunctionalities. In *The Structural Integrity of Carbon Fiber Composites: Fifty Years of Progress and Achievement of the Science, Development, and Applications*; Beaumont, P. W. R.; Soutis, C.; Hodzic, A., Eds.; Springer: Cham, 2017; pp 101-116.

152. Peijs, T. 6.7 Electrospun Polymer Nanofibers and Their Composites. In *Comprehensive Composite Materials II*; Beaumont, P. W. R.; Zweben, C. H., Eds.; Elsevier: Oxford, 2018; pp 162-200.

153. Bettge, D. J.; Hinrichsen, G. Continuous manufacturing of composites of high-performance polyethylene fibres. *Compos. Sci. Technol.* **1993,** *47* (2), 131-136.

154. Sloan, F.; Nguyen, H. Mechanical Characterization of Extended-Chain Polyethylene (ECPE) Fiber-Reinforced Composites. *J. Compos. Mater.* **1995,** *29* (16), 2092-2107.

155. Zhang, T. G.; Satapathy, S. S.; Vargas-Gonzalez, L. R.; Walsh, S. M. Ballistic impact response of Ultra-High-Molecular-Weight Polyethylene (UHMWPE). *Compos. Struct.* **2015,** *133*, 191-201.

156. Wang, Q.; Chen, Z.; Chen, Z. Design and characteristics of hybrid composite armor subjected to projectile impact. *Mater. Des.* **2013,** *46*, 634-639.

157. Cartwright, B. K.; Lex Mulcahy, N.; Chhor, A. O.; Thomas, S. G. F.; Suryanarayana, M.; Sandlin, J. D.; Crouch, I. G.; Naebe, M. Thermoforming and Structural Analysis of Combat Helmets. *J. Manuf. Sci. Eng.* **2015,** *137* (5).

158. Mangalgiri, P. D. Composite materials for aerospace applications. *Bull. Mater. Sci.* **1999,** *22* (3), 657-664.

159. Tham, C. Y.; Tan, V. B. C.; Lee, H. P. Ballistic impact of a KEVLAR® helmet: Experiment and simulations. *Int. J. Impact Eng.* **2008,** *35* (5), 304-318.

160. Liao, H.; Wu, Y.; Wu, M.; Zhan, X.; Liu, H. Aligned electrospun cellulose fibers reinforced epoxy resin composite films with high visible light transmittance. *Cellulose* **2012,** *19* (1), 111-119.

161. Pinto, E. R. P.; Barud, H. S.; Silva, R. R.; Palmieri, M.; Polito, W. L.; Calil, V. L.; Cremona, M.; Ribeiro, S. J. L.; Messaddeq, Y. Transparent composites prepared from bacterial cellulose and castor oil based polyurethane as substrates for flexible OLEDs. *J. Mater. Chem. C* **2015,** *3* (44), 11581-11588.

162. Capaccio, G.; Crompton, T. A.; Ward, I. M. Drawing behavior of linear polyethylene. II. Effect of draw temperature and molecular weight on draw ratio and modulus. *J. Polym. Sci., Part B: Polym. Phys.* **1980,** *18* (2), 301-309.

163. Kong, Y.; Hay, J. N. The measurement of the crystallinity of polymers by DSC. *Polymer* **2002,** *43* (14), 3873-3878.

164. Faick, C. A.; Finn, A. N. The index of refraction of some soda-lime-silica glasses as a function of the composition. *J. Am. Ceram. Soc.* **1931,** *14* (7), 518-528.

165. Gao, H.; Li, J.; Xie, F.; Liu, Y.; Leng, J. A novel low colored and transparent shape memory copolyimide and its durability in space thermal cycling environments. *Polymer* **2018,** *156*, 121-127.

166. Kurokawa, N.; Hotta, A. Thermomechanical properties of highly transparent self-reinforced polylactide composites with electrospun stereocomplex polylactide nanofibers. *Polymer* **2018,** *153*, 214-222.

167. Merzlyak, M. N.; Razi Naqvi, K. On recording the true absorption spectrum and the scattering spectrum of a turbid sample: application to cell suspensions of the cyanobacterium anabaena variabilis. *J. Photochem. Photobiol. B: Biol.* **2000,** *58* (2), 123-129.

168. Nogi, M.; Yano, H. Optically transparent nanofiber sheets by deposition of transparent materials: a concept for a roll-to-roll processing. *Appl. Phys. Lett.* **2009,** *94* (23), 233117.

169. Jarecki, L.; Meier, D. J. Ultra-high modulus polyethylene. 1 Effect of drawing temperature. *Polymer* **1979,** *20* (9), 1078-1082.

170. Meinel, G.; Morosoff, N.; Peterlin, A. Plastic deformation of polyethylene. I. Change of morphology during drawing of polyethylene of high density. *J. Polym. Sci., Part B: Polym. Phys.* **1970,** *8* (10), 1723-1740.

171. Liu, Y.; Russell, T. P.; Samant, M. G.; Stöhr, J.; Brown, H. R.; Cossy-Favre, A.; Diaz, J. Surface relaxations in polymers. *Macromolecules* **1997,** *30* (25), 7768-7771.

172. Kerle, T.; Lin, Z.; Kim, H.-C.; Russell, T. P. Mobility of polymers at the air/polymer interface. *Macromolecules* **2001,** *34* (10), 3484-3492.

173. Mai, F.; Tu, W.; Bilotti, E.; Peijs, T. The influence of solid-state drawing on mechanical properties and hydrolytic degradation of melt-spun poly(lactic acid) (PLA) tapes. *Fibers* **2015,** *3* (4), 523.

174. Peterlin, A.; Corneliussen, R. Small-angle x-ray diffraction studies of plastically deformed polyethylene. II. Influence of draw temperature, draw ratio, annealing temperature, and time. *J. Polym. Sci., Part B: Polym. Phys.* **1968,** *6* (7), 1273-1282.

175. Sumita, M.; Miyasaka, K.; Ishikawa, K. Effect of drawing on the melting point and heat of fusion of polyethylene. *J. Polym. Sci., Part B: Polym. Phys.* **1977,** *15* (5), 837-846.

176. Peijs, T.; Rijsdijk, H. A.; de Kok, J. M. M.; Lemstra, P. J. The role of interface and fibre anisotropy in controlling the performance of polyethylene-fibre-reinforced composites. *Compos. Sci. Technol.* **1994,** *52* (3), 449-466.

177. Ferry, J. D. *Viscoelastic Properties of Polymers*, Wiley: New York, 1980.

178. Rosato, M. G.; Rosato, D. V. *Concise Encyclopedia of Plastics*, Springer: New York, 2012.

179. Spalding, M. A.; Chatterjee, A. *Handbook of Industrial Polyethylene and Technology: Definitive Guide to Manufacturing, Properties, Processing, Applications and Markets Set*, Wiley: Hoboken, 2017.

180. Li, Y.; Akpalu, Y. A. Probing the Melting Behavior of a Homogeneous Ethylene/1-Hexene Copolymer by Small-Angle Light Scattering. *Macromolecules* **2004,** *37* (19), 7265-7277.

181. Lu, Y.; Wang, Y.; Chen, R.; Zhao, J.; Jiang, Z.; Men, Y. Cavitation in Isotactic Polypropylene at Large Strains during Tensile Deformation at Elevated Temperatures. *Macromolecules* **2015,** *48* (16), 5799-5806.

182. Whittaker, J. L.; Balu, R.; Knott, R.; de Campo, L.; Mata, J. P.; Rehm, C.; Hill, A. J.; Dutta, N. K.; Roy Choudhury, N. Structural evolution of photocrosslinked silk fibroin and silk fibroin-based hybrid hydrogels: A small angle and ultra-small angle scattering investigation. *Int. J. Biol. Macromol.* **2018,** *114*, 998-1007.

183. Hermans, P. H.; Weidinger, A. Quantitative X‐Ray Investigations on the Crystallinity of Cellulose Fibers. A Background Analysis. *J. Appl. Phys.* **1948,** *19* (5), 491-506.

184. Afeworki, M.; Brant, P.; Lustiger, A.; Norman, A. Solid-state 13C NMR and synchrotron SAXS/WAXS studies of uniaxially-oriented polyethylene. *Solid State Nucl. Magn. Reson.* **2015,** *72*, 27-40.

185. Xiong, B.; Lame, O.; Chenal, J. M.; Rochas, C.; Seguela, R.; Vigier, G. Temperature-Microstructure Mapping of the Initiation of the Plastic Deformation Processes in Polyethylene via In Situ WAXS and SAXS. *Macromolecules* **2015,** *48* (15), 5267-5275.

186. Butler, M. F.; Donald, A. M.; Ryan, A. J. Time resolved simultaneous small- and wide-angle X-ray scattering during polyethylene deformation: 1. Cold drawing of ethylene-α-olefin copolymers. *Polymer* **1997,** *38* (22), 5521-5538.

187. Rhodes, M. B.; Stein, R. S. Light Scattering Study of the Annealing of Drawn Polyethylene. *J. Appl. Phys.* **1961,** *32* (11), 2344-2352.

188. Lu, Y.; Men, Y. Cavitation-Induced Stress Whitening in Semi-Crystalline Polymers. *Macromol. Mater. Eng.* **2018,** *303* (11), 1800203.

189. Jiang, Z.; Chen, R.; Lu, Y.; Whiteside, B.; Coates, P.; Wu, Z.; Men, Y. Crystallization Temperature Dependence of Cavitation and Plastic Flow in the

Tensile Deformation of Poly(ε-caprolactone). *J. Phys. Chem. B* **2017,** *121* (27), 6673-6684.

190. Jiang, Z.; Tang, Y.; Men, Y.; Enderle, H.-F.; Lilge, D.; Roth, S. V.; Gehrke, R.; Rieger, J. Structural Evolution of Tensile-Deformed High-Density Polyethylene during Annealing: Scanning Synchrotron Small-Angle X-ray Scattering Study. *Macromolecules* **2007,** *40* (20), 7263-7269.

191. Men, Y.; Rieger, J.; Endeler, H.-F.; Lilge, D. Mechanical α-Process in Polyethylene. *Macromolecules* **2003,** *36* (13), 4689-4691.

192. Jiang, Z.; Tang, Y.; Rieger, J.; Enderle, H.-F.; Lilge, D.; Roth, S. V.; Gehrke, R.; Heckmann, W.; Men, Y. Two Lamellar to Fibrillar Transitions in the Tensile Deformation of High-Density Polyethylene. *Macromolecules* **2010,** *43* (10), 4727-4732.

193. Pawlak, A.; Galeski, A.; Rozanski, A. Cavitation during deformation of semicrystalline polymers. *Prog. Polym. Sci.* **2014,** *39* (5), 921-958.

194. Chang, B.; Schneider, K.; Heinrich, G. Microstructural Evolution of Isotactic-Polypropylene during Creep: An In Situ Study by Synchrotron Small-Angle X-Ray Scattering. *Macromol. Mater. Eng.* **2017,** *302* (10), 1700152.

195. Chang, B.; Schneider, K.; Xiang, F.; Vogel, R.; Roth, S.; Heinrich, G. Critical Strains for Lamellae Deformation and Cavitation during Uniaxial Stretching of Annealed Isotactic Polypropylene. *Macromolecules* **2018,** *51* (16), 6276-6290.

196. Choi, K.-J.; Spruiell, J. E.; White, J. L. Orientation and morphology of high-density polyethylene film produced by the tubular blowing method and its relationship to process conditions. *J. Polym. Sci., Part B: Polym. Phys.* **1982,** *20* (1), 27-47.

197. Smith, P.; Lemstra, P. J. Ultra-high-strength polyethylene filaments by solution spinning/drawing. *J. Mater. Sci.* **1980,** *15* (2), 505-514.

198. Fung, P. Y. F.; Carr, S. H. Morphology and deformation of melt-spun polyethylene fibers. *J. Macromol. Sci. B* **1972,** *6* (4), 621-633.

199. Zhang, X. M.; Elkoun, S.; Ajji, A.; Huneault, M. A. Oriented structure and anisotropy properties of polymer blown films: HDPE, LLDPE and LDPE. *Polymer* **2004,** *45* (1), 217-229.

200. Brew, B.; Ward, I. M. Study of the production of ultra-high modulus polyoxymethylene by tensile drawing at high temperatures. *Polymer* **1978,** *19* (11), 1338-1344.

201. Campbell, F. C. *Structural Composite Materials*, ASM international: Ohio, 2010.

202. Alcock, B.; Peijs, T. Technology and Development of Self-Reinforced Polymer Composites. In *Polymer Composites - Polyolefin Fractionation - Polymeric*

Peptidomimetics - Collagens; Abe, A.; Kausch, H.-H.; Möller, M.; Pasch, H., Eds.; Springer: Berlin, 2013; pp 1-76.

203. Owens, D. K.; Wendt, R. C. Estimation of the surface free energy of polymers. *J. Appl. Polym. Sci.* **1969,** *13* (8), 1741-1747.

204. Good, R. J.; Girifalco, L. A theory for estimation of surface and interfacial energies. III. Estimation of surface energies of solids from contact angle data. *J Phys Chem.* **1960,** *64* (5), 561-565.

205. Good, R. J. Contact angle, wetting, and adhesion: a critical review. *J. Adhes. Sci. Technol.* **1992,** *6* (12), 1269-1302.

206. Liu, Y.; Zhang, H.; Porwal, H.; Tu, W.; Wan, K.; Evans, J.; Newton, M.; Busfield, J. J. C.; Peijs, T.; Bilotti, E. Tailored pyroresistive performance and flexibility by introducing a secondary thermoplastic elastomeric phase into graphene nanoplatelet (GNP) filled polymer composites for self-regulating heating devices. *J. Mater. Chem. C* **2018,** *6* (11), 2760-2768.

207. ASTM D1876-08(2015)e1, Standard Test Method for Peel Resistance of Adhesives (T-Peel Test), ASTM International, West Conshohocken, PA, 2015, www.astm.org.

208. ASTM D3039 / D3039M-17, Standard Test Method for Tensile Properties of Polymer Matrix Composite Materials, ASTM International, West Conshohocken, PA, 2017, www.astm.org.

209. ASTM D6264 / D6264M-17, Standard Test Method for Measuring the Damage Resistance of a Fiber-Reinforced Polymer-Matrix Composite to a Concentrated Quasi-Static Indentation Force, ASTM International, West Conshohocken, PA, 2017, www.astm.org.

210. Waxler, R. M.; Horowitz, D.; Feldman, A. Optical and physical parameters of Plexiglas 55 and Lexan. *Appl. Opt.* **1979,** *18* (1), 101-104.

211. Bistac, S.; Kunemann, P.; Schultz, J. Crystalline modifications of ethylene-vinyl acetate copolymers induced by a tensile drawing: effect of the molecular weight. *Polymer* **1998,** *39* (20), 4875-4881.

212. Dhaliwal, A. K.; Hay, J. N. The characterization of polyvinyl butyral by thermal analysis. *Thermochim. Acta* **2002,** *391* (1), 245-255.

213. Wang, D.; Zhang, Z.; Li, Y.; Xu, C. Highly Transparent and Durable Superhydrophobic Hybrid Nanoporous Coatings Fabricated from Polysiloxane. *ACS Appl. Mater. Interfaces* **2014,** *6* (13), 10014-10021.

214. Wang, Z.; Lu, Z.; Mahoney, C.; Yan, J.; Ferebee, R.; Luo, D.; Matyjaszewski, K.; Bockstaller, M. R. Transparent and High Refractive Index Thermoplastic Polymer Glasses Using Evaporative Ligand Exchange of Hybrid Particle Fillers. *ACS Appl. Mater. Interfaces* **2017,** *9* (8), 7515-7522.

215. ASTM D1746-15, Standard Test Method for Transparency of Plastic Sheeting, ASTM International, West Conshohocken, PA, 2015, www.astm.org.

216. Ajji, A.; Zhang, X.; Elkoun, S. Biaxial orientation in HDPE films: comparison of infrared spectroscopy, X-ray pole figures and birefringence techniques. *Polymer* **2005,** *46* (11), 3838-3846.

217. Chatterjee, T.; Patel, R.; Garnett, J.; Paradkar, R.; Ge, S.; Liu, L.; Forziati, K. T.; Shah, N. Machine direction orientation of high density polyethylene (HDPE): Barrier and optical properties. *Polymer* **2014,** *55* (16), 4102-4115.

218. Mai, F.; Tu, W.; Bilotti, E.; Peijs, T. Preparation and properties of self-reinforced poly(lactic acid) composites based on oriented tapes. *Compos. Part A - Appl. S.* **2015,** *76*, 145-153.

219. Peijs, T.; Smets, E. A. M.; Govaert, L. E. Strain rate and temperature effects on energy absorption of polyethylene fibres and composites. *Appl. Compos. Mater.* **1994,** *1* (1), 35-54.

220. Davies, G. A. O.; Zhang, X. Impact damage prediction in carbon composite structures. *Int. J. Impact Eng.* **1995,** *16* (1), 149-170.

221. Clyne, T.; Hull, D. *An Introduction to Composite Materials*, Cambridge University Press: Cambridge, 2019.

222. Ashizawa, H.; Spruiell, J. E.; White, J. L. An investigation of optical clarity and crystalline orientation in polyethylene tubular film. *Polym. Eng. Sci.* **1984,** *24* (13), 1035-1042.

223. Van Der Werff, H. Modelling of ballistic impact on fiber composites. *Target* **2010,** *50*, 3.

224. Van der Werff, H.; Heisserer, U. High-performance ballistic fibers: ultra-high molecular weight polyethylene (UHMWPE). In *Advanced Fibrous Composite Materials for Ballistic Protection*; Woodhead Publishing: Cambridge, 2016; Chapter 3, pp 71-107.

225. Choy, C. L.; Greig, D. The low temperature thermal conductivity of isotropic and oriented polymers. *J. Phys. C: Solid State Phys.* **1977,** *10* (2), 169-179.

226. Gibson, A. G.; Greig, D.; Sahota, M.; Ward, I. M.; Choy, C. L. Thermal conductivity of ultrahigh-modulus polyethylene. *J. Polym. Sci., Part B: Polym. Lett.* **1977,** *15* (4), 183-192.

227. Shen, S.; Henry, A.; Tong, J.; Zheng, R.; Chen, G. Polyethylene nanofibres with very high thermal conductivities. *Nat. Nanotechnol.* **2010,** *5* (4), 251-255.

228. Zhu, B.; Liu, J.; Wang, T.; Han, M.; Valloppilly, S.; Xu, S.; Wang, X. Novel Polyethylene Fibers of Very High Thermal Conductivity Enabled by Amorphous Restructuring. *ACS Omega* **2017,** *2* (7), 3931-3944.

229. Ronca, S.; Igarashi, T.; Forte, G.; Rastogi, S. Metallic-like thermal conductivity in a lightweight insulator: Solid-state processed Ultra High Molecular Weight Polyethylene tapes and films. *Polymer* **2017,** *123*, 203-210.

230. Xu, Y.; Kraemer, D.; Song, B.; Jiang, Z.; Zhou, J.; Loomis, J.; Wang, J.; Li, M.; Ghasemi, H.; Huang, X.; Li, X.; Chen, G. Nanostructured polymer films with metal-like thermal conductivity. *Nat. Commun.* **2019,** *10* (1), 1771.

231. Verpaalen, R. C. P.; Varghese, S.; Froyen, A.; Pilz da Cunha, M.; Pouderoijen, M. J.; Severn, J. R.; Bhatti, M. R.; Peijs, T.; Bastiaansen, C. W. M.; Debije, M. G.; Engels, T. A. P.; Schenning, A. P. H. J. Fast, Light-Responsive, Metal-Like Polymer Actuators Generating High Stresses at Low Strain. *Matter* **2020,** *2* (6), 1522-1534.

232. Bhatti, M. R.; Bilotti, E.; Zhang, H.; Varghese, S.; Verpaalen, R.; Schenning, A.; Bastiaansen, C. W. M.; Peijs, T. Ultra-High Actuation Stress Polymer Actuators as Light-Driven Artificial Muscles. *ACS Appl. Mater. Interfaces* **2020,** *12* (29), 33210.

233. Bhatti, M. R.; Bilotti, E.; Zhang, H.; Bastiaansen, C. W. M.; Peijs, T. Photo-Thermal Actuation of Ultra-Drawn High-Density Polyethylene. *Polymer* **2020**, 122897.

234. Duckwall Jr, L. R.; Bostian, D. H.; Hatfield, E. Machine direction oriented high molecular weight, high density polyethylene films with enhanced water vapor transmission properties. US6391411, 2002.

235. Breese, D. R.; Beaucage, G. Effects of Machine Direction Orientation (MDO) on the Moisture and Oxygen Barrier Properties of HMW-PE Films. In *TAPPI PLACE Conference*; 2005.

236. Peijs, T. Composites for recyclability. *Mater. Today* **2003,** *4* (6), 30-35.

237. Cabrera, N.; Alcock, B.; Loos, J.; Peijs, T. Processing of all-polypropylene composites for ultimate recyclability. *Proceedings of the Institution of Mechanical Engineers, Part L: Journal of Materials: Design and Applications* **2004,** *218* (2), 145-155.

238. Zhang, J. M.; Reynolds, C. T.; Peijs, T. All-poly(ethylene terephthalate) composites by film stacking of oriented tapes. *Compos. Part A - Appl. S.* **2009,** *40* (11), 1747-1755.

List of Publications

1. **Yunyin Lin**, Ruhi Patel, Jun Cao, Wei Tu, Han Zhang, Emiliano Bilotti, Cees W. M. Bastiaansen, Ton Peijs. Glass-like transparent high strength polyethylene films by tuning drawing temperature. *Polymer* **2019,** *171*, 180-191.
2. **Yunyin Lin**, Wei Tu, Rob C. P. Verpaalen, Han Zhang, Cees W. M. Bastiaansen, Ton Peijs. Transparent, Lightweight, and High Strength Polyethylene Films by a Scalable Continuous Extrusion and Solid-State Drawing Process. *Macromolecular Materials and Engineering* **2019,** *304* (8), 1900138.
3. **Yunyin Lin**, Jun Cao, Meifang Zhu, Emiliano Bilotti, Han Zhang, Cees W. M. Bastiaansen, Ton Peijs. High Performance Transparent Laminates based on Highly Oriented Polyethylene Films. *ACS Applied Polymer Materials* **2020**, *2* (6), 2458-2468.
4. **Yunyin Lin**, Emiliano Bilotti, Cees W. M. Bastiaansen, Ton Peijs. Transparent Semi-crystalline Polymeric Materials and their Nanocomposites: A Review. *Polymer Engineering and Science* **2020**, https://doi.org/10.1002/pen.25489.
5. **Yunyin Lin**, Ton Peijs, Cees W. M. Bastiaansen. Transparent Drawn Article. GB1820429.7, 2018.
6. Jun Cao, Vladimir Koval, Hangfeng Zhang, **Yunyin Lin**, Jiyue Wu, Nan Meng, Yan Li, Zheng Li, Hongtao Zhang, Haixue Yan. Crystal structure and electrical properties of textured Ba2Bi4Ti5O18 ceramics. *Journal of the European Ceramic Society* **2019,** *39* (4), 1042-1049.